Optical and photoelectrical applications of langmuir blodgett films

M.T Fowler

OPTICAL AND PHOTOELECTRICAL APPLICATIONS OF LANGMUIR-BLODGETT FILMS

by

M.T.Fowler, B.Sc.

A Thesis submitted for the Degree of Doctor of Philosophy in the University of Durham

February 1985

DECLARATION

I hereby declare that the work reported in this thesis has not previously been submitted for any degree and is not being currently submitted in candidature for any other degree.

Signed _____

The work reported in this thesis was carried out by the candidate.

Signed _____

_____

Directors of Studies

_____

Candidate

ABSTRACT

The Langmuir-Blodgett (LB) technique is well known for the deposition of thin, uniform films of precisely defined thickness. These films can be used in electronic devices as an active layer, or in a passive role as insulators. Results are presented of investigations using films of both types. Novel LB films of a merocyanine dye have been developed for use as a spectral sensitiser, and films of phthalocyanine used as insulators for the enhancement of the electroluminescent (EL) properties of a metal-semiconductor structure.

The merocyanine dye used has none of the clear amphiphilic molecular substitutions associated with classical LB film materials, but behaves well as a Langmuir film. Incorporated into a matrix of cadmium arachidate the dye can be deposited onto various substrates using the LB technique. The optical properties of such deposited films are characterised and compared with those of a merocyanine dye featuring amphiphilic substitutions. For both dyes these properties indicate that good quality LB films have been deposited, and that some dimeric structure is present in these films. The feasibility of using these films for the spectral sensitisation of semiconductors is demonstrated by their modifying effect on the photoconductive response of polycrystalline zinc sulphide.

The incorporation of LB films of phthalocyanine into the gold/ZnSeS system enables low voltage forward bias d.c EL to be observed with a threshold ~1V. Measurement of the increase in intensity of emitted EL with bias suggests that the presence of the insulating layer increases the minority current available for radiative recombination by supporting realignment of energy bands in the metal and semiconductor. EL efficiency of devices is shown to increase with insulator thickness up to ten deposited layers of phthalocyanine a thickness of ~23nm. A simple energy band model for the system is proposed which takes into account series resistance effects.

ACKNOWLEDGEMENTS

In producing this thesis I have become indebted to a great many people to whom I would like to express my gratitude. Primarily I must thank my supervisors, Professor Gareth Roberts and Dr Mike Petty for successfully combining their talents to guide, assist, encourage and when necessary cajole me during the course of this research. I consider myself privileged to have been a member of their LB film research group, and can only hope that I live up to its high standards in the future. I would like to thank everyone in the group for both their friendship and the constant sharing of ideas and expertise, in particular Mr Steve Baker and Dr John Batey whose own studies made much of this research possible. My time in the Department of Applied Physics and Electronics at the University of Durham has been made enjoyable and constructive by many people. I am particularly indebted to the technical staff, headed by Mr Frank Spence, and the secretaries Mrs Pauline Morrell and Mrs Sylvia Mellanby for contributing their skills, knowledge and patience. The excellent diagrams drawn by Ms Elizabeth Thompson, Mrs Julie Smart and Mr Norman Thompson, and the assistance of the Computer Centre staff in printing this thesis are much appreciated.

I would like to acknowledge financial support from the SERC and RSRE, Malvern, and thank RSRE and ICI Ltd for the provision of materials. Dr Mervyn Daniel (RSRE) has also contributed much in the way of assistance and encouragement.

A great many close personal friends have helped make life bearable for me during my years in Durham. It is impractical to name them all, but Phill Christie and Doug Buchanan deserve special thanks. Warm thanks too to the various loves in my life (who all did their bit), and to Michael Webster and everyone at The Victoria for providing a second home. Lastly, but most importantly, thanks to my parents, sisters and brother for their distant but constant support, encouragement and faith.

CONTENTS

CHAPTER 1

INTRODUCTION

The Langmuir-Blodgett (LB) film technique has provoked much interest and research activity in recent years. The technique allows the deposition onto materials of uniform films down to a thickness of one molecular layer. Much of the initial interest of physicists was in the use of LB films as insulating layers of precisely controllable thickness, but latterly increasing attention has been centred on the possibility of the films playing an active role in devices. In this thesis investigations of the use of LB films in each of these roles are described, both involving the enhancement of optical properties associated with semiconductor materials. The first branch of the research was aimed at increasing the photoresponse of a wide bandgap semiconductor to lower energies of visible light by sensitising it with a dye in LB film form. The second aim was to increase the electroluminescent output of a semiconductor device by the incorporation of insulating LB film layers.

The spectral sensitisation of silver halides by the incorporation of small amounts of dye material is a technique well known to photographic science. The photoresponse of the semiconductor to visible light can be much enhanced in the spectral region where the dye absorbs most strongly. It has also been shown in the past that the technique is applicable to other wide bandgap semiconductors, and that the efficiency of the effect is critically dependent upon the amount of dye

adsorbed on the semiconductor surface. Depositing dyes by the LB technique should offer a fine degree of control of this effect for its application in devices. Sensitising dyes in LB film form have been studied before, but invariably requiring gross hydrophobic and hydrophilic substitutions to make them behave like 'classical' LB film materials. Part of this research was aimed at developing an LB film dye without these substitutions, which should thus have a greater stability and suffer less dilution of its optical properties. The sophisticated LB trough facilities at Durham University aid the characterisation of novel materials. Such films have been successfully produced with a merocyanine dye, and preliminary measurements of their effect upon the photoconductive response of zinc sulphide suggest that a clear sensitisation effect should be detected given more suitable semiconductor substrates.

There are many electroluminescent (EL) devices which operate by the injection of minority carriers into the luminescent region of a semiconductor. This is normally achieved with pn junctions where the minority carrier injection ratio (γ) is high. However, many of the semiconductors which are potentially the most efficient phosphors for the production of EL (i.e II-VI compounds) are difficult to obtain in low resistivity p-type form due to self compensation effects, i.e they are poor amphoteric semiconductors. An alternative device structure for such compounds is the metal-semiconductor (Schottky barrier) structure. For these devices γ is small ($< 10^{-4}$) and severely limits their EL efficiency. However, γ increases exponentially as the difference in barrier heights presented

to majority and minority carriers is reduced. One way of achieving such a change is by the incorporation of a thin insulator between the metal and semiconductor. Voltage dropped across the insulator causes a realignment of the relative positions of energy bands in the metal and semiconductor and hence can increase δ. This effect is critically dependent upon the quality and thickness of the insulating layer, which has suggested an application for the LB technique. Past work with LB films has concentrated upon model systems for evaluating the technique, in particular the incorporation of well characterised fatty acid monolayers into the gold/n-type GaP system. The aim of this study was to extend this to a II-VI material, and use more stable LB film materials. Devices have thus been fabricated using LB films of phthalocyanine deposited onto epitaxial films of ZnSeS grown by the MOCVD technique.

The thesis begins with discussions of the basic physics upon which this research was based. Chapter 2 is an account of the fundamental properties of dyes, and of their use for spectral sensitisation. Chapter 3 explains some of the physics of electroluminescent devices, with particular emphasis on the Schottky barrier and MIS structures relevant to this work. In Chapter 4 the technology of LB films is reviewed, and the techniques used for characterisation and deposition of the films used in both branches of this work are described. The chosen deposition conditions for the LB films, and other aspects of device fabrication and the measurement techniques employed in the characterisation of structures are recounted in Chapter 5. Chapter 6 details the results of an investigation into the use of merocyanine dyes

as LB films. The film-forming properties of the dyes are assessed, followed by a discussion of the optical characteristics of the dyes in solution and as LB films. The chapter concludes with the results obtained when LB films of dyes were deposited upon zinc sulphide crystals with the aim of demonstrating a dye-sensitisation effect. The results are explained in terms of an electron transfer process. In Chapter 7, the results of an investigation of gold - zinc sulphur selenide MS and MIS structures are presented. Phthalocyanine LB films were incorporated as insulating layers, and the effects of these films on the electrical and electroluminescent properties of the devices are shown. The data are explained using a modified version of the conventional tunnel injection theory. Chapter 8 concludes the thesis with a summary of the results obtained in this work, and some suggestions for the future development of the lines of research discussed.

CHAPTER 2

DYES AND DYE-SENSITISATION

This chapter discusses the properties of dyes and the processes involved in dye-sensitisation. Firstly the origins of the characteristic optical properties of dyes are explained in terms of their molecular structure. Following a brief history of the use of dyes as spectral sensitisers, the mechanisms of dye-sensitisation are discussed in terms of energy level considerations and the structures of dye molecules, both individually and collectively. The chapter concludes with brief reviews of the properties of some specific dye materials, and past work on dyes as Langmuir-Blodgett films.

2.1 OPTICAL PROPERTIES OF DYES

Dyes and pigments are classes of organic materials characterised by their colour. They are generally classed as those compounds which absorb light in the visible region (400nm to 800nm), but this loose definition is often extended into the ultra-violet and infra-red regions of the spectrum. Dyes are usually distinguished as being materials which impart their colour to a system by being incorporated at a molecular level, whereas pigments exist as aggregations within the system being coloured.

2.1.1 Origins of Energy Levels

As with most organic materials the bonding between dye

molecules is weak and is ascribed to van der Waals forces. Thus the absorption of light by these materials is essentially molecular in nature and corresponds to transitions between ground and excited electron states. Extra structure will occur in the absorption characteristic of the material due to vibrational energy levels (electron-phonon interaction is significant since electron exchange processes are relatively weak). This contrasts with the absorption processes in inorganic semiconductors where strong electron exchange dominates, characterised by a distinct absorption edge.

The electronic properties of an organic solid are governed by the electron transitions which can take place in the molecule. These electron transitions are in turn characterised by the spectroscopic properties of the system. When a molecule in its ground state absorbs a photon of light, one of the electrons in the highest filled molecular orbital is raised to the lowest unfilled molecular orbital. In general, the λ_{max} of absorption indicates the energy difference between the ground and excited states of the molecule. Changing the environment of absorbing electrons in a molecule (i.e by changing substituents) will cause small shifts in λ_{max}. Conjugated systems of π-electrons are stabilised (i.e attain lower energy) by resonance, and it is found that the increased resonance with the number of double bonds in conjugation raises λ_{max}. Stabilisation is apparently greater in the excited state than in the ground state since the energy difference between the two states is reduced. Conjugated π-electron systems are termed chromophores. Some largely empirical but quite successful

rules have been developed for calculation of the absorption maxima of a number of kinds of chromophore, and the modifying effects of substituents. The simpler chromophores absorb in the ultra-violet (e.g benzene has λ_{max} = 200nm), so for a compound to have λ_{max} in the visible generally implies a rather extensively conjugated chromophore. Dyes and pigments are accordingly usually rather complex molecules with extensive π-electron systems. A simple alkene chain has to be quite lomg to absorb in the visible (e.g C22 in β-carotene which has λ_{max} = 450nm). However, with the presence of heteroatoms such as nitrogen, chromophores need not be so extended for their absorptions to reach the visible region. For instance, the cyanines are a broad class of dyes with variously substituted chromophores of the general form

$$-\ddot{N}-(C=C)_n-C=\overset{+}{N}- \rightleftharpoons -\overset{+}{N}=C-(C=C)_n-\ddot{N}-$$

They exhibit strong resonance since the two resonance forms shown are identical, and are intensely coloured. The merocyanines studied in this research are a sub-group of the cyanines.

2.1.2 Intramolecular Relaxation of Electrons

When an electronic transition has taken place a molecule will tend to lose its excess energy and return to its ground state. The normal photophysical processes by which a molecule loses this energy are in competition with net charge carrier generation. A molecule in its ground electron state will normally contain two electrons of equal and opposite spin in each filled molecular orbital. This is the ground singlet state. If the spin of an excited electron continues to oppose that of the remaining electron then the resultant

state is called an excited singlet. If its spin is the same as the ground electron it is called an excited triplet. Singlets and triplets (hence the 'multiplicity' of a state) result in differing energy degradation processes. These processes are shown diagrammatically in Figure 2.1 (also shown are the vibrational levels associated with extra structure in the absorption characteristic). Fluorescence is the emission of light resulting from an electron dropping between states with the same multiplicity. This almost invariably occurs from the lowest excited state of a given multiplicity, and has extra structure associated with vibrational levels of the ground state. Thus the spectrum of the fluorescence of a molecule is often a mirror image of the absorption characteristic. The natural lifetime of this process is generally very short, of the order 10^{-8} seconds, depending upon the strength of the corresponding absorption process. Phosphorescence is the emission of light resulting from an electron dropping between states with different multiplicity, invariably from the lowest triplet to the ground state. Since the corresponding absorption process is strongly forbidden the natural lifetime of this process is much longer, from 10^{-3} seconds up to several seconds. These are the two processes one would expect to be quenched when electron or energy transfer from a dye occurs in a system.

There are also two types of non-radiative transition, as shown. Internal conversion occurs between states of the same multiplicity, and results from the relative crowding of higher excited states and the overlap of their vibrational levels. The times for these transitions are of the order of 10^{-12} seconds. The process is rarely effective across the

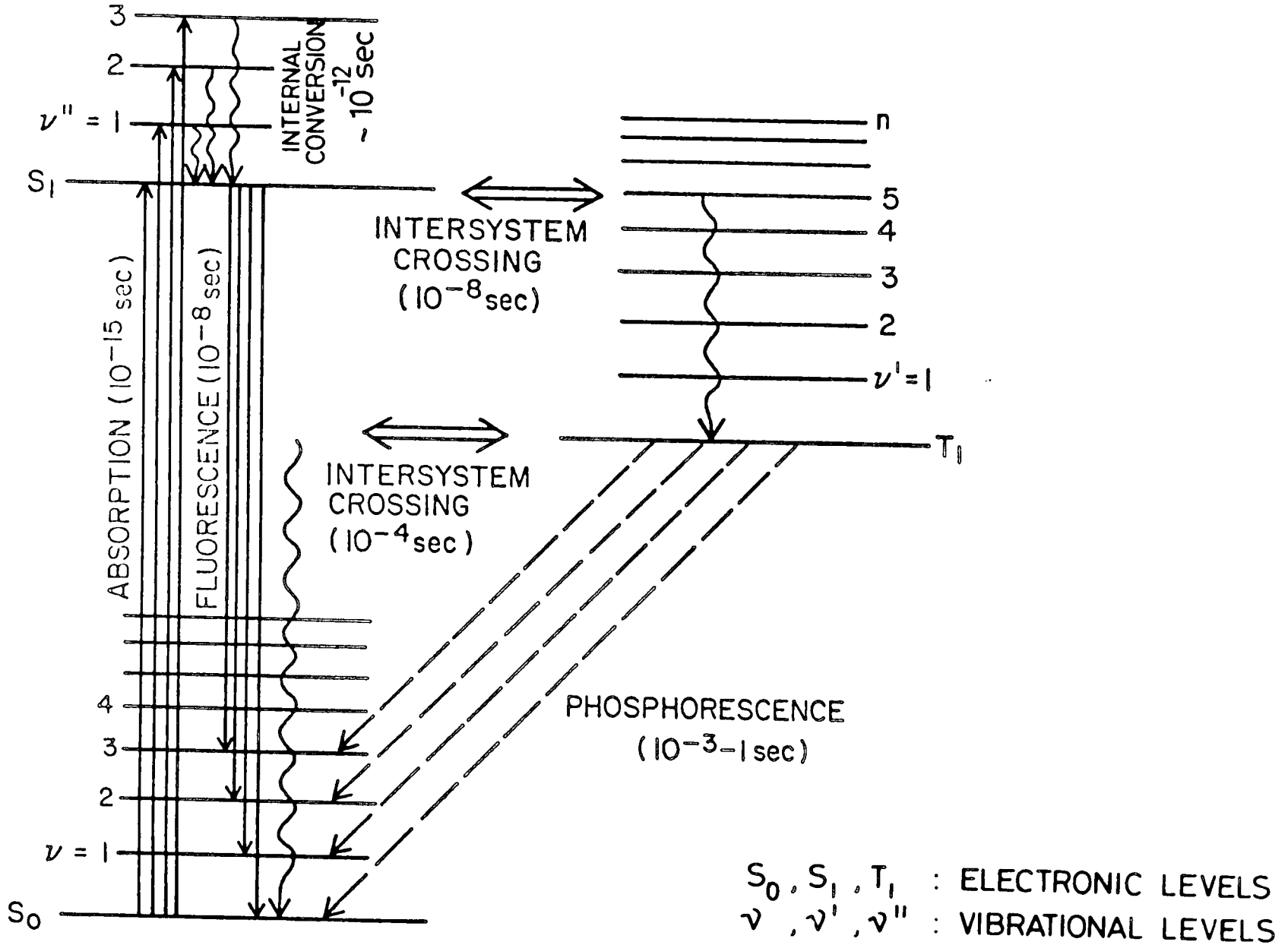

Figure 2.1 Schematic representation of intramolecular energy transitions of organic materials.

relatively large energy interval between the lowest excited singlet state and the ground state, which is characterised by strong fluorescence. The equivalent process between multiplicities is intersystem crossing, which normally only occurs between the lowest excited singlet state and the lowest triplet, or the lowest triplet and the ground singlet. From the lowest excited singlet to the lowest triplet the process competes with fluorescence (i.e lifetimes $\sim 10^{-8}$ seconds), but is slower from the lowest triplet to the ground state because the energy difference is usually much larger. It can still, however, compete favourably with phosphorescence.

2.1.3 Visible Light Spectroscopy

Because of the relatively weak van der Waals interaction between molecules the organic solid state is still primarily molecular in nature. Thus, the absorption characteristics of an organic compound in the solid state are closely related to those of the free molecule. The measurement of light absorption is governed by two closely related laws. Lambert's law is applicable to the absorption of light by a solid, and takes the form

$$\ln(I_o/I_T) = \alpha b \qquad (2.1)$$

where I_o and I_T are the intensities of the incident and transmitted light respectively, b is the sample thickness (usually expressed in cm) and α is the absorption coefficient. More suitable for solutions, where concentrations vary, is Beer's law

$$\log(I_o/I_T) = A = \varepsilon bc \qquad (2.2)$$

A is the absorbance or optical density and is the quantity

normally measured by a spectrophotometer, c is the solution concentration in moles/litre, and ε is the molar absorptivity or molar extinction coefficient, which normally has the units of litres/mole-cm. For most dyes, ε is of the order 10^5 at λ_{max}. The two quantities, α and ε, are useful for characterising the magnitude of absorption at a particular wavelength, but are not truly representative of the molecular absorption process. However, integrating an absorption curve plotted against frequency (and hence energy) will give a measure of the absolute strength of an electron transition. i.e

$$f_{if} \propto \int \varepsilon d\nu \qquad (2.3)$$

Here ν is the frequency of absorption and f_{if} is known as the oscillator strength. It is possible to relate the oscillator strength to the quantum mechanical dipole strength of an electronic transition.

Although it has already been stated that the photophysical processes in the organic solid are primarily those of the free molecule, it is clear that some molecular interaction will occur. A solid state absorption spectrum will usually exhibit spectral broadening due to weak coupling between electron orbitals. Though this interaction is weak, the times associated with it are only 10^{-11} s. Since the lifetime of an excited state is 10^{-8} s (Figure 2.1), an absorption process initiated in a single molecule in the solid can transfer energy to a whole assembly of interacting molecules. These interacting molecules are called Frenkel excitons, and can transport energy over relatively large distances in the organic solid state. Additional transitions can also occur due to some dimeric structure appearing in the

solid, since the two molecules in the dimer will interact through dipole-dipole coupling. When the arrangement of dye molecules is influenced by their adsorption onto, say, a semiconductor surface these transitions can give rise to very sharp and strong absorption. These 'J' bands and other aggregation bands have been widely reported by workers on dye-sensitisation(1). Another important interaction of excited states is excimer formation. An excimer is an excited state dimer and results from the interaction between an excited singlet state and an unexcited molecule. Excimer emission is usually broad, structureless and somewhat red-shifted from the normal molecular fluorescence. The formation and dissociation of excimers can be represented as

$$A(S_o) + h\nu \longrightarrow A^*(S_1)$$
$$A^*(S_1) + A(S_o) \longrightarrow (AA)^*$$
$$(AA)^* \longrightarrow A(S_o) + A(S_o) + h\nu' \qquad (2.4)$$

where A and A^* represent ground and first excited singlet states and $(AA)^*$ is the excited dimer or excimer state. In molecular crystals excimer emission is observed when the crystal structure is such that adjacent molecules form parallel-plane dimers which allow appreciable overlap of the delocalised π-electrons.

2.2 DYE SENSITISATION

Dye sensitisation or spectral sensitisation is defined as a selective increase in the sensitivity of a system to a spectral region by the addition of a dye. In practice, this means an increase in the sensitivity to wavelengths longer than those strongly absorbed by the undyed photosensitive system. This selectivity distinguishes it from chemical

sensitisation which increases sensitivity to all spectral regions absorbed by the system, usually by a factor which is nearly the same for all the regions. Dye sensitisation is primarily associated with photographic science and the improvement of the response of silver halide grains in emulsions. However, Akimov(2) has shown that several inorganic semiconductors can be sensitised by the adsorption of dyes from a vapour. This has paved the way for the possible development of semiconductor solar cell and photodetector devices with a spectral response matched to that of the incoming radiation.

2.2.1 A Brief History

The first observation that organic dyes could extend the spectral sensitivity of silver halide emulsions was by Vogel in 1873. While studying the spectral response of supposedly pure emulsions he noticed that a particular type of commercial plate had a high green sensitivity. Vogel found that this plate incorporated a dye, put there for the purpose of anti-halation (i.e the prevention of blurring by the reflection and dispersal of light), and that if the dye was washed out with alcohol the green sensitivity disappeared. He found that incorporating the magenta dye coralline in silver bromide emulsions produced a strong response in the green, and hence verified his assumption that the dye was responsible for the extra sensitivity. After the publication of Vogel's findings(3) there was considerable controversy in the photographic world, the concept of the transfer of the energy absorbed by a foreign substance to the silver halide being regarded by some as "contrary to the accepted laws of

molecular physics". However, confirmation by Becquerel and others of the effect soon led to the process being accepted as fact. Over the next thirty years or so dye sensitisation developed with the discovery of more and more sensitising dyes, though there was generally little knowledge of the true structures of dyes, or of the mechanisms responsible. West(4) has written an entertaining history of the progress in spectral sensitisation at this time.

Major progress in the field began with the introduction of efficiently sensitising cyanine dyes after the turn of the century. Though these dyes were not very stable to light, and consequently of little use as textile dyes, their high absorptivity and the relative purity with which they could be synthesised made them ideal for photographic sensitisation. Some of the properties of this class of dyes are discussed in section 2.3. Particularly important, as knowledge of the structure of the dyes grew after 1920, was the discovery that increasing the chain length in a symmetrical cyanine dye caused a spectral shift in solution of ~100nm to longer wavelengths per additional double bond. Since the position of the absorption band for a fixed chain length depends upon the structure of the heterocyclic nuclei, a great variety of absorptions and sensitisations were potentially available. In fact, it is now accepted that only the cyanines and related dyes (i.e polymethine dyes) can be regarded as efficient spectral sensitisers. The next few years saw increasing lengths of cyanine chains for sensitising into the infra-red. An innovation of this period was the discovery of the useful class of non-ionised dye sensitisers, the merocyanines. This important subclass of cyanines is also

discussed in section 2.3.

Although the search for efficient spectral sensitisers has continued unabated since the early days, much of the fundamental research undertaken into sensitisation since the last war has been aimed at definitively establishing the mechanism involved. Possible mechanisms are discussed in the next sub-section.

2.2.2 Electron Transfer vs Energy Transfer Mechanisms

It is universally accepted that the process of dye sensitisation involves the elevation of an electron to the conduction band of a semiconductor, when incorporated dye molecules are excited by incident light (assuming an n-type semiconductor). However, the mechanism by which the electron reaches the conduction band has been, and to some extent remains, incompletely understood. There are essentially two possible transfer mechanisms, represented by Figure 2.2. This energy level diagram shows schematically sensitisation by electron transfer (A) and by energy transfer (B). In terms of electron transfer theory one starts by reasoning that in the dark and even immediately after the absorption transition in the dye, the semiconductor and the dye retain their individuality (this is shown by the relatively minor spectral changes which accompany adsorption of a dye). The dye and semiconductor must therefore be separated by a potential barrier which prevents the two electron systems from completely merging. According to quantum theory there is a certain probability that an excited electron in the dye molecule at the same energy as a conduction level of the semiconductor will pass through the barrier into the

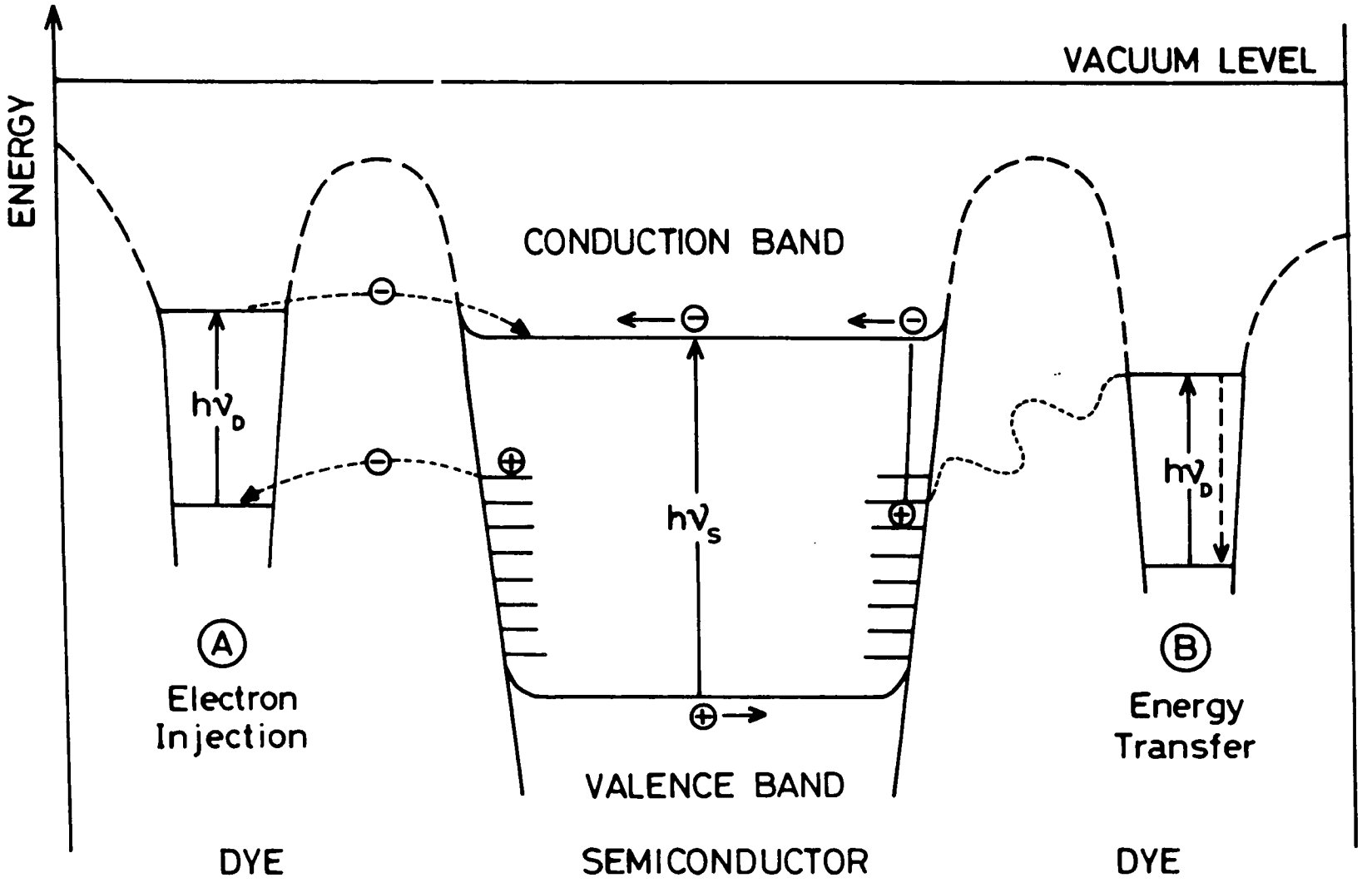

Figure 2.2 Energy levels of dyes and a semiconductor depicting spectral sensitisation (a) by electron transfer, (b) by energy transfer (after West(4)).

conduction band, leaving a dye positive hole in the form of a semioxidised dye free radical. By a corresponding tunnelling of an electron from a localised surface site in the semiconductor, into the partially empty ground state of the dye free radical, the original dye molecule is regenerated and a positive hole left trapped in the semiconductor surface. There is a certain probability that, if sufficient thermal energy is available, this surface hole may be liberated into the valence band of the semiconductor. The absorption spectrum of a dye adsorbed onto a semiconductor reproduces, in broadened and perhaps shifted form, the structure of the spectrum in solution. Hence the time for the sensitising interaction must exceed that of the absorption process $\sim 10^{-15}$ s. From the quenching of the fluorescence of sensitising dyes it has been deduced that the interaction must be complete in less than 10^{-9} s - from the degree of fluorescence quenching the interaction time has been estimated at 10^{-11} s(5). In Figure 2.2 it can be seen that the height of the barrier and, to some extent, its width is greater for the regeneration of the dye by the generation of a surface hole than for electron transfer into the conduction band. The dye free radical should therefore exist for some time after the sensitisation transfer, mooting the possibility of its detection. It is possible that in the near future the electron transfer process could be proved definitively using time-resolved picosecond laser spectroscopy to detect the radical(6).

In energy transfer (case B)(7), the dye resonates with a surface site in the semiconductor so that at the expense of the electronic excitation energy of the dye, an electron is

liberated from the surface site into the conduction band of the semiconductor, leaving a positive hole trapped in the surface. In this case, of course, the end result is the same as for the electron transfer theory - an electron in the semiconductor conduction band, the dye in its ground state, and an electron removed from a site at an intermediate level in the semiconductor. Evidence to support the theory of sensitisation by energy transfer was supplied by Kuhn and his associates in a series of ingenious experiments(8) using the LB film technique. They produced monolayers of cyanine dyes and transferred them intact onto silver bromide crystals, either directly on the surface or onto intermediate insulating layers of known thickness of cadmium arachidate. They demonstrated the excitation of fluorescence, the spectral sensitisation of photoconductivity, and the sensitisation of image formation in silver bromide, all with insulating layers between the dye and the halide to prevent electron transfer. The efficiency of the energy transfer through the layers fell off with increasing insulator thickness in accordance with theories of resonant transfer. The fact that they were able to demonstrate sensitisation effects with over 30nm of cadmium arachidate layers between the dye and the silver halide, showed that tunnelling of the excited electrons to the crystal was very unlikely during the lifetime of the excited dye.

Though Kuhn et al appear to have demonstrated the existence of an energy transfer mechanism, current opinion is mostly, though not unanimously, convinced of the possibility of electron transfer on energetic grounds. There is strong evidence to suggest that the excited levels of typical

sensitisers are equi-energetic with conduction levels in semiconductors, particularly in silver halides. This conviction results from experimental determination of the energy levels of dyes from spectral data and quantum-chemical calculations(9). These energy levels have been shown to be much higher than was thought when the energy transfer model was first proposed. It is now widely accepted that where dyes are directly adsorbed onto a crystal surface, the energy transfer model does not explain anything that cannot equally well be explained by direct electron transfer(10). There is also no evidence for energy transfer under these circumstances, while increasing confirmation of electron injection is found. For example, photoacoustic spectroscopy (11) has shown the transient presence of absorption spectra which suggest the presence of intermediate dye radicals.

2.2.3 Desensitisation

As shown in Figure 2.3 sensitisers and semiconductors may interact in a variety of possible ways, depending on the dye orbital energies relative to the band edges of the semiconductor. The relevant dye orbitals are shown as HOMOs (highest occupied molecular orbitals) and LUMOs (lowest unoccupied molecular orbitals). In the ground state the HOMO of a dye can release an electron (or trap a hole). Excitation of the dye results in the promotion of an electron from its HOMO to its LUMO, thus reversing, in the first excited singlet state, the ability of the dye orbitals to trap and release electrons. Therefore the dye acts as a spectral sensitiser if its LUMO is positioned above the bottom of the conduction band (case B). On the other hand,

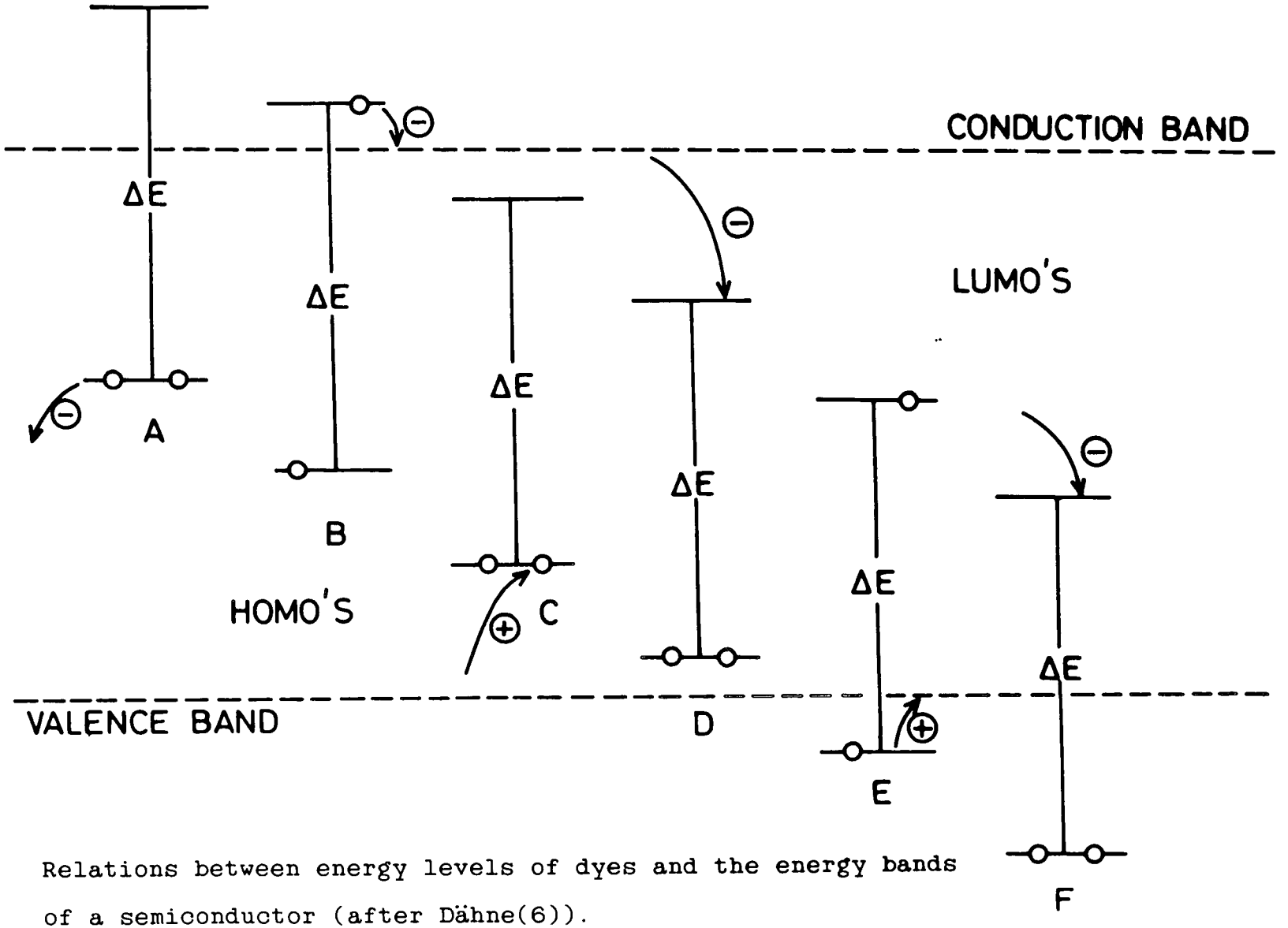

Figure 2.3 Relations between energy levels of dyes and the energy bands of a semiconductor (after Dähne(6)).

the dye in the excited state can trap an electron or release a photohole. Thus if the dye's HOMO is below the top of the valence band it acts (case E) as a desensitiser by hole injection. (In cases C and D the dye acts as a hole or electron trap, and in cases A and F as an electron or hole injector, in all four cases when the dye is in the ground state). One implication of this scheme for n-type semiconductors is that the lower the location of the conduction band, the easier will be the sensitisation of the transfer of an electron from the dye to the semiconductor. Also, the lower the valence band, the less likely are desensitisation effects from dye photohole injection. This is the case with zinc oxide, which can be sensitised by any common dye, whereas desensitisation is nearly impossible because of its low energy bands(6).

It is interesting to note that the semiconducting properties of organic dyes, investigated by Meier and others(9), can be applied to adsorbed layers. It has been proposed that a sensitising dye/semiconductor can be considered as a solid state diode, i.e the adsorption of a dye onto a semiconductor surface results in a rapid equalisation of Fermi levels. Many of the dyes used to sensitise n-type semiconductors have themselves been characterised as p-type semiconductors(9), suggesting the formation of a type of pn-junction structure. This idea is supported by the fact that good sensitisers of n-type materials have been shown to become desensitisers on some p-type materials, and vice versa(6).

2.2.4 Aggregation Effects

Aggregation effects have already been briefly mentioned in section 2.1. The tendency of dyes to form dimers and higher polymers has been of considerable practical and theoretical interest, since these will influence the absorption and hence the sensitising properties of a dye. The most important effect in terms of sensitisation is the formation of 'J' bands (named after E.E.Jelley who published the first description of them(12)). These are strong bands in solution spectra, red-shifted from the molecular absorption, and of unparalled sharpness for organic materials at room temperature. They also appear in the spectra of a wide variety of adsorbed cyanines and some adsorbed merocyanines. These bands have been of particular value in sensitisation for colour photography, allowing sharp differentiation between red and green. They are attributed to the formation of molecular aggregates held together by van der Waals forces, and seem to be strengthened with increasing length of the conjugated chain in cyanines, i.e the delocalisation of π-electrons(6). They are also influenced by the crystal structure onto which the dye is adsorbed, since this influences the arrangement of and hence the interactions between dye molecules. These bands are not essential for strong sensitisation, and indeed the dye is often a less efficient sensitiser than when absorbing molecularly. However, the presence of aggregates in molecular crystals of dyes are expected to yield interesting results in the fields of nonlinear optics and organic conduction(6).

2.5.1 Sensitisation of Semiconductors

Because of the photochemical decomposition inherently associated with the photographic effect in silver halide crystals, an alternative semiconductor system will allow a clearer determination of the photoeffects involved in dye sensitisation. Terenin and later Akimov(2) have observed the sensitisation by dyes of photoeffects in bound powders of zinc, cadmium and lead oxides, and in cadmium and zinc sulphides(13). ZnO in particular has been studied in some detail in connection with its uses in electrophotographic systems. Figure 2.4 reproduces some of Akimov's results for the enhancement of photoconductivity in ZnO by the incorporation of various sublimed dyes. One particularly interesting result reported in this work was that for the optimum sensitisation effects shown in Figure 2.4. It was found that the coverage of the semiconductor surface corresponded to ~40% of one monolayer(13). If this value were critical, the fine control available through the LB film technique should allow accurate optimisation of dye deposition. It was also reported that the presence of at least some photoelectric sensitivity to longwave light by the undyed semiconductor was required for the subsequent detection of the sensitisation effect. It was suggested that this was indicative of the need to have electron trapping levels at the semiconductor surface to participate in the sensitisation process. Charge transfer via these traps allows the regeneration of the dye molecule into its ground state.

Heiland(14,15) has undertaken measurements of the sensitisation effect of dye sublimated in ultrahigh vacuum

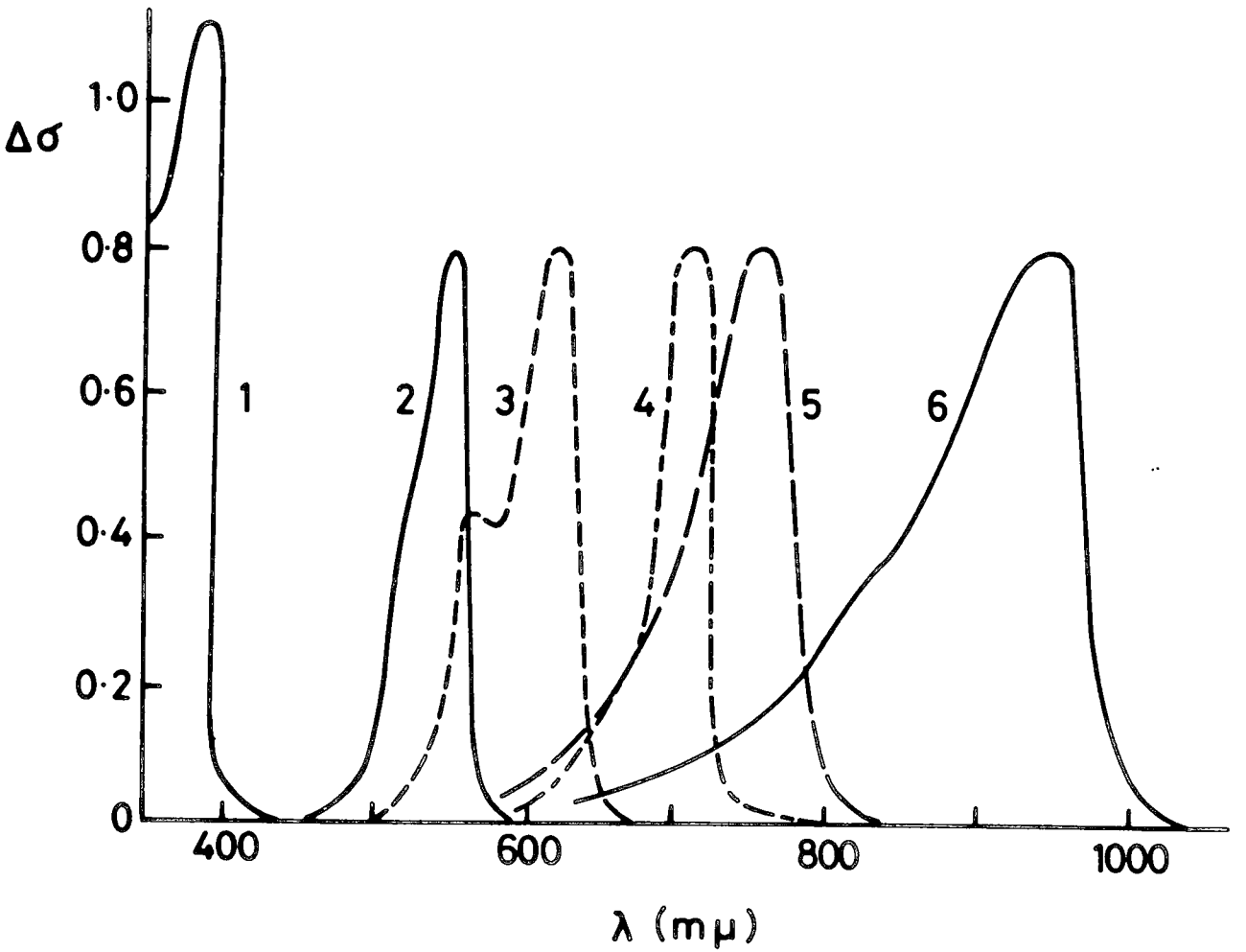

Figure 2.4 Spectral distribution of the photoconductivity of ZnO powder. 1) Unsensitised; dyed with: 2) erythrosine; 3) pinacyanol; 4) cryptocyanine; 5) neocyanine; 6) xenocyanine (after Akimov(2)).

onto single crystal ZnO cleaned by annealing. This eliminated some of the complications associated with binder systems, and allowed charge transfer in the dye and crystal to be studied by measurements of the electric field normal to the surface in conjunction with the sensitised photoconductivity. This, and somewhat similar studies by other workers(16,17), appeared to confirm the electron transfer theory. Another technique allowing a well-defined surface preparation is the technique developed by Gerischer(18) of immersing a ZnO electrode into a galvanic cell and adding dye to the solution. This technique has been followed and adapted by a number of workers for SnO_2 and TiO_2, as well as ZnO(19-21). The fabrication of a photovoltaic cell based on a dye-ZnO sandwich structure has been reported(22). Dyes adsorbed onto anthracene and other molecular crystals have also been shown to have a sensitising effect on photoconductivity(23).

2.3 SENSITISING DYES

The properties conferred by a sensitising dye are clearly dependent upon the absorption of the dye itself. The relationships between the chemistry and absorption of dyes are a highly complicated subject, discussed briefly in section 2.1. However, the dyes used in practice for sensitisation are all from a broad class known as polymethine dyes, the largest subclass of which are the cyanines. Polymethine dyes contain two or three nuclei connected by conjugated chains of carbon atoms. This section briefly reviews some of the properties of cyanine and merocyanine dyes.

2.3.1 Cyanines

As has already been shown, the cyanines are resonance hybrids of the general form

$$-\ddot{N}-(C=C)_n-C=\overset{+}{N}- \rightleftharpoons -\overset{+}{N}=C-(C=C)_n-\ddot{N}-$$

where n is an odd positive integer. In most of these dyes the nitrogen atoms and the terminal carbon atoms of the chromophore are part of a heterocyclic ring which may take a number of forms. By varying the conjugated chain length the absorption characteristics of these dyes have been extended throughout the visible spectrum and into the near infra-red. These are the 'classical' dyes for the sensitisation of photoeffects, and their development and syntheses have been comprehensively reviewed(24). These dyes are generally insoluble in non-polar solvents, but sparingly soluble in water. They have poor stability to light, this instability increasing with conjugated chain length. Most of the work carried out by Kuhn et al(6) used cyanine dyes with long aliphatic substitutions which rendered them soluble in chloroform and suitable for incorporation into LB films.

2.3.2 Merocyanines

The merocyanines are a class of non-ionic polymethine dyes of the general form

$$-N-(C=C)_n-C=O \rightleftharpoons -\overset{+}{N}=C-(C=C)_n-\overset{-}{O}$$

where in this case n is an even positive integer. They are resonance hybrids between a covalent and a charge separated dipolar form, and generally have a low solubility in water and other polar solvents. They are somewhat soluble in non-polar solvents, in contrast with the cyanines. The optical properties of many merocyanines are

well-documented(25). The low solubility of these dyes in water, even in a form unsubstituted with aliphatic chains, suggests that they may fulfil the first requirement of a material that is to be used as an LB film, i.e stability on the water surface. A selection of merocyanine dyes were studied in the course of this work (Chapter 6), with the specific aim of isolating a merocyanine without long substitutions to act as an LB film. It was hoped that the omission of the aliphatic regions would give a more stable film than those obtained to date.

2.4 DYES AS LANGMUIR-BLODGETT FILMS

The technology of LB films is reviewed more fully in Chapter 4, but this section briefly summarises some of the research which has been carried out by other workers utilising the technique with dyes. In fact the growth of interest in these films in recent years can be traced to the start of a series of elegant experiments involving dyes by Kuhn et al. They were looking for a novel method of studying experimentally the distance dependence of energy transfer from an excited donor molecule to a nearby acceptor molecule. The idea was to physically separate donor and acceptor by a well defined distance, and then to examine the fluorescence of the donor or acceptor as a function of the separation. This work was initially done with layers of adsorbed dyes separated by fatty acid monolayers(26), but with the development of improved techniques monolayers of dyes themselves were incorporated into these systems(8). Various energy transfer processes involving dyes have been demonstrated(8,27), including the work with silver halides

mentioned in section 2.2. A striking example of the effectiveness of the technique is demonstrated by the systems shown in Figure 2.5(8). S is a sensitising dye and A an acceptor dye, i.e in this case S absorbs in the ultra-violet and fluoresces in the blue, A absorbs in the blue and fluoresces in the yellow. If the system is irradiated with UV light with a sufficiently large distance (arachidic acid monolayers) between S and A the blue fluorescence of S appears since A does not absorb the UV radiation (case 2). If, however, there is only a very small distance between them ($\lesssim 100\text{Å}$), the excitation energy of S is transferred to A and yellow fluorescence appears (case 1). The energy transfer process is confirmed by case 3 where no fluorescence is observed. Mobius and co-workers are continuing this fundamental work(28-32), with the ambitious aim of constructing artificial organised aggregates (organisates) which could simulate some of the complex systems existing in nature(33).

Sugi et al have extended the work of Kuhn by studying photoelectrical effects in systems incorporating LB films of dyes. They have demonstrated a marked anisotropy in the photoconductivity of dye LB films, with that in the plane of the film being 10^3 to 10^4 times larger than that normal to the plane(34,35). By varying a single atom in the chromophore structure of merocyanine dyes they have shown that the lateral photoconductivity increases with the degree of aggregation occurring between dye molecules, evinced by the increased tendency for the dyes containing heavier atoms to exhibit J-band absorption. This work is continuing with the aim of optimising the necessary criteria to produce an

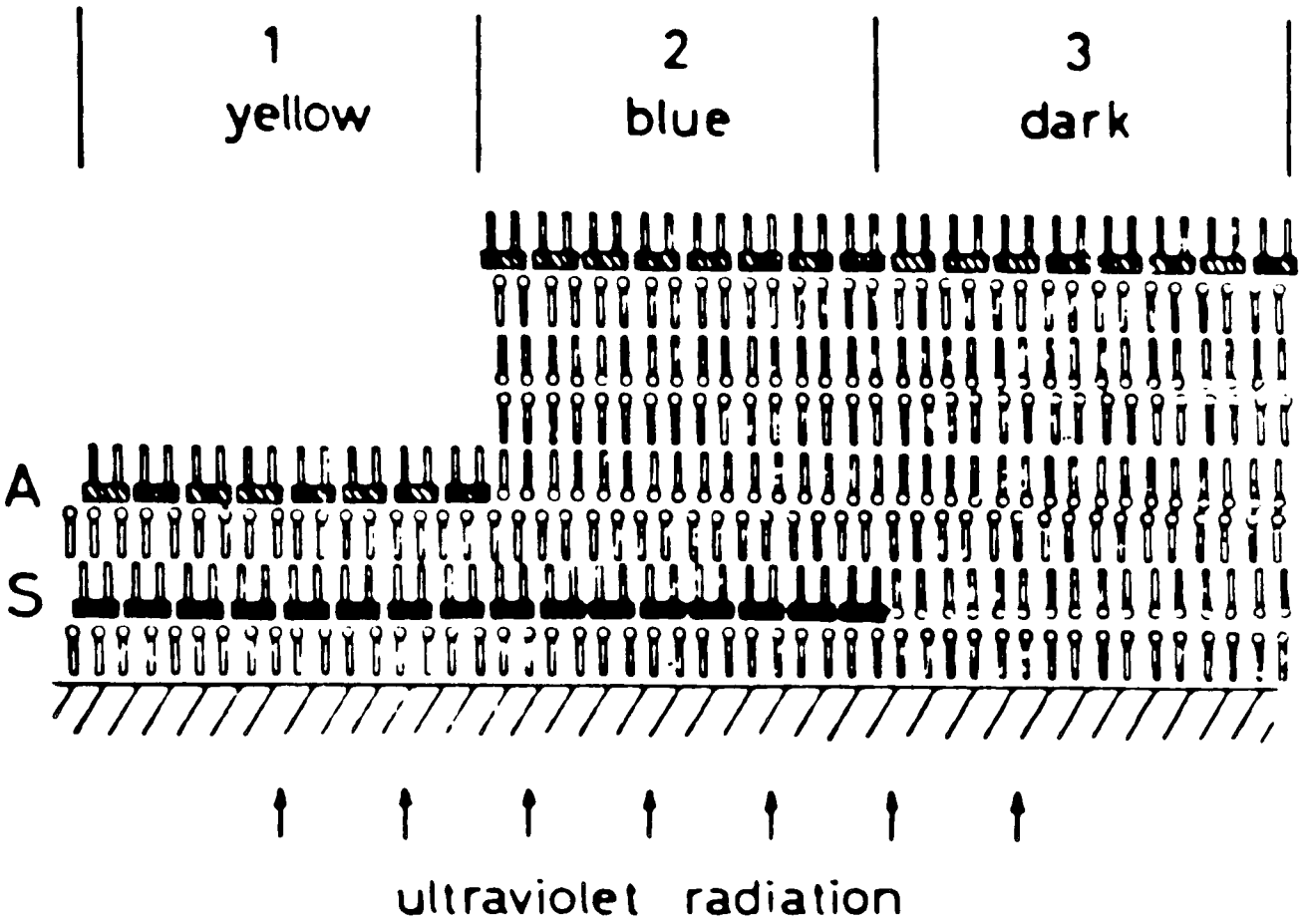

Figure 2.5 Demonstration of energy transfer by the fluorescence of LB film structures incorporating dyes (after Kuhn et al(8)).

efficient organic photovoltaic cell(36,37).

Recent work with dye LB films has included studies of their effects upon surface plasmon resonance of metallic substrates(38). The coupling which occurs between the dye excitons and the surface plasmons suggests a potential for application in the development of transducers based upon optical fibres and related systems.

Characterisation and development of stable phthalocyanine dyes in LB film form is also continuing(39). Utilisation of the insulating properties of these films is discussed later in this thesis.

2.5 SUMMARY

This chapter has discussed the origins of the optical properties of dyes, and the physical basis for the process of dye sensitisation. Past work has suggested that dyes in LB film form may be used in this process, though most dyes used have required the substitution of long hydrocarbon chains onto the molecules. The results of the characterisation and use of an unsubstituted merocyanine dye in LB film form are presented in Chapter 6, using the LB film technology discussed in Chapter 4.

CHAPTER 3

ELECTROLUMINESCENT DEVICES

Electroluminescence (EL) is the direct conversion of electrical energy into light, as distinct from other possible energy to light processes such as thermoluminescence. This chapter discusses the physics of the processes involved in EL and some of the structures used to achieve it. The account of the theory of Schottky barriers and thin-MIS diode structures is given in some detail, since it was these structures that were studied in this research.

3.1 INTRODUCTION

In general, luminescence is the emission of light by a material when supplied with energy. The method of excitation of the material distinguishes the types of luminescence - (a) photoluminescence, where excitation is by light or X-rays; (b) cathodoluminescence, by fast electrons; (c) radioluminescence, by other fast particles or high energy radiation; (d) thermoluminescence, by heating effects; and (e) electroluminescence, by d.c or a.c electrical fields. EL, as studied here, has spectral characteristics of relatively narrow bandwidth. Of particular interest are devices emitting visible light, i.e in the wavelength range 400nm to 700nm. EL requires that a system must be capable of being excited electrically, and that it relaxes from its excited state via processes some of which are radiative, usually electron-hole recombination. In the following

section the processes of excitation and recombination are discussed in general terms.

3.2 EXCITATION AND RECOMBINATION PROCESSES

3.2.1 Excitation

This section deals first with the increase in the free carrier population in semiconductors by electrical excitation processes. Four processes are considered: avalanche multiplication, internal field emission, minority carrier injection and exciton formation.

Avalanche multiplication occurs in rectifying structures such as p-n junctions and Schottky barriers under strong reverse bias. At low reverse fields ($\lesssim 10^3 Vm^{-1}$) electrons have average energies no higher than the equilibrium value kT. However, at high fields ($\gtrsim 10^7 Vm^{-1}$) electrons have much higher energies and are termed 'hot' (a reflection of the high temperatures needed to attain such energies thermally). These hot electrons can create electron-hole pairs by impact ionisation of lattice or impurity atoms, and these excited carriers can themselves create further pairs, leading to an avalanche effect. If breakdown does not occur, the increased population of electrons and holes in the depletion region will result in recombination. An alternative high field effect in Schottky barriers is internal field emission, where free carriers are generated by field enhanced quantum mechanical tunnelling. At a sufficiently high reverse bias, the degree of band bending will reduce the spatial separation between bound electrons and the conduction band to a tunnellable distance. Electrons may reach the conduction band from the metal, from impurity atoms, or even from the

semiconductor valence band (Zener effect), resulting again in an increased population of free carriers in the depletion region. These two high field effects are usually complementary, the dominance of one being a function of the system used.

It is normally preferable to be able to operate devices at lower fields, and this can be achieved with minority carrier injection. When, for example, a p-n junction is forward biased the potential barrier between the two semiconductor regions is lowered and a current will flow. One component of this current will be the diffusion of electrons into the p-type region and of holes into the n-type region, where they become minority carriers. These may combine with the majority carriers, possibly radiatively. Alternative current mechanisms and other factors complicate this simplistic view of minority carrier injection; furthermore the p-n homojunction cannot be fabricated with some semiconductors and MIS diodes are used to achieve injection EL. As this restriction applies to materials studied here, minority carrier injection in MIS structures is discussed in detail in 3.5.

An exciton is formed by a free electron and a free hole becoming bound together in a hydrogenic orbit as a result of the Coulombic force acting between them. Electrons can enter excitonic states through a number of excitation processes. Excitons have slightly lower energies than free carriers and exist in the forbidden gap just below the conduction band. They can move through the crystal lattice without a net flow of current as their energy is transferred from one atom to the next. If an exciton becomes bound to an impurity centre,

the high localisation of the electron will extend its wave function in momentum space. This increases the probability of phonon-free recombination in indirect gap materials at near bandgap energies (see 3.2.2.), and is of significance to the EL efficiency of nitrogen doped GaP, for instance.

3.2.2. Radiative Recombination

There are also a number of processes by which an excited carrier may lose its excess energy. Some of these are radiative processes desirable for EL; in direct competition are non-radiative processes. The predominance of the first over the second is necessary for efficient EL. Those methods of recombination resulting in the emission of light are depicted by Figure 3.1.

Interband recombination (a) will occur if a conduction electron encounters a valence hole, producing a photon of energy $\sim E_g$. Some spectral broadening occurs due to the thermal distribution of carriers, but higher energy emission (b,c) is limited because radiative decay times are much longer than the lattice scattering times of the hot carriers (an exception is at low temperatures and at very high excitation levels such as for avalanche multiplication). The relative position in momentum space of the conduction band minimum and valence band maximum dictate whether these transitions are direct or indirect. Transitions between bands can only occur if both momentum and energy are conserved. Hence an indirect transition is less likely as the emission of a number of phonons with specific energy is required (i.e a change in momentum by interaction with lattice vibrations). Note, however, that near bandgap

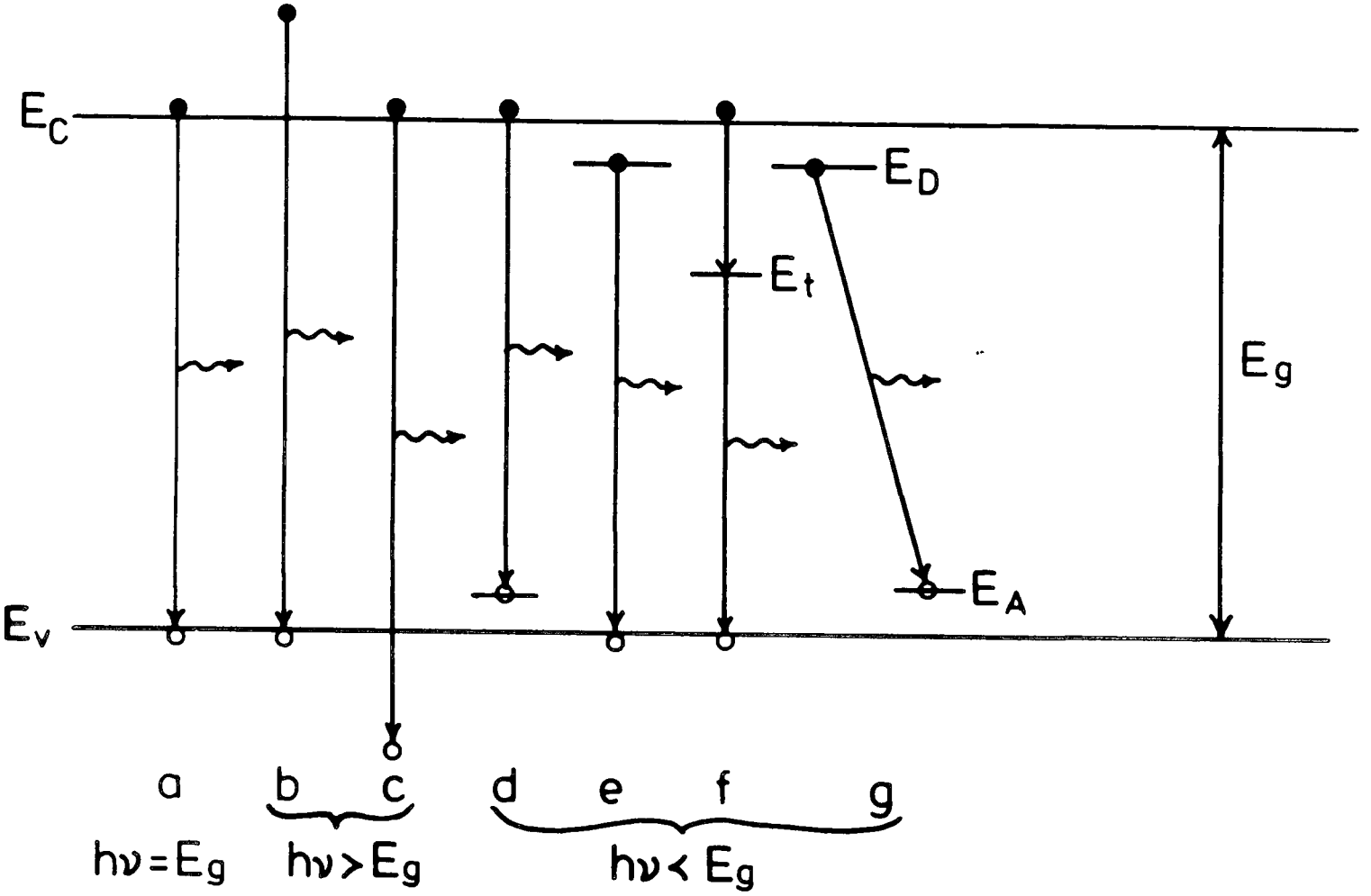

Figure 3.1 Radiative recombination mechanisms in a semiconductor.

emission can be obtained from a bound exciton without this limitation, since the binding impurity can be involved in conserving momentum.

Impurity levels in the forbidden gap can give EL from either conduction band to acceptor (d) or donor to valence band (e) transitions. To act as efficient radiative recombination centres they must be fairly deep in the gap if thermal activation of the captured carrier is not to dominate. The use of deep centres for visible EL (f) is limited to wide bandgap semiconductors since the energies of emitted photons are clearly significantly less than for interband recombination.

Finally, the Coulombic force between donors and acceptors in highly doped semiconductors can cause them to associate into pairs, between which recombination can occur (g). Again this process is in competition with thermal activation, and is also limited by the spatial separation of the pair.

3.2.3. Non-Radiative Recombination

Clearly the recombination of carriers without the production of light is undesirable in EL devices. However, certain processes do have this property. In Auger recombination an excited electron dropping from the conduction band to a lower energy state can impart its energy to another conduction band electron, promoting it to a higher level in the band. This second electron merely dissipates its excess energy as heat as it returns to the band bottom. Other combinations of carriers may be involved in this process. An electron may also lose energy by multiphonon

emission. As phonon energies are small in comparison to bandgaps this is only probable where impurity levels break the transition into smaller stages. Finally, the presence of a large number of defect states at the semiconductor surface can significantly increase losses in efficient light output.

3.3. ELECTROLUMINESCENT EFFICIENCY

There are a number of ways of defining the efficiency of an EL device. Different methods are relevant to the characterisation of a system, the assessment of a practical device and the applicability of a device to a particular requirement. This section discusses each of these methods.

3.3.1. Internal Quantum Efficiency

The internal quantum efficiency of a system (n_i), also known as the light generation efficiency, is a measure of the ratio of radiative to non-radiative recombination. Since the probabilities of recombinations are given by

$$P_r = 1/t_r \qquad (3.1)$$

and $$P_{nr} = 1/t_{nr} \qquad (3.2)$$

where t_r and t_{nr} are the radiative and non-radiative lifetimes, it follows that

$$n_i = 1/(1 + t_r/t_{nr}) \qquad (3.3)$$

This is the efficiency of the luminescent process itself and may also be defined as the number of photons generated within the device per electron supplied.

3.3.2. External Quantum Efficiency

The overall efficiency of a device is further limited by light extraction difficulties resulting from absorption and

internal reflection. Near bandgap light in particular will be strongly absorbed on its way to the semiconductor surface, and with devices fabricated on strongly absorbing substrates, such as the ZnSeS-GaAs system used here, light can only escape upwards. For MS and MIS structures, further absorption will occur in the top electrode, resulting in a net attenuation $\exp\{-(\alpha_s d_s + \alpha_m d_m)\}$, where d_s and d_m are the distances traversed in the semiconductor and metal, and α_s and α_m their absorption coefficients (themselves wavelength dependent). Since the semiconductor will always have a refractive index (n) greater than that of air ($n_{air} = 1$), light will be partially reflected at the interface with a reflection coefficient

$$R = (n-1)^2/(n+1)^2 \qquad (3.4)$$

Also light incident on the surface at an angle greater than the critical angle, $\theta_c = \sin^{-1}(1/n)$, will be totally reflected. These factors together give the light extraction efficiency

$$n_{ext} = (1-R)\,(1-\cos\theta_c)\exp\{-(\alpha_s d_s + \alpha_m d_m)\} \qquad (3.5)$$

Note that reflection effects alone limit the light extraction efficiency of a simple MIS LED to <7% for a typical semiconductor with n = 2.5. This can be improved with index matching encapsulents and optimised device geometry. A final factor is of course that the minority carrier injection ratio (γ) limits the number of carriers actually available for recombination from those supplied. Hence, an external quantum efficiency can be defined

$$n_e = n_i\, n_{ext}\, \gamma \qquad (3.6)$$

3.3.3. Power Conversion Efficiency

In practice, it is easiest to measure efficiency as the total energy of the emitted light as a function of the electrical energy supplied to the device. The radiant flux can be measured with a suitable calibrated photodetector and compared with that of a device of known efficiency. This efficiency would be equal to the quantum efficiency if the bias applied to the device multiplied by the electronic charge (e) was equal to the energy of the emitted photons - in practice, the voltage is also dropped elsewhere (e.g at the interfacial barrier in the ZnSeS-GaAs system). Power conversion efficiencies have been measured in this work, but it is possible to estimate both external and internal quantum efficiencies from these.

3.3.4. Luminous Efficiency

If a device is to be used as a visible LED the sensitivity of the human eye must be considered. This is not uniform, but varies with wavelength as shown in Figure 3.2, with a maximum at 556 nm. If the spectral emission of a device is significant at wavelengths where eye sensitivity changes rapidly, the output and eye response should be integrated together to give the luminous efficiency in lumens per watt (maximum eye sensitivity = 680 lmW^{-1}). Similar considerations apply when matching an LED to a photodetector.

The following sections describe EL device structures. The p-n homojunction used to achieve minority carrier injection in most commercial III-V devices is discussed first. There follows a more detailed consideration of

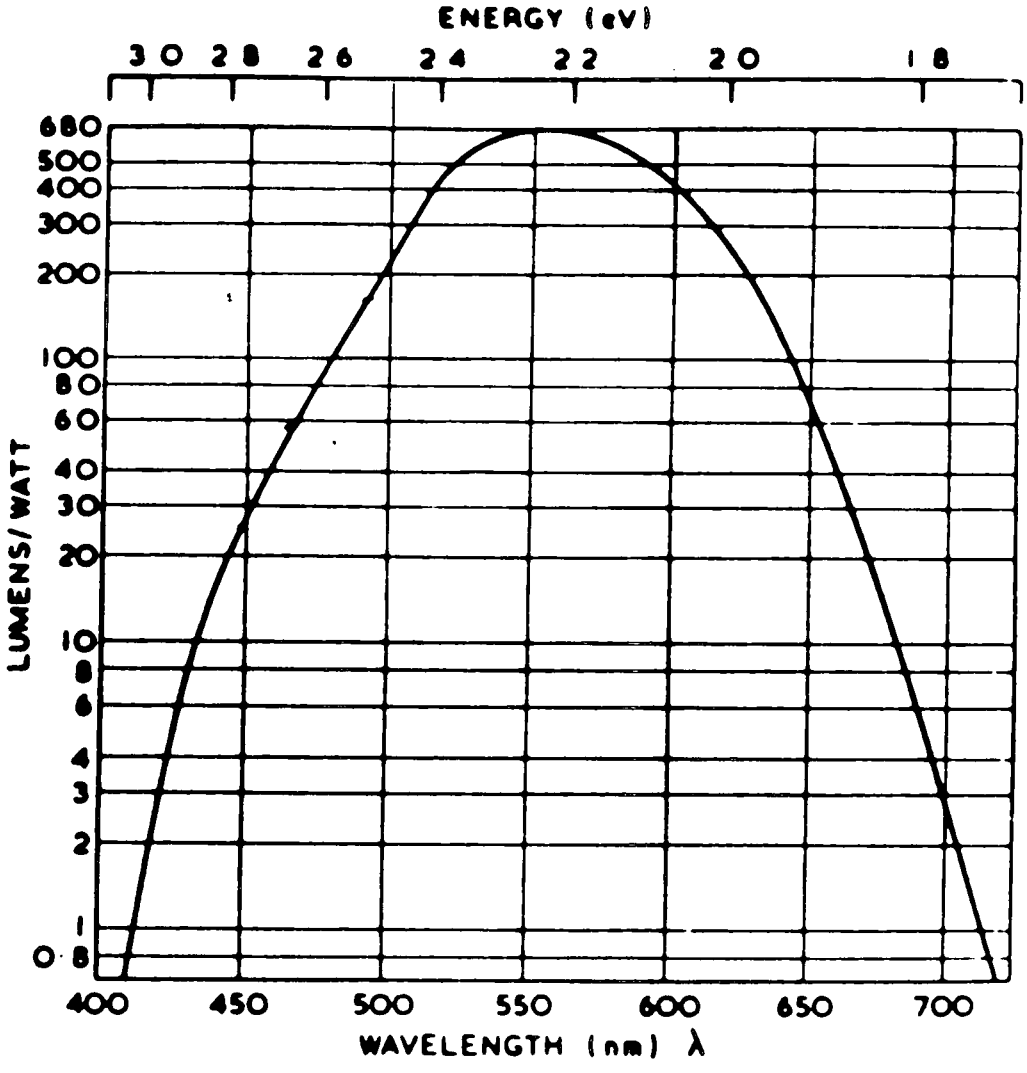

Figure 3.2 Luminous efficiency of the human eye vs incident light wavelength.

near-ideal Schottky barriers and practical MIS diodes as used in this work. Finally some alternative EL device structures are summarised.

3.4 THE p-n HOMOJUNCTION

When p-type and n-type materials are brought together to form a p-n junction, minority carriers will flow from each of the regions until their Fermi levels are aligned. The charge on the impurities thus ionised in the region of the junction will cause an electrostatic diffusion potential V_{do}, as shown in Figure 3.3(a). The region depleted of majority carriers (the depletion region W) is of much higher resistivity than the bulk of the semiconductor; consequently, any applied bias will be primarily dropped there. It can be shown that

$$V_{do} = \ln(n_n/n_p)kT/e$$
$$= \ln(p_p/p_n)kT/e \qquad (3.7)$$

where n_n is the electron concentration in the n-type region etc. Typically $V_{do} \sim 1V$ and $w \sim 1\mu m$. Reverse bias can create large electric fields in the depletion region leading to avalanche multiplication and internal field emission (see 3.2.1). More significant, however, is forward bias which lowers the potential barrier by the applied voltage V, as shown in Figure 3.3(b), and causes current to flow. The diffusion current, J_d, is the injection of minority carriers according to the Shockley equation

$$J_d = e(D_n n_{po}/L_n + D_p p_{no}/L_p)\{\exp(eV/kT) - 1\} \qquad (3.8)$$

where D_n and D_p are the carrier diffusion coefficients, L_n and L_p the carrier diffusion lengths, n_{po} and p_{po} the equilibrium minority carrier concentrations, and $V = V_{do} - V_d$. For practical EL devices the carrier component giving

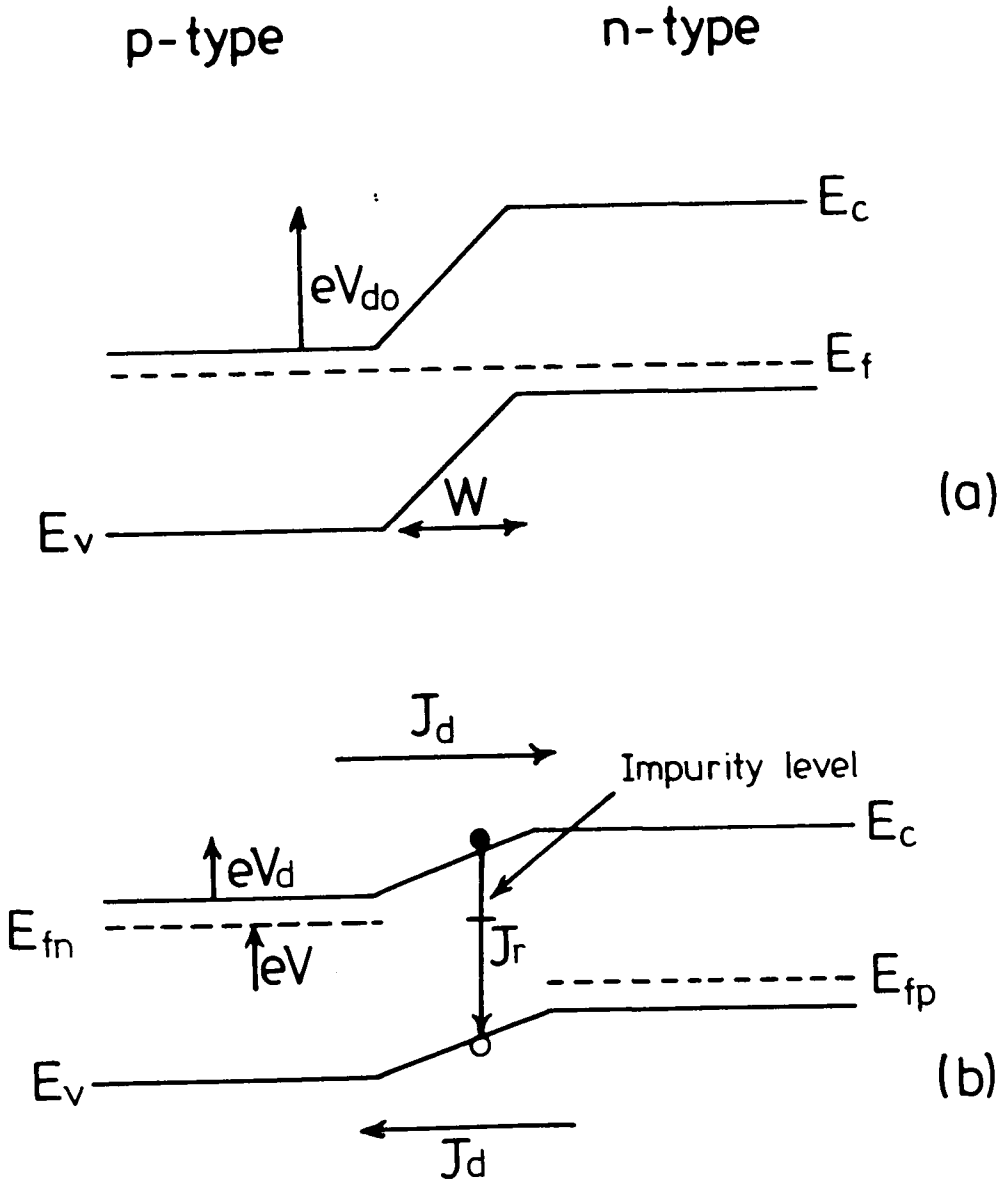

Figure 3.3 Schematic diagram of a p-n homojunction (a) in equilibrium and (b) under forward bias.

the most efficient radiative recombination will be made to dominate. Practical p-n homojunction LEDs can achieve values of γ (see 3.3.2) approaching unity, hence their appeal.

An unwelcome contribution to the current flow is due to non-radiative recombination via impurity levels around the depletion region. This is given by

$$J_r \propto \exp(eV/nkT) \qquad (3.9)$$

where n is normally between 1 and 2. This loss mechanism is minimised by careful control of impurities during crystal growth. Other deviations from equation (3.8) are caused by interband tunnelling, the 'high injection condition' (occurs when the field across the semiconductor bulk is not negligible), and surface leakage. These are generally insignificant at the operating voltages of conventional p-n junction LEDs.

3.5 THE NEAR-IDEAL SCHOTTKY BARRIER

This section considers the use of Schottky diodes as EL structures, firstly the ideal case of an abrupt metal-semiconductor interface, and then with allowance for the presence of an interfacial region. The electrical properties of such devices (conductivity, capacitance, photoresponse) are then discussed.

3.5.1 The Ideal Schottky Barrier

Figure 3.4a shows a band diagram for the ideal case of a metal in contact with an n-type semiconductor. For this case, where the metal work function (ϕ_m) is greater than the semiconductor electron affinity (χ_s), charge has flowed from the semiconductor to the metal to align their Fermi levels in

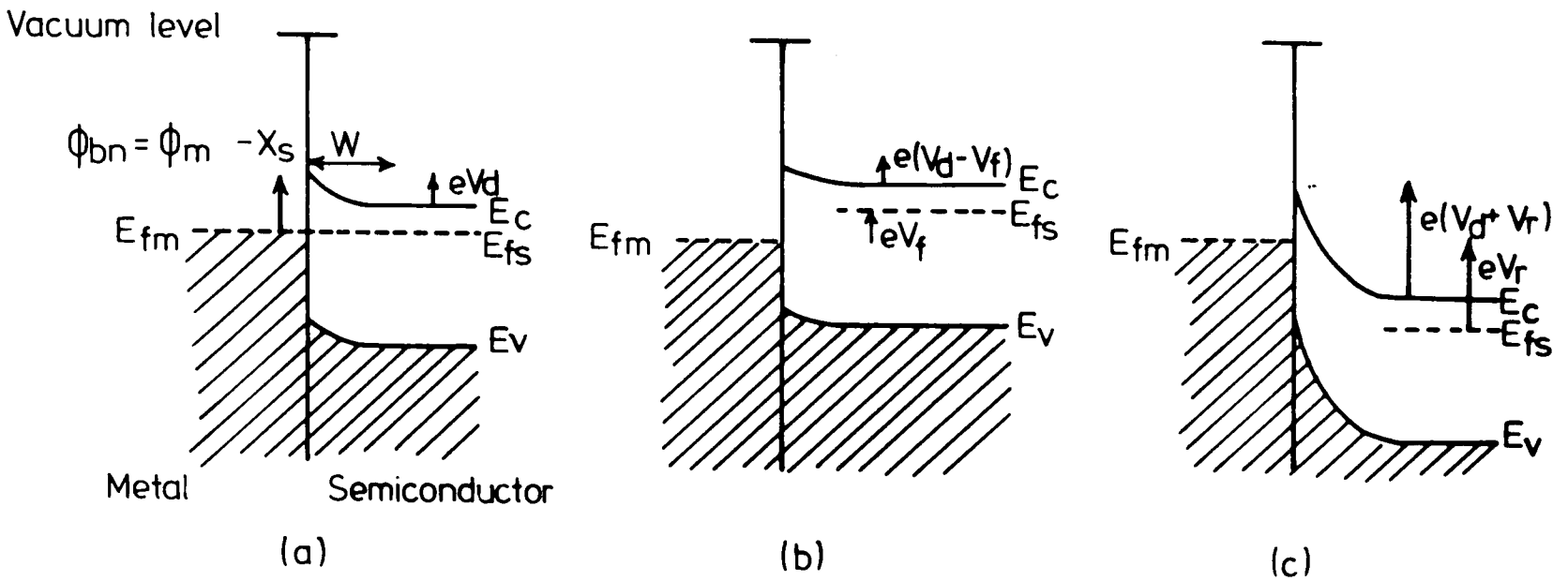

Figure 3.4 Energy band diagram of an ideal Schottky barrier (a) in equilibrium, (b) under forward bias and (c) under reverse bias.

equilibrium. The resultant build up of charge at the metal surface is balanced by a distributed space charge region of width w in the semiconductor (also known as the depletion region). A barrier of height

$$\phi_{bn} = \phi_m - \chi_s \qquad (3.10)$$

exists at the junction, though the barrier to electrons in the semiconductor conduction band is only V_d, the diffusion voltage (i.e the degree of band bending). Figures 3.4b and 3.4c show the band diagrams for forward and reverse bias. In reverse bias EL may be produced by avalanche multiplication or internal field emission, as described in 3.2.1. In forward bias the band bending is reduced and a current flows. Minority carriers (in this case holes) injected into the semiconductor are a source of EL via radiative recombination with majority carriers. A typical minority carrier injection ratio (γ) for such a structure is $\sim 10^{-4}$, insufficient for an efficient EL device. However, the relative ease of fabrication of this device compared with p-n junctions, and indeed the lack of viable p-n junctions with II-VI semiconductors, make this commercially attractive. And significant improvements in γ are possible, as shown in 3.6.

Equation 3.10, known as the Schottky-Mott relation(1,2), is limited by the assumption that surface contributions to ϕ_m and χ_s are not altered by their intimate contact. Interface states, most simply pictured as the 'dangling bond' of an unpaired electron associated with a surface atom, cause the experimentally observed deviation of ϕ_{bn} from the linear relationship to ϕ_m of equation 3.10. Bardeen(3) proposed that the charge localised in these intrinsic surface states, and extrinsic states due to defects and impurities, could be

dominant in the formation of the semiconductor depletion region. Figure 3.5a shows this case where band bending occurs before the metal and semiconductor are in equilibrium, due to localised charge in a high density of surface states. When brought together in 3.5b the movement of charge required to align the Fermi levels is accomodated by the surface states, giving a barrier height

$$\phi_{bn} = E_g - \phi_o \qquad (3.11)$$

as the density of surface states, $D_s \rightarrow \infty$. The surface semiconductor Fermi level remains unchanged with respect to its conduction and valence band edges - this is Fermi level 'pinning'. ϕ_o is defined as the level to which the surface states of the semiconductor are filled to achieve a neutral surface, E_g is the semiconductor bandgap. In this case the barrier height is independent of the metal work function, though in general it is dependent to some extent on both interfacial charge and work function.

The Bardeen model, extended in the next section to allow for the necessary presence of some interfacial layer, has been found to be satisfactory for the analysis of most practical Schottky diodes. However, many extensions and revisions to this theory have been proposed, and the reader is referred to some of these(4,5,6,7). In particular these draw attention to the effects of surface chemical reactions on barrier formation.

3.5.2 Interfacial Layer Effects

The near-ideal Schottky barrier is one in which a very thin insulating region exists between the metal and semiconductor. Its presence is required for analysis of the

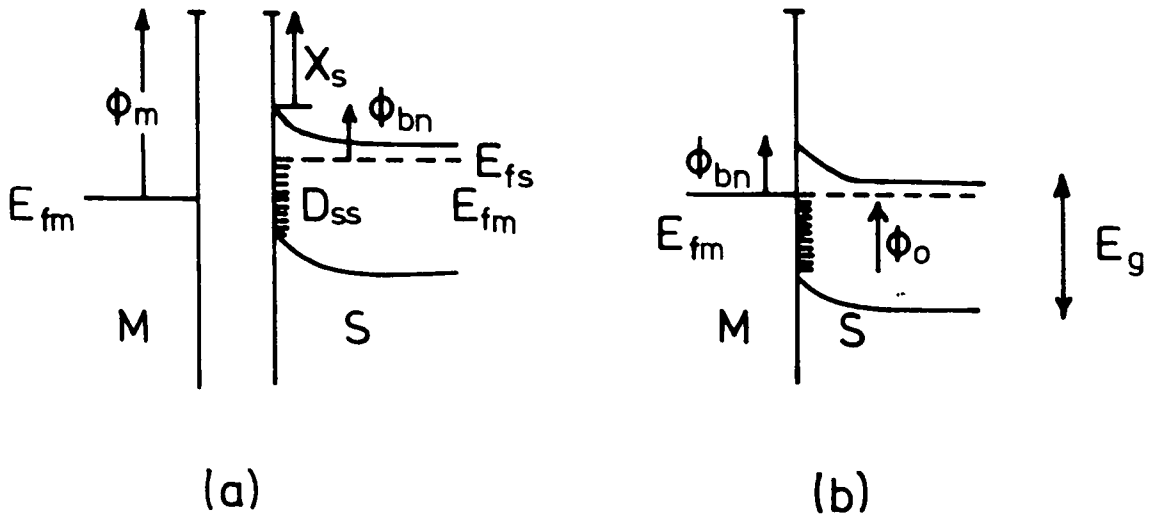

Figure 3.5 Energy band diagram depicting the formation of a Schottky barrier with a high surface state density. (a) Metal and semiconductor separate, (b)in equilibrium.

Bardeen model since otherwise the metal would act as if to screen the effect of the surface states. In the analysis by Cowley and Sze(8) it is assumed to be capable of withstanding a potential, but transparent to quantum mechanical tunnelling of electrons and generally of negligible effect upon the current transport properties of the diode. By also assuming that interface states were only present at the surface of the semiconductor, and that they were evenly distributed across the energy gap, they derived an approximate equation

$$\phi_{bn} \sim K(\phi_m - \chi_s) + (1 - K)(E_g - \phi_o) - \Delta\phi_{bn} \qquad (3.12)$$

where $K = \varepsilon_i/(\varepsilon_i + e\delta D_s)$

Here ε_i and δ are the permittivity and thickness of the interfacial layer, and $\Delta\phi_{bn}$ the barrier image force lowering due to the Schottky effect (see Figure 3.6a). This lowering effect(9) is due to the attraction between an electron away from the metal surface and the positive charge it induces at that surface. A maximum in the Schottky barrier potential is hence created a small distance from the metal-semiconductor interface. This is only a small effect (~0.04eV), but being bias dependent the change in barrier height will alter the exponentially related current characteristics (see section 3.5.3). Note that in the limits $D_s \rightarrow 0$ and $D_s \rightarrow \infty$, equation 3.12 gives the Schottky-Mott relation and the Bardeen equation respectively. If a negligible proportion of any applied bias V is assumed to be dropped across the insulating layer, V will contribute wholly to band bending in the semiconductor, as in the forward bias case shown in Figure 3.6b. Hence at the surface the conduction and valence band edges will not be shifted relative to the metal Fermi level. The amount of charge stored in the interface states,

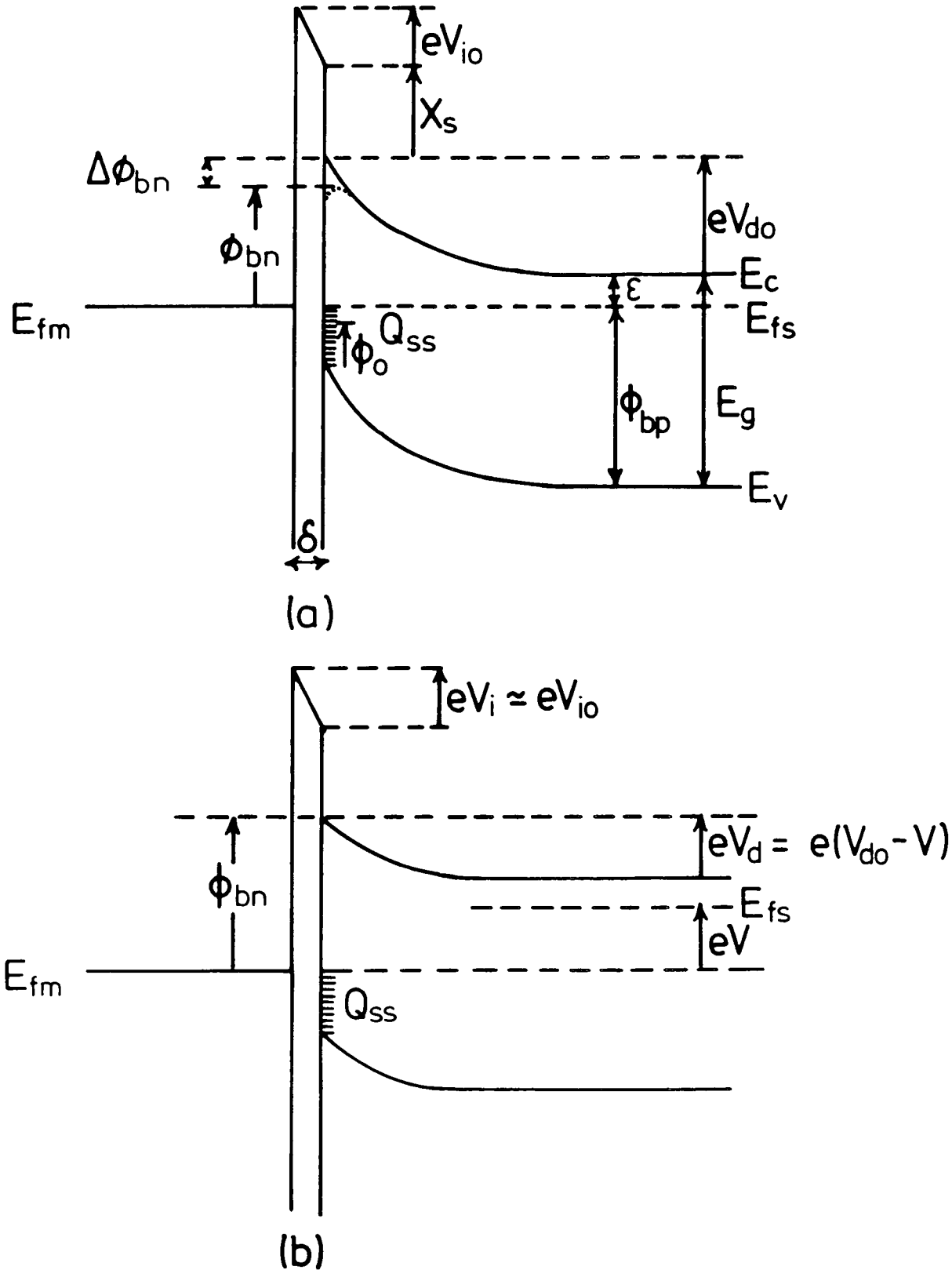

Figure 3.6 Energy band diagram of a Schottky barrier incorporating a thin interfacial layer (a) in equilibrium and (b) under forward bias.

dependent on the relative position of the metal Fermi level will thus remain constant with changing bias. This further justifies treating the effect of the insulator as negligible in most analysis.

The characteristics of diodes fabricated with the aim of minimising the interfacial layer can be close to those of this near-ideal model. These are discussed in the next section.

3.5.3 Electrical Properties

(a) Conductivity -- There are a number of mechanisms by which current could flow through a Schottky diode. Electrons with sufficient energy will be emitted over the barrier; electrons with slightly lower energies may tunnel through it. If holes are injected into the semiconductor they may recombine with electrons either in the depletion region or the semiconductor bulk. The last of these processes is that desired for EL, but as has already been stated δ is very low for these devices(10) and recombination currents are negligible. Quantum mechanical tunnelling effects are also very small except at low temperatures or with heavy doping densities. As it is electron emission over the barrier that will dominate, only this process is considered here. To maintain emission electrons must diffuse and drift through the semiconductor bulk to the surface, and for a time it was disputed which process limited current flow(2,11). However, it is now accepted that even where electron mobilities are low, the thermionic emission theory proposed by Bethe(11) best accounts for the current-voltage characteristics of these devices.

The thermionic emission theory is favoured since its necessary assumption that the electron quasi-Fermi level remains flat throughout the depletion region has been shown to be valid (quasi-Fermi levels will not be discussed here, but the reader is referred to (12) and (13)). This implies for an applied bias V that at the interface the electron concentration

$$n = N_c \exp\{-e(\phi_{bn} - V)/kT\} \qquad (3.13)$$

where N_c is the effective density of states in the conduction band

$$N_c = 2(2\pi m^* kT/h^2)^{3/2} \qquad (3.14)$$

An isotropic velocity distribution for electrons in the semiconductor is assumed, with mean thermal velocity $\bar{v}$ (for a Maxwellian velocity distribution $\bar{v} = (8kT/\pi m^*)^{1/2}$). The number of electrons crossing unit area of the interface per second will be $n\bar{v}/4$, giving a current density into the metal of

$$J_{sm} = (eN_c\bar{v}/4)(\exp\{-e(\phi_{bn} - V)/kT\}) \qquad (3.15)$$

Since there is no net flow of current at zero bias, there must be a flow of electrons from the metal dictated by the barrier height. Thus the net current density

$$J = (eN_c\bar{v}/4)(\exp\{-e(\phi_{bn} - V)/kT\}) - (eN_c\bar{v}/4)\exp\{-e\phi_{bn}/kT\}$$
$$= J_o(\exp\{eV/kT - 1\}) \qquad (3.16)$$

J_o is the reverse saturation current density and is given by

$$J_o = A^* T^2 \exp\{-e\phi_{bn}/kT\} \qquad (3.17)$$

where A^* is the effective Richardson constant

$$A^* = 4\pi m^* ek^2/h^3 \qquad (3.18)$$

(m^* = electron effective mass).

Diffusion theory is based upon current flow in the depletion region, and proposes(14) that current density is given by

$$J = J_d\{\exp(eV/kT) - 1\} \qquad (3.19)$$

where $J_d = eN_c\mu_n E.\exp(-e\phi_{bn}/kT)$ (3.20)

(μ_n = electron mobility; E = electric field in barrier). Note that J_d is not a saturation current, but dependent upon E and hence the applied bias.

Crowell and Sze(15) have combined these two theories to give a general expression

$$J = eN_c v_r/(1 + v_r/v_d) \times\{\exp(-e\phi_{bn}/kT)\}\{\exp(eV/kT) - 1\} \qquad (3.21)$$

where v_r is an effective recombination velocity and v_d an effective diffusion velocity at the potential energy maximum created by the Schottky effect. However, except for very low mobilities the thermionic emission theory suffices(12). Nonetheless, real diodes show a characteristic better described for $V \gtrsim 3kT$ by

$$J = J_o\exp(eV/nkT) \qquad (3.22)$$

where n here is called the ideality factor. In practice n is always greater than unity as a result of barrier height bias dependence and a finite interfacial layer (see section 3.6). For the same reasons the reverse current will not saturate. For values of n close to one a plot of ln(J) against V is linear and gives the barrier height ϕ_{bn} using equation 3.17. However, it should be noted that for large biases series resistance associated with the semiconductor bulk and its back contact will begin to dominate the characteristic.

(b) Capacitance -- The depletion region charge opposing the charge on the metal in a Schottky barrier leads to a capacitance. This capacitance is bias dependent since depletion region width varies with voltage. Making the approximation that in the depletion region the charge density

is a constant eN_d (N_d = donor density) and zero elsewhere. Gauss's Law(16) gives the depletion region charge at zero bias as

$$Q_d = (2\varepsilon_s e N_d V_{do})^{1/2} \qquad (3.23)$$

This capacitance is usually measured by applying an ac modulation to a dc reverse bias, leading to a differential capacitance

$$C_d = dQ_d/dV = \left\{e\varepsilon_s N_d/2(V_d - kT/e)\right\}^{1/2} \qquad (3.24)$$

Here the equilibrium diffusion voltage has been replaced by $V_d = V_{do} - V$; the kT/e term arises when the depletion approximation is not made. Note that this derivation assumes that only ionised donor charge is present in the semiconductor - the effect of interface states is considered in section 3.6. When equation 3.24 is valid it is clear that a plot of C_d^{-2} against V should be linear, with an intercept on the voltage axis

$$V_o = V_{do} - kT/e = \phi_{bn} - \varepsilon - kT/e \qquad (3.25)$$

(symbols as Figure 3.6). A barrier height can thus be deduced from this plot, but it should be noted that this value will not take into account image force lowering of the barrier by the Schottky effect. This is because carriers do not actually cross the barrier as they do in conductivity measurements.

(c) Photoelectric Effect -- Studies by Fowler(17) on the photoresponse of metal surfaces to monochromatic light led to the theory that the photocurrent per absorbed photon (R) for a Schottky barrier is given by

$$R = C(h\nu - h\nu_o)^2 \qquad (3.26)$$

where ν is the frequency of the light, $h\nu_o$ equals the barrier height, and C is a constant. This requires that the photon

energy is at least 3kT greater than the barrier height, and considerably less than the energy gap between the barrier top and the bottom of the metal conduction band. A plot of $R^{1/2}$ against $h\nu$ is linear with an intercept giving the height of the barrier actually presented to electrons. However, the problem exists of free carriers being generated in the semiconductor depletion region as $h\nu$ approaches the band gap energy. This can only be overcome by use of a top electrode thick enough to absorb most incident light, but thin enough to allow photoexcited electrons from the metal to reach the semiconductor (~50nm for gold)(18). Since thick top contacts are unsuitable for the EL devices geometries required in this research, little use of this technique has been made here.

3.5.4 Minority Carrier Injection

The minority carrier injection ratio, γ, is defined for an n-type material as the ratio of the hole current to the total current

$$\gamma = J_p/(J_p + J_n) \qquad (3.27)$$

$$\sim J_p/J_n \qquad \text{(for low injection } J_n >> J_p\text{)}$$

Although expressions for γ can be derived by analysis of hole current(15) components, it is sufficient here to note that

$$\gamma \propto \exp\{(-e/kT)(\phi_{bp} - \phi_{bn})\} \qquad (3.28)$$

such that γ is highly dependent on $(\phi_{bp} - \phi_{bn})$ (see Figure 3.6). Since ϕ_{bp} is considerably larger than ϕ_{bn} the value of γ will be very small, and will remain so since $(\phi_{bp} - \phi_{bn})$ does not change significantly with bias. The incorporation of an insulating layer, however, allows the band realignment required to increase γ. This is discussed in the following section.

3.6 THE METAL-INSULATOR-SEMICONDUCTOR DIODE

This structure takes the form shown in Figure 3.7a in equilibrium and 3.7b under forward bias. The insulator is now considered to have a significant effect on carrier transport, and a significant part of an applied voltage is dropped across the insulator (V_{io}). The band edges are no longer 'pinned' relative to the metal Fermi level - the interface charge and barrier height are both now bias dependent, as shown in Figure 3.7b. In simple terms the metal Fermi level can now move with respect to the semiconductor band structure allowing both an increase of the barrier to electrons and a decrease of the barrier to holes. Hence the minority current can be enhanced. The next sections relate the necessary modifications to Schottky barrier theory to account for the insulating layer.

3.6.1 Modifications to Electrical Properties

(a) Conductivity -- The change in conductivity due to the presence of an insulator was analysed by Card and Rhoderick(19). They suggested that the main result would be to alter the value of J in equation 3.22 to a term dependent upon the thickness of the insulator (δ in Angstroms) and the mean value of the barrier its energy gap constituted to current flow (χ), i.e

$$J = J_{\infty} \exp(eV/nkT) \qquad (3.29)$$

where $J_{\infty} = J_o \exp(-1.01 \chi^{1/2} \delta)$

The ideality factor n was also shown to vary as a result of the bias dependence of ϕ_{bn}. When the density of interface states is low this approximates to(15)

$$n = 1 + \delta \varepsilon_s / w \varepsilon_i \qquad (3.30)$$

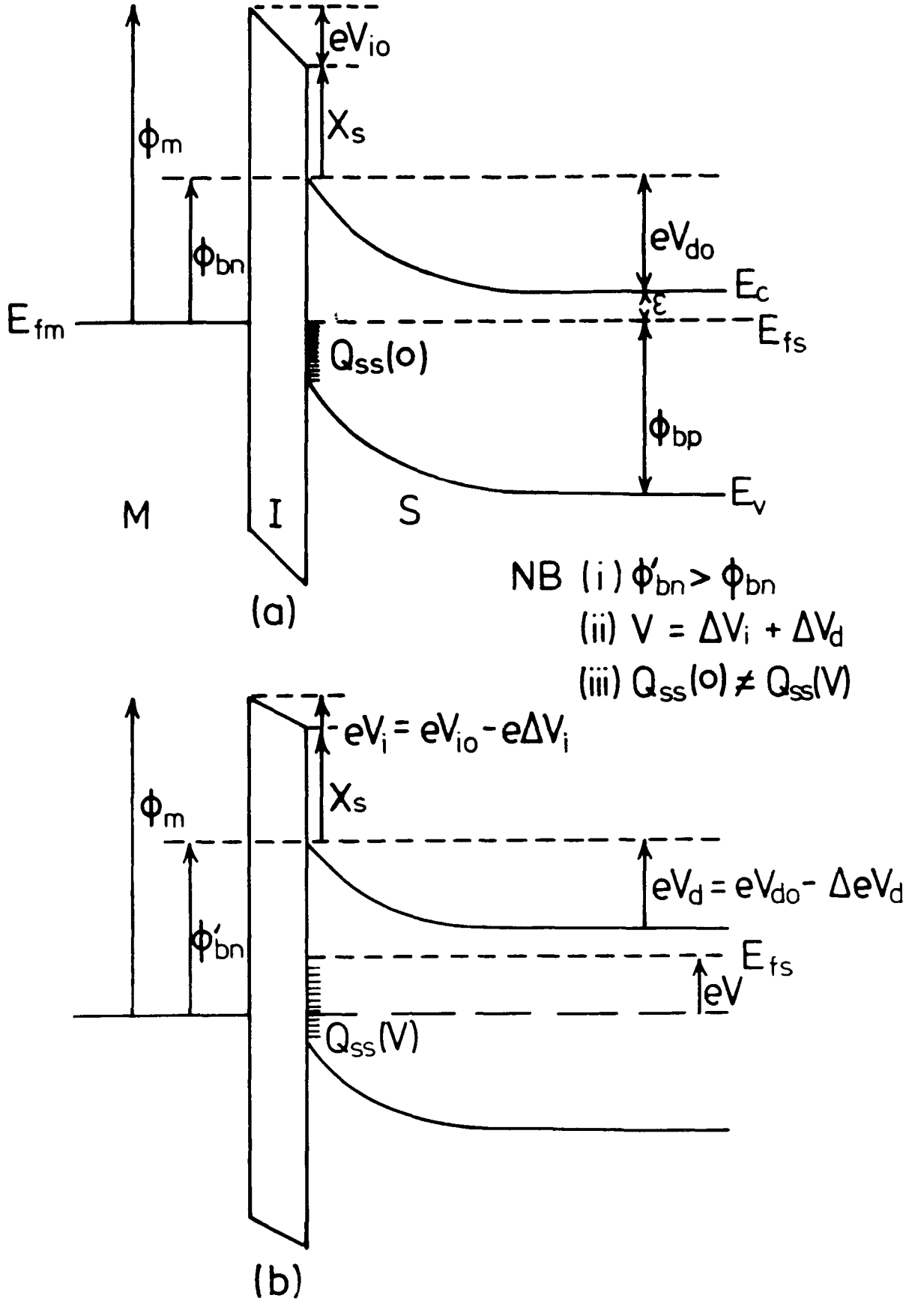

Figure 3.7 Energy band diagram of an MIS structure (a) in equilibrium and (b) under forward bias.

(ϵ_s, ϵ_i = permittivity of semiconductor and insulator respectively, w = depletion region width). Card and Rhoderick also derived an expression for n as a function of the density of interface states communicating with the metal and semiconductor, which is not considered here.

In reverse bias the insulator has the effect of preventing saturation, as in this case ϕ_{bn} will decrease with bias. This decrease is much larger than the Schottky effect lowering.

(b) Capacitance -- The first attempt to extend the analysis of C_d^{-2} vs V plots from Schottky barriers to MIS diodes was by Cowley(20). His analysis considered the effects of both the insulator and bias-dependent charge in interface states. By deriving relationships in terms of the sums of potentials due to charges in the model (essentially that of Figure 3.7), he found expressions for the non-equilibrium band bending (V_d) in the semiconductor. These gave the space charge in the semiconductor as a function of bias, which he differentiated with respect to bias to give the differential capacitance. For the case of no surface states at the interface he showed

$$C_d^{-2} = (2/e\epsilon_s N_d)(V + V_{do} + V_i/4 + V_i^{1/2} V_{do}^{1/2}) \qquad (3.31)$$

where $V_i = 2e\epsilon_s N_d (\delta/\epsilon_i)^2$

and assuming the depletion approximation. Although this predicts a linear relationship with the same slope as that for a Schottky diode (equation 3.24), note that the intercept is considerably larger. Later work based on that of Cowley extended his model(21) to account for interface states both at the metal and semiconductor surfaces. By assuming D_{sa} and D_{sb} (the densities of interface states communicating with the

metal and semiconductor respectively) are constant as a function of energy, it is possible to derive an expression for differential capacitance such that

$$C_d^{-2} = \left\{2(1 + \alpha_1 + \alpha_2)/e\varepsilon_s N_d(1 + \alpha_1)\right\} \qquad (3.32)$$
$$\times \left\{V_1/4(1 + \alpha_1 + \alpha_2)(1 + \alpha_1) + V_1^{1/2} V_{do}^{1/2}/(1 + \alpha_1)\right.$$
$$\left. + V_{do}(1 + \alpha_1 + \alpha_2)/(1 + \alpha_1) + V\right\}$$

where $\alpha_1 = eD_{sa}\delta/\epsilon_i$ and $\alpha_2 = eD_{sb}\delta/\epsilon_i$

Again this gives a linear relationship with the slope as for a Schottky barrier, and of course reduces to equation 3.31 for the case $D_{sa} = D_{sb} = 0$.

However, a fundamental error in these derivations has been discussed by Fonash(22). He has pointed out that relationships of potentials assuming quasistatic changes in bias have been used to derive a differential capacitance. Where the charge in interface states cannot respond quickly enough to a high frequency a.c measuring signal these quasistatic values are invalid - the variation of V_d with the signal is not accurately described. Developing the model with a more correct a.c analysis of V_d, Fonash has shown that C_d^{-2} vs V is only linear for $D_{sa} = D_{sb} = 0$ (i.e equation 3.31), or if all the interface states are communicating with the metal (i.e D_{sb} and hence $\alpha_2 = 0$ in equation 3.32). For all other cases he predicts a non-linear plot. Interestingly, none of his models predict a linear characteristic with a slope and intercept dependent on insulator thickness. This is in contrast to many results presented here and elsewhere.

These analyses show that interpretation of C-V characteristics for MIS structures is far from simple, and cannot be expected to directly give an accurate measure of

diffusion voltage. This problem is considered further in the discussion of results presented in Chapter 7.

3.6.2 Enhancement of Minority Carrier Injection

The increase in γ due to the presence of an insulating layer, as suggested in section 3.5.4, has been analysed theoretically(23). In simple terms the optimum conditions are that the insulator be thick enough to allow the necessary realignment of bands between the metal Fermi level and the semiconductor, while thin enough to allow the minority carriers to tunnel through it.

For very thin insulators where band realignment is insignificant, and minority carrier current is limited by bulk diffusion rather than the insulator, Card and Rhoderick(23) derived J_p to show that

$$\gamma = (eD_p N_v / LA^* T^2)\exp(\gamma_n^{1/2}\delta)\exp\{e(\phi_{bn} - \phi_{bp})/kT\} \times \exp\{eV(1/n_h - 1/n_e)/kT\} \quad (3.33)$$

N_v is the effective density of states in the valence band (cf N_c), n_h and n_e act as hole and electron ideality factors, and L is the depletion region width (strictly, the width of the region in which carrier quasi-Fermi levels remain flat).

For insulators sufficiently thick to limit the tunnelling of minority carriers, Card and Rhoderick considered hole currents at different biases. When the bias voltage is greater than that needed to align the metal Fermi level and the semiconductor valence band edge (i.e $V > \phi_{bp}$), they derived the minority carrier injection ratio as

$$\gamma = (m_p^*/2m_n^*)\{e(V - \phi_{bp})/kT\}^2 \times \exp(\gamma_n^{1/2}\delta_n - \gamma_p^{1/2}\delta_p)\exp(e\phi_{bn}/kT) \quad (3.34)$$

where γ_n, δ_n, γ_p and δ_p apply for electrons and holes

respectively as introduced in equation 3.29. This expression gave good agreement with silicon-silicon dioxide experimental results, where γ could be increased from 10^{-4} to over 10^{-1} for an optimum insulator thickness. The derivation of 3.34 assumes an ideal insulator where quantum mechanical tunnelling is the limiting carrier transport process. For an imperfect case the insulator presents less of a barrier to current flow, and arguing qualitatively one would expect the optimum insulator thickness to be greater than for an ideal one. Indeed, in their work with Au-LB film-GaP MIS diodes Batey et al(24) found optimum insulator thicknesses ~27nm for two film materials, well beyond the accepted thickness limit for tunnelling (~5nm). Although they appeared to find an optimum thickness of 5.6nm when using phthalocyanine LB films(25), recent preliminary ellipsometry measurements(26) have suggested this optimum may have been ~16nm.

3.6.3 MIS Light Emitting Diodes

Clearly a significant increase in minority carrier injection will increase the electroluminescent efficiency of an MIS stucture (section 3.3). In fact, enhancement of γ is well established as a method of obtaining light from semiconductors, particularly the non-amphoteric II-VI compounds. Of particular interest is the work by Livingstone(27) on ZnSe, who found a 10^{4}-fold increase in efficiency with insulator thicknesses up to 50nm, with little subsequent change up to 200nm. In this case minority carriers cannot have been injected by tunnelling. One possible explanation(28) is that hot electrons arriving in the metal undergo an Auger recombination process, and

transfer sufficient energy to create energetic holes capable of entering the valence band of the semiconductor. The inherent inefficiency of such a process is thought to be the reason why to date achieved efficiencies have been well short of the theoretical levels mentioned in 3.3. It is possible that a more efficient tunnelling injection could be achieved given a good, well defined insulator. Batey et al(24,25) have already shown that LB films can be used to fabricate MIS EL structures on GaP. In the present work the process has been extended to a II-VI semiconductor.

3.7 OTHER EL STRUCTURES

Alternative structures do exist for obtaining EL from II-VI materials. The p-n heterojunction is another low field injection device which has been investigated(29), but fabrication difficulties have limited these to low efficiency emission of mainly red light. Most research interest in new EL structures is aimed at large area devices, e.g for flat panel displays. Thin films of suitably doped ZnS phosphors have been successfully incorporated into a.c EL devices using an MISIM structure. Progress with the equivalent d.c driven devices has been less encouraging to date, due to breakdown at 'hot-spots' caused by a lack of current limiting between electrodes and the phosphor. Extensive reviews are available on such thin film EL devices(e.g 30). It should be noted that these generally require high (~100V) operating voltages.

3.8 SUMMARY

This chapter has discussed the physics of electroluminescence, and some of the devices used to attain

it. Particular emphasis has been placed upon metal-semiconductor and metal-insulator-semiconductor stuctures. These have been shown to allow the injection of minority carriers, a source of radiative recombination and hence EL in II-VI materials (in the absence of viable pn homojunctions). The predicted enhancement of minority carrier injection by the presence of an insulating layer suggests an application for Langmuir-Blodgett films. An account of the current technology of these films is presented in the next chapter.

CHAPTER 4

LANGMUIR-BLODGETT FILMS

4.1 INTRODUCTION

When solutions of some organic materials are introduced onto a water surface, they spread out to form a layer one molecule thick. This monolayer will remain present after evaporation of the solvent. By decreasing the area available this monolayer can be laterally compressed and will exhibit properties analogous to that of a gas undergoing compression; as surface pressure increases the molecules in the film will exist in phases which can be likened to a two-dimensional gaseous , liquid and eventually solid state. Such monolayers are termed Langmuir films. If the monolayer can be maintained in its solid phase it is sometimes found that it will transfer to a substrate passing through the monolayer-subphase interface. Hence the substrate will receive monolayer coverage of the organic material or, in the case of repeated traversal of the interface, coverage by multiple layers. These transferred coatings are known as Langmuir-Blodgett (LB) films. Ultra-thin films of such precisely controllable thickness have many potential applications in physical, chemical and biological sciences, (including the work reported here).

In this chapter, following a brief historical introduction, a description is given of the equipment used to both characterise and deposit LB films. Well established and novel materials for use as LB films are discussed , and the methods for assessing monolayer formation and deposition

described. Finally, a summary is given of the potential applications for these films.

4.1.1 A Brief History

Although the spreading of organic films on water has been observed since ancient times ("pouring oil on troubled waters"), it was Benjamin Franklin in 1773 who first speculated on the extreme thinness of such films. He observed that a few cubic centimetres of oil could cover several hundred square metres when applied to the surface of water. True scientific study of such films began when the work of Agnes Pockels attracted the attention of Lord Rayleigh in 1891(1). Her experiments introduced the concepts of surface pressure-area diagrams, the spreading of materials in volatile solvents, and the use of a forerunner to the Langmuir trough (section 4.2). In 1899 Rayleigh suggested for the first time that these films were only one molecule thick(2). However, most of today's interest in monomolecular layers is based on the research carried out by Irving Langmuir and Katherine Blodgett at the General Electric Research Laboratory between the first and second world wars. Using fatty acids with long hydrocarbon chains, Langmuir's initial characterisation led him to conclude that these films were indeed one molecule thick(3). Furthermore, he established that the long chains were effectively standing vertically on the water surface, implying a monolayer thickness equal to the chain length of the molecule. Later collaboration with Blodgett(4) led to the development of apparatus to control and transfer monomolecular films onto solid substrates, upon which most modern LB film methods are

still based. This and other work prior to 1966 has been well documented by Gaines(5).

Much of the recent interest in LB films stems from Kuhn's use of the technique to investigate optical and energy transfer mechanisms(6). Influenced by this work and the wish to incorporate well-defined organic films into solid state electronic devices, Roberts et al developed a Langmuir trough featuring electronic control instrumentation and superior mechanical construction(7). It is now widely believed that this level of sophistication is necessary for producing LB films of reproducible high quality. A broadly similar trough has been used to characterise the LB films used in this research. The next section describes its construction in some detail.

4.2 THE LANGMUIR TROUGH

4.2.1 Previous Designs

The production of good quality LB films depends greatly upon the reliability of the deposition system used. It must be free from contamination and vibration, capable of controlling surface pressure precisely, and give smooth movement of a substrate through a monolayer for film deposition. In their pioneering work Langmuir and Blodgett(4) used a waxed thread lying on the surface of the water to act as a barrier between two halves of their trough. The monolayer forming material was spread on one side of the thread, then a drop of a piston oil placed on the surface on the other side. As this oil spread out it exerted a constant pressure on the barrier of approximately $30mNm^{-1}$. Substrates were raised and lowered using a windlass. Kuhn et al(6)

originally used a modification of this technique which avoided oil contamination. A polypropylene float ran in between side barriers within the trough. A weight was connected to the float by a thread running over a pulley. exerting the desired surface pressure. Pressure was monitored with a Wilhelmy balance, and again a windlass was used to raise and lower the substrate.

4.2.2 A Modern Trough

Several Langmuir troughs are in use at Durham University, all based on the design of Roberts et al(7). The trough described below has been dedicated to research on LB films of dye materials, but is broadly similar to other troughs in operation. Figure 4.1 shows a schematic diagram of this form of trough.

Mechanical Construction

A photograph of the main structure of the trough is shown in Figure 4.2. The glass trough itself is supported on a metal platform within a framework of metal beams. The platform can be lowered to allow removal of the trough for cleaning. The active area of the water surface is defined by a constant perimeter variable area barrier. The barrier is formed by a 2cm wide PTFE-coated glass fibre belt, held taut around six PTFE rollers. The area is changed by movement of the two pairs of rollers mounted on cross-members. The cross-members have V-shaped rollers set on steel rods and are pulled by toothed rubber belts driven from a single motor. The speed of the motor is externally controlled, and microswitches define the limits of barrier movement. The

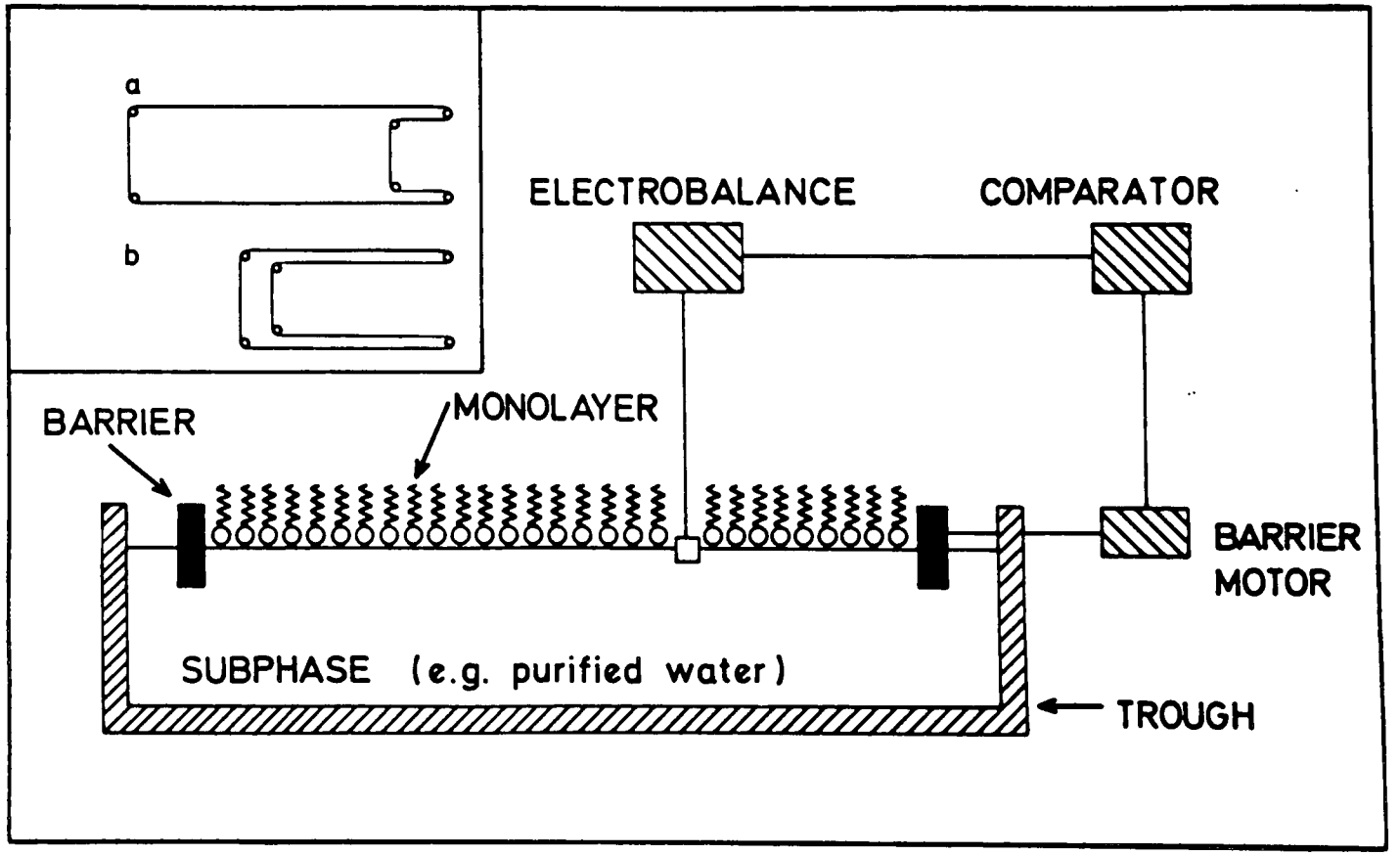

Figure 4.1 Schematic diagram of a modern Langmuir trough. The inset shows a plan view of the constant perimeter barrier (a) fully open and (b) fully compressed.

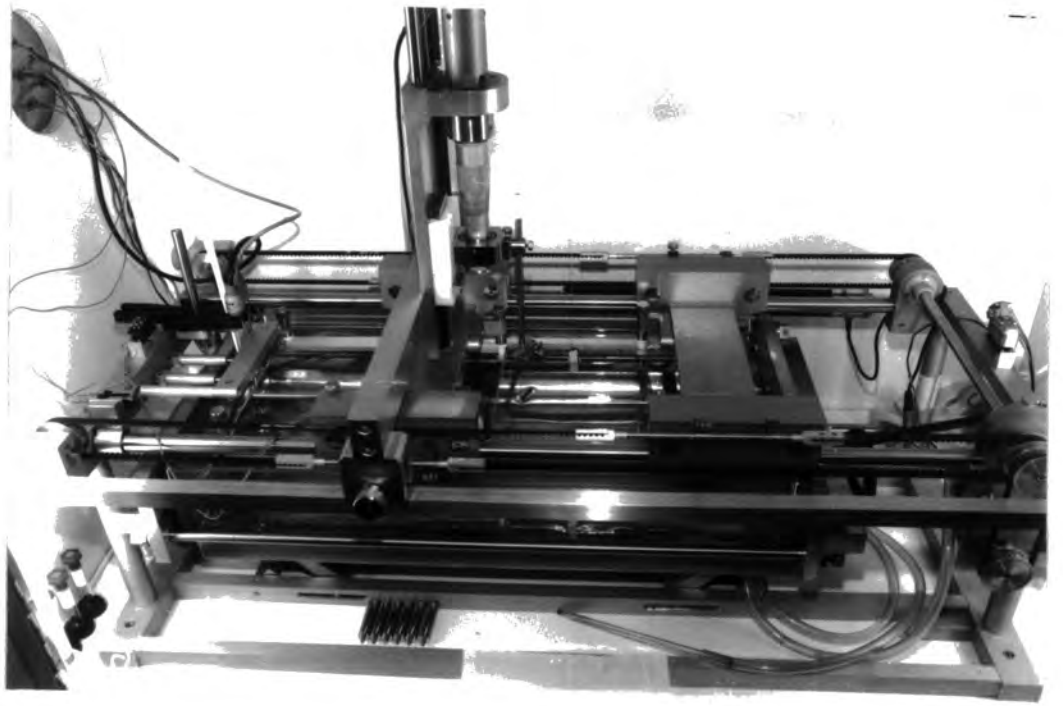

Figure 4.2 The Langmuir trough at Durham University used for this work.

Figure 4.3 Control instrumentation associated with the Langmuir trough.

deposition mechanism, or dipping head, is a motor driven micrometer screw mounted above the water on a moveable crossbeam. Substrates are held by a metal screw clamp which can be affixed to the dipping head. The speed and range of the dipping cycle are externally controlled. The surface pressure is monitored using a Wilhelmy plate consisting of a 1cm wide strip of filter paper; this is suspended in the water by a thread from a microbalance head above the trough. Changes in the effective weight of the plate reflect surface pressure. The complete structure is housed in a glass-doored cabinet mounted upon a Newport XJ-A pneumatic anti-vibration table. An extractor fan in the wall of the cabinet aids solvent evaporation. Where possible the structure has been made from PTFE and stainless steel, or metal surfaces anodized, to ease cleaning and lower the risk of contamination.

Instrumentation

A photograph of the instrumentation associated with the trough is shown in Figure 4.3. Several of the functions of the trough are automated using the purpose built control unit. The barrier may be operated in four modes, 'forward', 'reverse', 'control' and 'auto'. In 'forward' and 'reverse' modes the barrier will compress or expand at speeds adjustible by front panel knobs. In 'control' mode a differential feedback system is used to compress the barrier until a film reaches a preselected surface pressure. The force acting upon the Wilhelmy plate is monitored by a Beckman LM600 microbalance. An electrical signal representing the difference in pressure from that preset on

the microbalance is passed to the control unit. The gain of the feedback system can be varied using a front panel knob. This mode is normally used during deposition. 'Auto' mode is used exclusively for the deposition of phthalocyanine LB films. Characteristics of this material require that the film is only compressed when the substrate is moving up out of the subphase (this aids 'Z-type' deposition, which is discussed later - see section 4.5.3). In this mode the barrier will compress the film after the substrate has been lowered into the subphase, and the film is allowed to stabilise for a preset time of up to six minutes before deposition commences. A further delay of up to thirty minutes may be selected to allow the LB film to stabilise in air. The number of dipping cycles required is set by switches and loaded into a counting circuit. The upper and lower limits of the dipping head movement, and its speed are preset by front panel knobs. High-resolution linear potentiometers attached to the barrier cross-members and the dipping head allow precise monitoring of film area and substrate position. A Bryans 29000 X-Y chart recorder is used for plotting surface pressure (the microbalance output) against area, or area against substrate position (for monitoring film deposition). Area and pressure may also be plotted against time on a Bryans 312 two-channel Y-t chart recorder. The acidity of the subphase is continuously monitored by a Pye-Unicam PW9409 pH-meter. The electrodes for this and a mercury thermometer are mounted at one end of the glass trough.

Environment

A dust-free environment is essential for the production of good LB films, and consequently all the troughs at Durham are housed in a class 10000 microelectronics clean room. A rigorous cleaning procedure is undertaken frequently when the glass trough is cleaned with chloroform, isopropyl alcohol and purified water. The belt and PTFE rollers are cleaned for several hours in hot isopropyl alcohol in a Soxhlet refluxing system. On reassembly, the subphase and Wilhelmy plate are renewed, and the trough instrumentation recalibrated. The water used as a subphase and in cleaning undergoes double deionisation, activated charcoal organic removal and 0.2μm filtration before being delivered to the troughs via high purity polypropylene tubing. This ultrapure water has a typical resistivity of 10MΩcm. Before spreading films the subphase surface is cleaned with a fine nozzled glass pipe connected to a water driven pump. The surface is considered clean if closing the barrier to minimum area results in a surface pressure change $<0.05 mNm^{-1}$.

4.2.3 Alternative Designs

It is worth noting that although the trough described here is well suited to the characterisation of LB films and incorporating structures, any commercial utilisation of the technique would require significant design improvements. Barraud and Vandevyver(8) have described a trough which continuously replenishes a compressed Langmuir film during deposition. At the GEC Hirst Research Centre workers are developing a rotary deposition mechanism for continual build up of alternate layer structures(9), and a trough featuring

this facility is already operational at Durham University.

4.3 LANGMUIR-BLODGETT FILM MATERIALS

Only a limited range of organic materials are suitable for LB film applications. In this section an account is given of some of those that have been used. For the purpose of this study all materials previously investigated have been considered 'classical', and the merocyanine and phthalocyanine dyes used in this research termed 'novel' materials.

4.3.1 Classical Materials

The traditional requirements for a material to form an LB film are that it is highly insoluble in water, that the constituent molecules have distinct hydrophobic and hydrophilic regions, and that it possesses suitable mechanical properties to enable transfer to a substrate. Such molecules can form a stable monolayer on a water surface with predictable orientation. Typical hydrophobic and hydrophilic groups found are long hydrocarbon chains (about twenty carbons), and acid or alcohol groups respectively. Fatty acids (e.g stearic and arachidic acid) are good examples of LB film forming materials. With these films enhanced stability can be achieved by the presence of divalent metal ions (usually Cd^{2+}) in the subphase(10). This converts some of the acid to its salt, the degree of conversion being dependent upon the pH of the water. A large amount of research has been carried out over many years on

fatty acid LB films, and on other molecules with broadly similar structures e.g phospholipids(11), chlorophyll(12) and cholesterol(13).Greater film stability has been achieved by using long chain polymeric materials, diacetylene(14) and, more recently, ω-tricosenoic acid(15).

Current interest in the possible photoactive properties of LB films has led to the study of materials without long hydrocarbon chains. The presence of these chains has a diluting effect upon the interesting electrical properties of the delocalised electronic orbitals of aromatic and heterocyclic ring structures. Vincett et al(16) have shown that with careful control of deposition conditions it is possible to fabricate multilayer structures of only lightly-substituted anthracene. Their success stimulated the work on the novel LB film materials which are described in the next two sections.

4.3.3 Merocyanines

The merocyanines are a wide range of non-ionic dyes characterised by a double bond or even-numbered methine chain uniting two heterocyclic rings. They exist as a resonant hybrid between a covalent form and a charged dipolar form, as shown in Figure 4.4. The optical properties of this class of dyes(17) are well known to photographic science and engineering where they have for many years been used for the spectral sensitisation of silver halide emulsions. Conventional film deposition techniques (e.g evaporation, adsorption from solution) have been used to show that merocyanine thin films can be used to spectrally sensitise other inorganic semiconductors(18,19), and also to fabricate

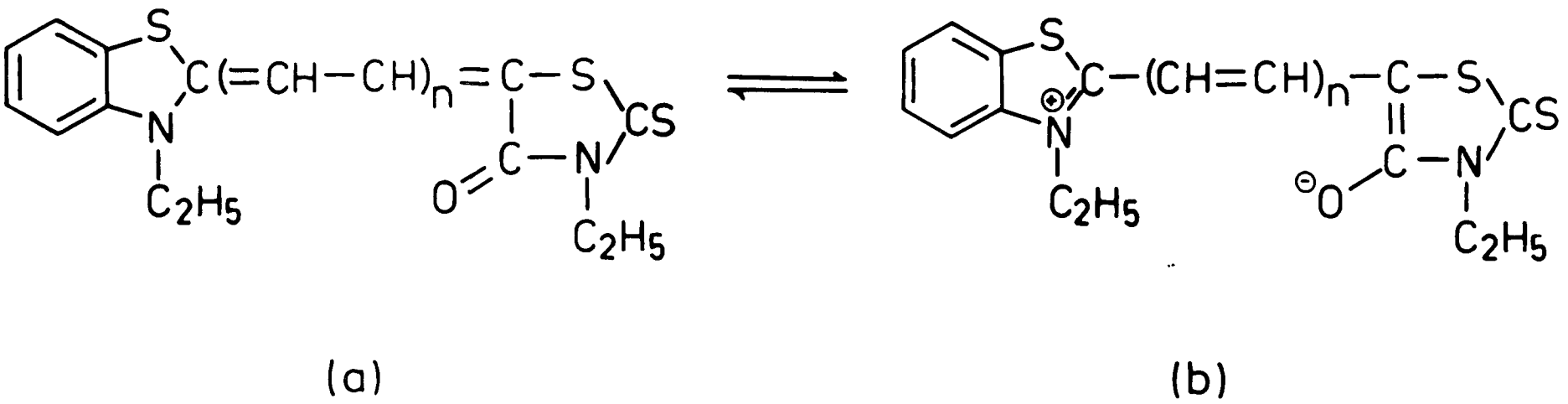

Figure 4.4 The molecular structure of a typical merocyanine dye showing (a) the covalent and (b) the charge-separated dipolar forms(17).

organic solar cells(20). Also of note are reports that a merocyanine dye has been shown to have a very large second order molecular polarisability(21). That this is far higher than any reported for inorganic materials, suggests an application in the field of non-linear optics.

Merocyanines with long hydrocarbon chain substitutions have been investigated as LB films by Kuhn(6) , more recently by Sugi(22), and have also been used in this research. However, one aim of this research was to find an LB film forming dye from the large range of dyes commercially available with no such substitution. The steps required to characterise such a material are detailed in Section 4.4.

4.3.3 Phthalocyanines

The phthalocyanines are a well defined class of synthetic macrocyclic tetramines, known in the chemical industry for exceptional stability to acids, alkalis and heat (Figure 4.5). It was this stability, and the potentially interesting electrical properties of the molecules' cyclic π-electron systems, which provoked investigations into the use of phthalocyanines as LB films. Baker(23) has shown that it is possible to prepare stable LB films of metal-free phthalocyanine (Figure 4.5a) and a tetra-tert-butyl substituted phthalocyanine. These films are of reproducible quality but are not single monolayers, and are polycrystalline in form with no long range order. Recent work with an asymmetrically substituted copper phthalocyanine (Figure 4.5b) has shown that mono- or bimolecular layers may now be produced which display a distinctive electron diffraction spot pattern(24). This material has been used in

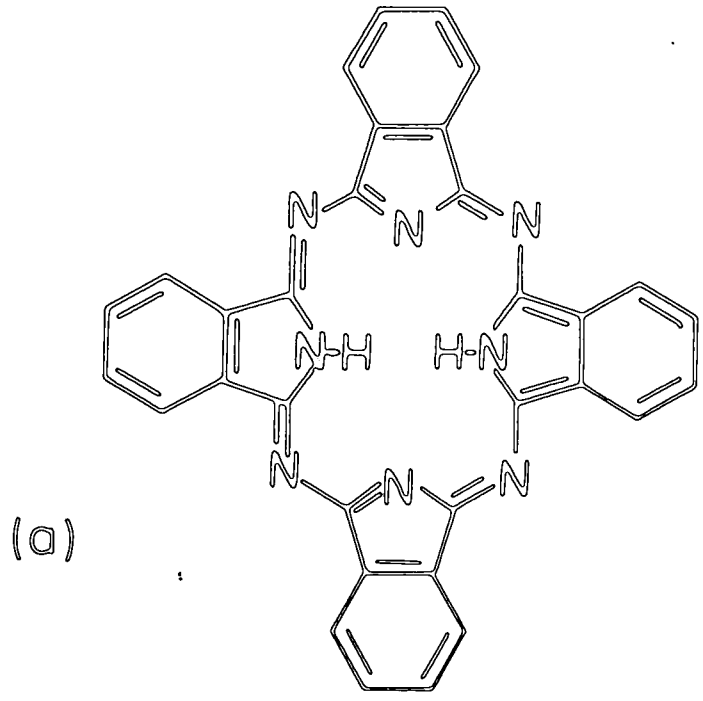

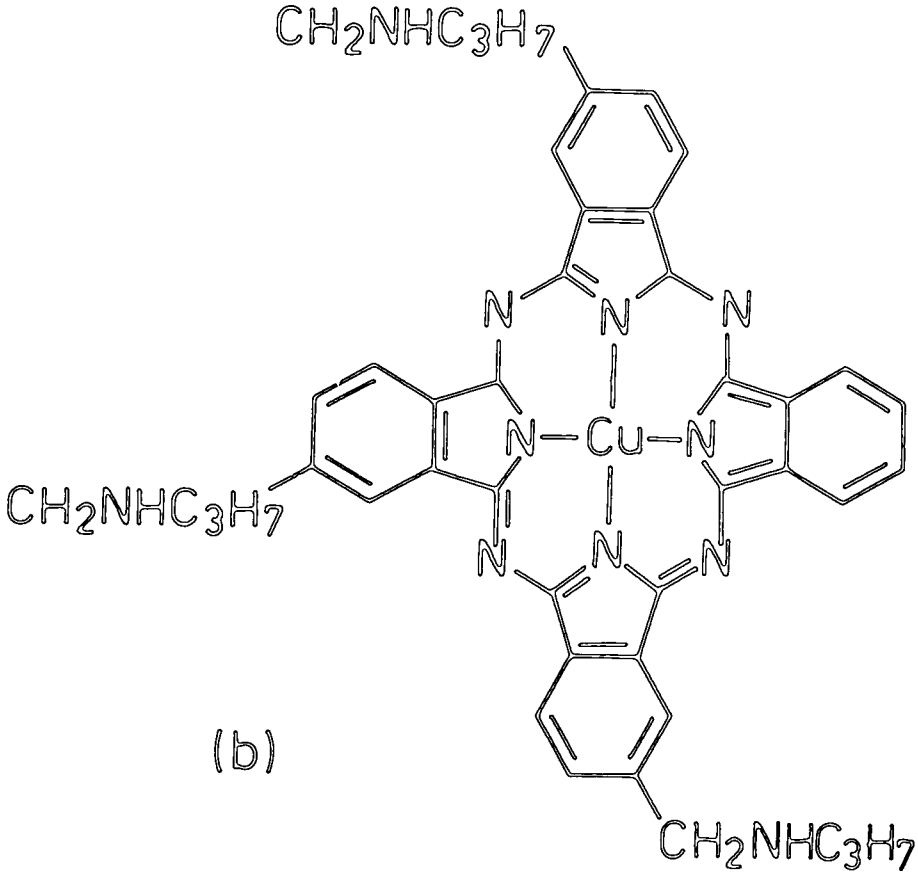

Figure 4.5 The molecular structures of (a) metal-free phthalocyanine and (b) asymmetrically substituted copper phthalocyanine.

this research as an insulator of finely controllable thickness, though the optical and electrical properties of phthalocyanines also lend themselves to potential applications as organic semiconductors, sensitisers, and in thin film gas detectors.

4.4 ASSESSMENT OF MONOLAYER PROPERTIES

With the present limited understanding of the relationships between molecular structure and the ability to form LB films, some procedure is clearly necessary for assessing the usefulness of materials. While there are good grounds for expecting materials similar to the fatty acids to form stable monolayers, the unsubstituted LB film molecules currently being sought are not so predictable. In this section some techniques for characterising materials prior to deposition are discussed.

4.4.1 Molecular Structure

A fundamental requirement for the formation of a useful monolayer film is that the substance used is insoluble in the water subphase. However, it must be noted that a material regarded by chemists as insoluble in significant quantities may rapidly dissolve into the subphase when dispersed as a very thin film over a relatively large volume of water. Some idea of the relative solubility of an organic in water can be gained by considering the number and strength of polar substituents incorporated in each molecule. For instance, replacing a methyl group on a molecule with a cyano group will increase its solubility in water. Thus a collection of similar materials can be ranked in order of suitability for

film formation before commencing actual characterisation.

When a material shows promise as a Langmuir film it is then useful to examine both physical and computer-generated models of the molecules. These can give clues to the orientation of and possible interactions between molecules in the film. Such modelling is done in conjunction with a study of the surface pressure-area characteristics of the film.

4.4.2 Pressure-Area Isotherms

When a monolayer forming substance is spread over the water surface of a trough the Wilhelmy plate will register a differential surface pressure which increases steadily as the film is compressed by the barrier. The result is plotted as a pressure-area (π/A) curve, or isotherm, where surface pressure is shown as a function of the surface area occupied by one film molecule. This molecular area is deduced simply from the area within the barrier by calculating the number of molecules spread from a solution of known concentration. Figure 4.6 shows typical isotherms for (a) stearic acid and (b) asymmetrically substituted copper phthalocyanine. As is shown, by extrapolating the solid phase region of the curve down to the x-axis the molecular area is obtained for a state of zero pressure. The assumption is made that this is the true cross-section of each molecule for its favoured orientation.

The shape of an isotherm gives clues to the behaviour of molecules as a film is compressed. That shown for stearic acid is the 'ideal' situation in which three distinct regions are present, the final region showing the steep, linear curve characteristic of a two-dimensional solid. The

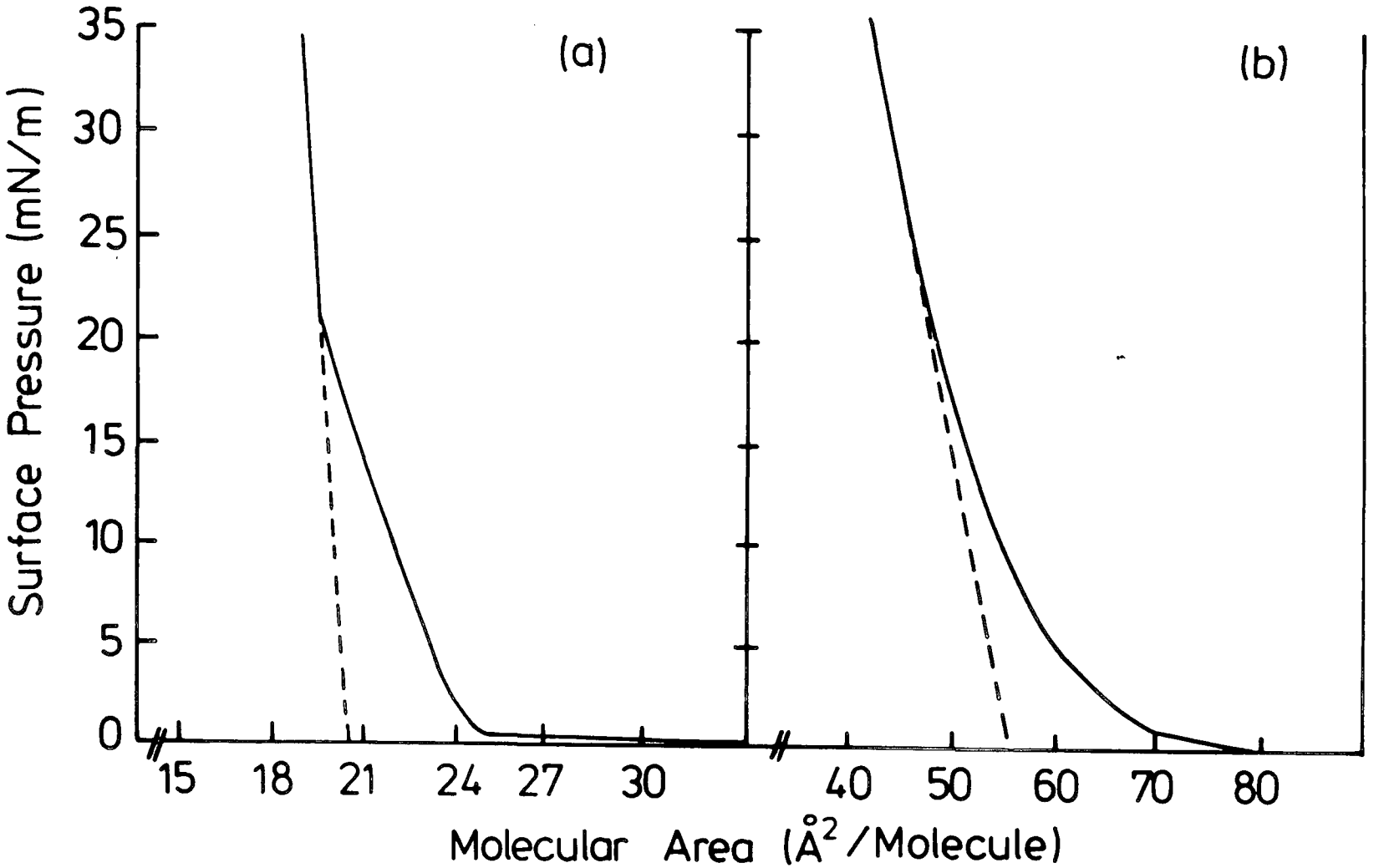

Figure 4.6 Typical compression isotherms for (a) stearic acid and (b) asymmetrically substituted copper phthalocyanine.

phthalocyanine isotherm, like most for novel materials, does not show this distinct structure but does exhibit a condensed 'solid phase' region. It is possible to interpret the curvature of such isotherms, and any change in curvature with recompression, in terms of molecular rearrangement and interaction. This will be discussed further in Chapter 6.

4.4.3 Collapse Mechanisms

An ideal Langmuir film held in its quasi-solid phase at a constant surface pressure will maintain its surface area coverage with time. In practise, all Langmuir films show some collapse due to the effects of (a) buckling of the film and/or (b) the gradual dissolution of material into the subphase. Preventing a film from buckling and collapsing in on itself normally only requires that the surface pressure is kept below that at which the film becomes unstable. The rate of dissolution, however, may depend on several factors, in particular the temperature, pH and contents of the subphase. Though this process can be rendered insignificant in most classical materials (by partial conversion of acid to salts),it can be quite rapid with novel materials. Thus it is useful to find the optimum conditions for slowing film collapse. Studies of Langmuir films which dissolve at an appreciable rate are described by Gaines(5). These show an initial rapid desorption, followed by a process obeying the equation

$$\ln(N) = -kt + C \qquad (4.1)$$

where N is the number of molecules remaining on the surface, t time, and k and C constants. Measuring the surface area of a collapsing film against time for varying subphase

conditions allows a minimum value for k to be determined.

Although film collapse is undesirable, it is important that a film should remain mobile on the surface if it is to be deposited onto a substrate. A simple check on the mobility of a film is the 'suction test'; the film is held at constant pressure and a small amount of material removed from the water surface using the vacuum nozzle mentioned in section 4.2.2. An adequately mobile film should collapse immediately to maintain surface pressure.

4.5 FILM DEPOSITION

Once a material has been established as a viable Langmuir film, its deposition characteristics as an LB film onto substrates may be studied. After cleansing of the trough water surface as described in 4.2.2, the deposition process may be considered as three stages - monolayer spreading, compression and actual deposition. Before investigating applications of films deposited they must also undergo some quality assessment. The next sections describe these steps.

4.5.1 Monolayer Spreading

Solutions for use in film spreading were normally made in ARISTAR grade chloroform to a concentration of approximately $1 mg cm^{-3}$. Accurate weighings for the determination of concentration were made with an Oertling R52 balance. Films were spread in solution one drop at a time using an Agla microlitre syringe held close to the water surface. This syringe has a micrometer driven plunger which allowed accurate measurement of volumes for molecular area

calculations. Typically 100µl of solution would be spread, invariably from the centre of the trough to lessen the effect of any residual contamination. After spreading, the extractor fan was switched on for about five minutes to ensure solvent evaporation.

4.5.2 Monolayer Compression

As a matter of course, a π/A isotherm was plotted for each film spread as an initial check on film quality. This was done by compressing the film at a fixed rate in 'forward' mode until the linear solid phase region was found. Having established this, the film was then recompressed in 'control' mode to a pressure near the middle of the solid phase. As can be seen from Figure 4.6, a film held at this point in its isotherm will change its structure very little for relatively large surface pressure deviations. Prior to deposition the film was left to stabilise for about five minutes to allow for any continuing molecular rearrangement. Alternatively, this was the stage at which the collapse mechanisms referred to in section 4.4.3 were studied.

4.5.3 Deposition Modes

During their pioneering work Langmuir and Blodgett discussed and named three possible modes of film deposition(25), as illustrated in Figure 4.7. Normal deposition is Y-type (b), where pick up occurs with the substrate moving in both directions. This mode is observed with the vast majority of LB film materials, though since most substrates are hydrophilic, pick up does not normally commence until the first upstroke. X-type deposition (a) is

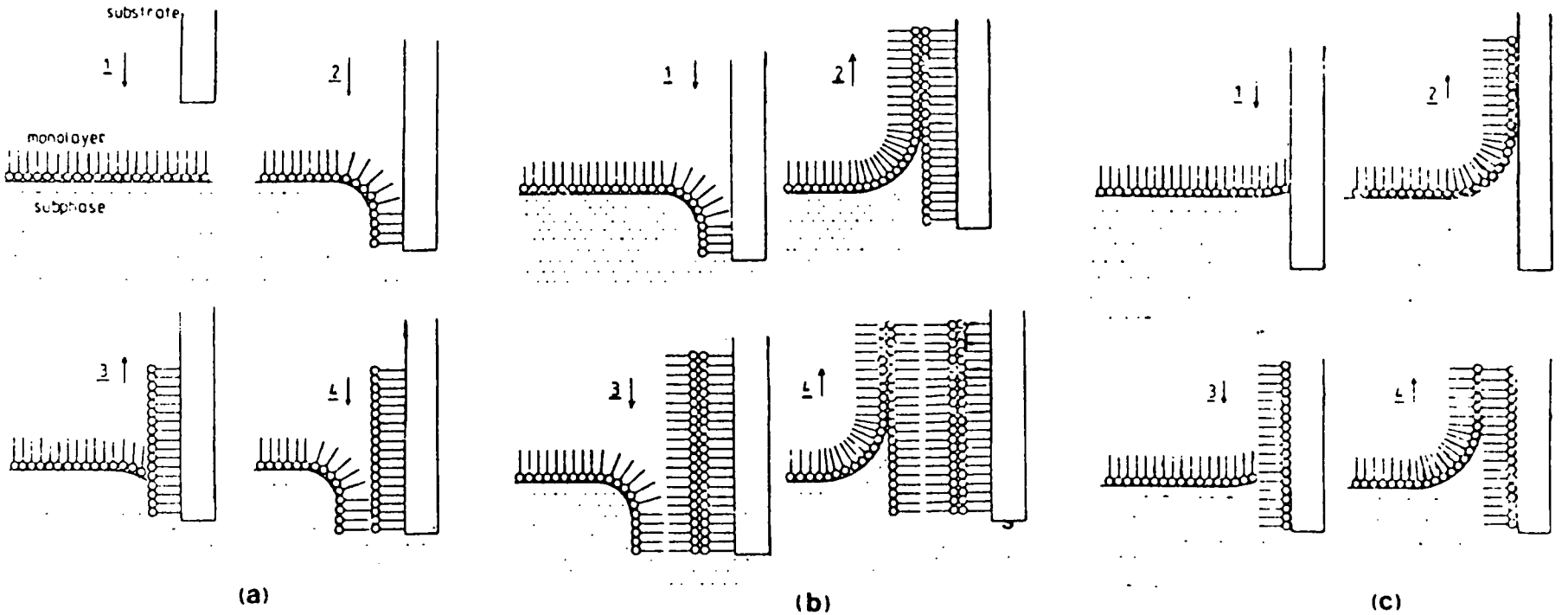

Figure 4.7 The three recognised deposition modes for LB films, (a) X-type, (b) Y-type and (c) Z-type.

the situation where pick up occurs only on the downstroke, sometimes found at extremes of subphase pH levels. Z-type deposition (c), pick up on the upstroke only, had never actually been observed when described by Langmuir and Blodgett. Since then, however, it has been found with some materials(16), but in particular with the asymmetrically substituted copper phthalocyanine used here. The techniques used for Y- and Z-type deposition are described below. The exact dipping conditions for different materials are discussed in detail in Chapter 6.

Y-Type Deposition

The quality of the first monolayer deposited upon a substrate is of particular importance. Not only might faults in the monolayer be propagated into subsequently deposited layers, there is also clearly a fundamental difference between the way it is bonded to the substrate and the way in which succeeding layers bond to each other. For this reason the first layer was always deposited very slowly ($\sim 2.5 mm min^{-1}$), and immediately after the final surface treatment of the substrate (i.e etching, refluxing etc - these treatments are discussed in Chapter 5). As the film was removed from the trough surface during deposition, the feedback system decreased the barrier area to maintain surface pressure. If the surface area of the substrate was known, then deposition ratios (i.e the percentage coverage by a film) could be calculated by monitoring the change in film area against time, or against dipping head position. Examples are shown in Figures 4.8a and 4.8b, where each part of the dipping cycle can be seen as a change in the film

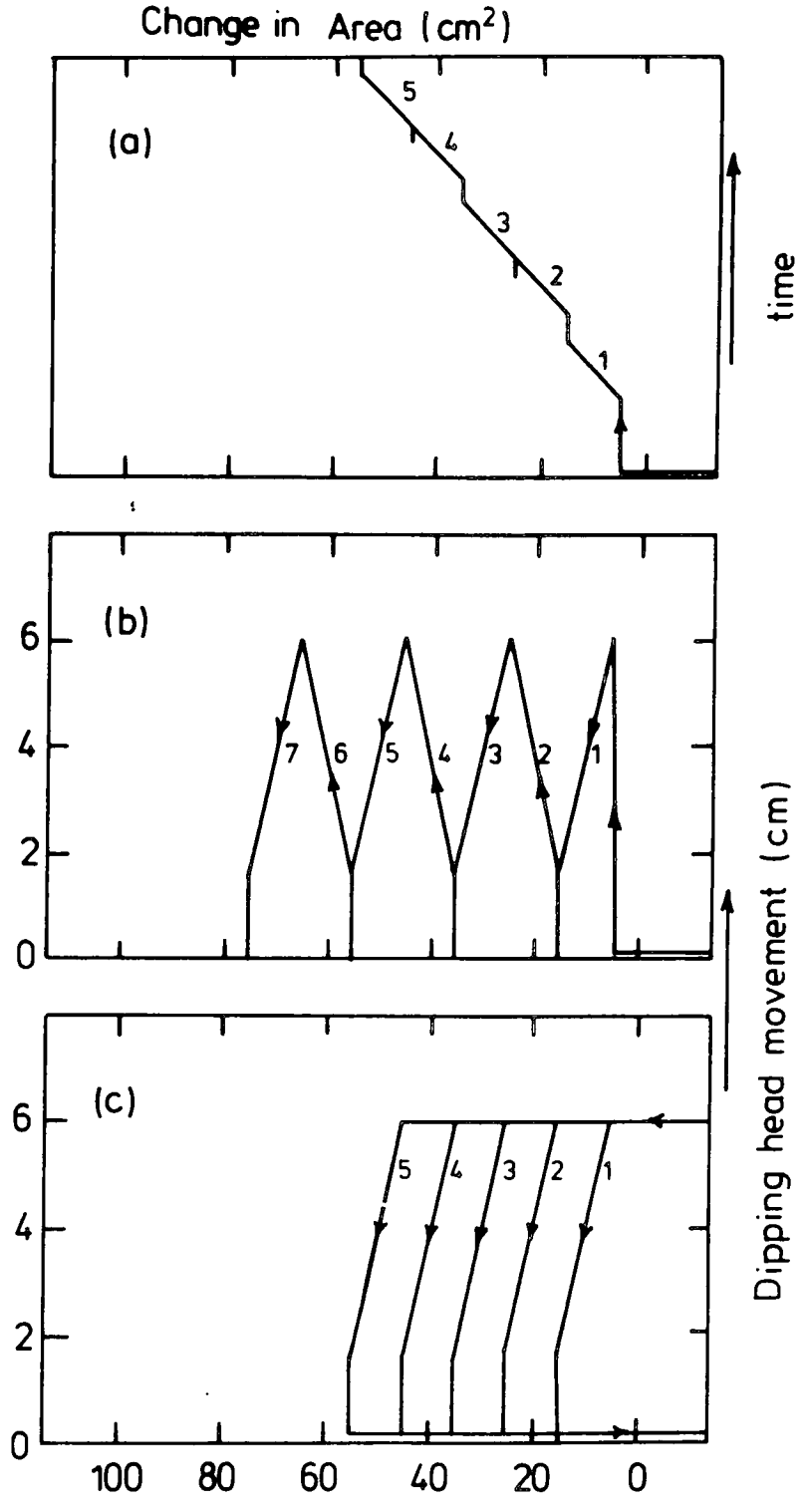

Figure 4.8 Idealised deposition records for (a) and (b) Y-type deposition and (c) Z-type deposition.

surface area.

Z-Type Deposition

Phthalocyanine LB films displaying Z-type deposition required extra precautions. To prevent any partial pick up during the downstroke the film should ideally be removed from the water surface. However, it has been found that simply expanding the film before lowering the substrate into the subphase does not reduce the quality of the films. This was done automatically by the trough control unit as described in section 4.2.2. The slightly different form of deposition record for the Z-type case is shown in Figure 4.8c. In this diagram the surface area changes during the upstroke only - the downstroke occurs with the barrier expanded.

4.5.4 Quality Assessment

There are two widely practised methods for assessing the quality of multilayer LB films. The first is to plot reciprocal capacitance against number of layers in a metal-insulator-metal structure. The standard technique is to deposit an LB film of stepped thickness onto an aluminised glass microscope slide, and then to evaporate on gold top contacts. The total capacitance per unit area, C, will be given by

$$1/C = Nd/\varepsilon_{lb} + d_{ox}/\varepsilon_{ox} \qquad (4.2)$$

where N is the number of film monolayers, d the thickness of a single monolayer and ε_{lb} the permittivity of the LB film. A plot of C^{-1} against N should be linear with a slope d/ε_{lb} and an intercept of d_{ox}/ε_{ox} due to the capacitance of the interfacial metal oxide. Alternatively it is possible to

measure optical absorption as a function of film thickness. This technique is particularly useful for dye films absorbing strongly in the visible, and will give a linear characteristic if interference effects are small. The use of this assessment technique is described in Chapter 6.

4.6 LB FILM APPLICATIONS

The study of LB films has been continuing for over half a century, but much of the upsurge in interest during the past decade stems from the realisation that these films have potential for use in electronic and optical devices. For a comprehensive review of possible device applications the reader is referred to (26), and to (27) and (28) for publications on LB film research in general. To give an idea of developments in the field, this section briefly reviews research by the Durham LB film group.

The metal-insulator-semiconductor (MIS) structure is of great interest because of its applications in integrated circuits and planar electronic devices. Only silicon among semiconductors has a native oxide with good insulating properties, but LB films offer an alternative form of insulating layer for others. The Durham group have deposited LB films onto many semiconductors. MIS field effect transistors (FETs) have been fabricated based upon InP(29) and amorphous silicon(30). The narrow band gap materials InSb and HgCdTe have been used in MIS structures with the aim of improving infra-red detectors(31). MIS solar cells based upon CdTe(32) have achieved a significant improvement in efficiency over equivalent Schottky barrier cells. The LB film technique allows this improvement to be conveniently

studied as a function of insulator thickness. In a similar fashion, Batey et al have studied the efficiency of electroluminescent MIS diodes on GaP(33). The electroluminescence results reported here are the logical extension of this work to II-VI materials, which cannot form good p-n junctions and hence require an MIS structure to function as LEDs. Investigations have been carried out into the use of LB films as electron beam resists for microlithography in integrated circuit fabrication. Polymerisable films of ω-tricosenoic acid, which can be deposited upon silicon at speeds as high as $15mms^{-1}$ (15), give far greater resolution than conventional spun photoresists(34). The same material has been used to considerably improve the breakdown strength of silicon - silicon dioxide structures(35).

As well as these primarily passive applications, LB films have potential applications as active layers. Films of semiconducting organic materials are of particular interest. Structures prepared using lightly substituted anthracene have been shown to exhibit electroluminescence and photoconductive properties(36). Phthalocyanines, though used as insulators, have interesting semiconducting properties. With appropriate substitutions it should be possible to obtain films exhibiting p- or n-type conductivity. The electrical conductivity of this material in MIM structures has already been shown to be very sensitive to gas ambients(24). The use of dye molecules in LB films for dye sensitisation(22), as studied in this work, has potential for improving the photoresponse of semiconductors to selected wavelength ranges.

There are also areas in which research is still at an early stage. Within the group attempts are being made to produce piezo- and pyroelectric films by depositing different alternate monolayers to build in a dipole moment, or by X-type deposition of a single material with its own large dipole moment. LB films are being used as insulators in MISS switch structures on GaAs and silicon. Materials are being screened as LB films for use in non-linear optical applications, following reports by Zyss(21) of very high figures of merit for some merocyanine dyes. Finally, a potentially exciting application being investigated for LB films is in the field of biological sensors. FET structures are envisaged incorporating films sensitive to particular ions, enzymes etc. Research is also being followed on an alternative approach: biological species may alter the optical properties of LB films. This is being investigated by studying surface plasmon resonance in LB film structures, which could later be incorporated in optical fibre sensors.

4.7 SUMMARY

This chapter has reviewed the history, technology, requirements, analysis and applications of LB films. In Chapter 6 results are presented for materials investigated here as potential LB films.

CHAPTER 5

EXPERIMENTAL METHODS

In this chapter a general description is given of the techniques used to fabricate and characterise structures when investigating both dye sensitisation and MIS electroluminescence.

5.1 MATERIALS

5.1.1 LB Film Materials

(a) Merocyanine dyes - two merocyanine dyes were deposited onto semiconductor substrates in the course of this research. Figure 5.1a shows 3-carboxyl- 5[2-(3-octadecyl-2-benzothiazolinylidene) ethylidene] rhodanine as supplied by the Japanese Research Institute for Photosensitizing Dyes Co. Ltd. The amphiphilic nature of this material, similar to dyes studied by other workers(1,2), made it a good comparison for less conventional LB film materials. It is henceforth referred to by its catalogue number NK2684.

Figure 5.1b shows the structure of 2-benzyl- 4[2-(1,3,3-trimethyl-2-indolylidene) ethylidene] 1,3-oxazol-5-one, as supplied by Dr D.Thompson of ICI Organics Division. This was found to be the best LB film material of a range of dyes supplied, after characterisation described in Chapter 6. Henceforth it is referred to by its ICI code number SC58497.

(b) Phthalocyanines - the phthalocyanine used in this work was that shown in Figure 4.5b, copper phthalocyanine

(a) NK 2684

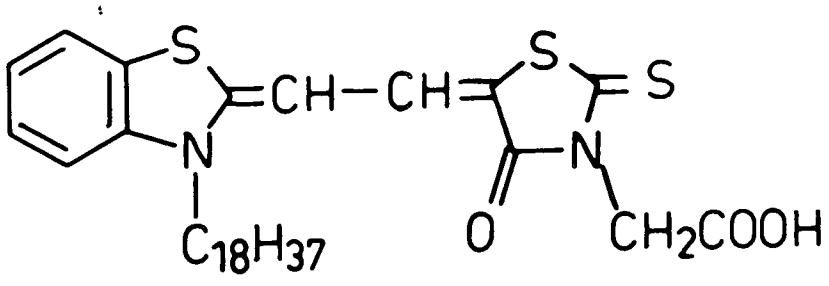

(b) SC 58497

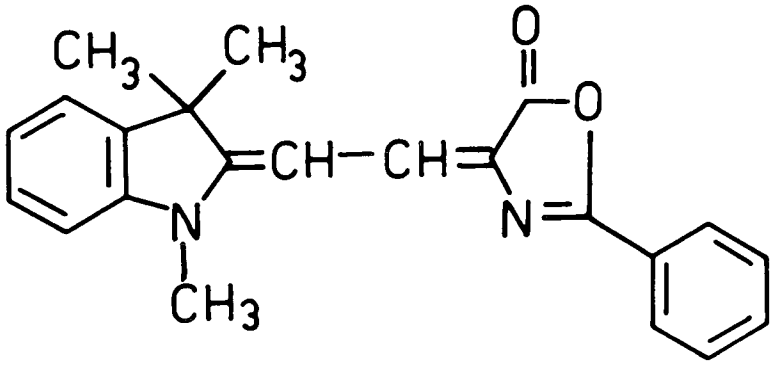

Figure 5.1 The molecular structures of (a) merocyanine dye NK2684 and (b) merocyanine dye SC58497.

tris($CH_2NHC_3H_7$-iso), again supplied by Dr D.Thompson. The characterisation of this material has been described elsewhere(3).

5.1.2 Semiconductor Materials

(a) Zinc Sulphide - in the absence of zinc oxide or silver halides in suitable form for photoconductivity measurements, low resistivity n-type polycrystalline zinc sulphide was obtained from Mr A.E.Thomas of this department. Having a bandgap ~3.7eV it was thought a suitable material for studying dye sensitisation effects. The production of this material in low resistivity form, and the making of ohmic contacts to it, is a complex problem, but surmountable(4). As supplied, samples were cut to an approximate size 8mm x2mm x1mm with 2mm surface ohmic contacts at either end of the largest face.

(b) Zinc Selenide Sulphide - this material was used for the investigation of MIS electroluminescent structures incorporating LB films, and was supplied by Dr P.J.Wright of the Royal Signals and Radar Establishment (RSRE), Malvern. The samples used consisted of thin (~3μm) film single crystal layers of $ZnSe_xS_{1-x}$ (x~0.94) grown on n-type GaAs (100) substrates by the technique of organometallic chemical vapour deposition (MOCVD)(5). The films had a carrier concentration $\sim 10^{18}$ cm^{-3}. This alloy composition was used to optimise the lattice match of the film with the GaAs substrate - ZnSe (lattice constant 5.6686Å) does not match perfectly with GaAs (lattice constant 5.6535Å). Preliminary measurements by Batey(6) with pure ZnSe films had indicated a large series resistance associated with the GaAs-ZnSe interface which

severely limited device efficiency.

5.2 MEROCYANINE-SEMICONDUCTOR DEVICE FABRICATION

As stated in Chapter 4, cleanliness is of paramount importance in the production of structures incorporating LB films. Through all fabrication stages described in this section precautions were taken to avoid contamination of samples and materials. Disposable polythene gloves were worn whenever handling materials or working in the Langmuir trough. Glassware was cleaned prior to use in an ultrasonic bath with chromic acid, 'Decon 90' detergent and purified water. Surface preparation of substrates was carried out in a fume cupboard in the clean room immediately before film deposition. Film materials were stored with desiccants in a refrigerator when not being used. Between measurements, devices incorporating LB films were stored under a low pressure of dry oil-free nitrogen. Specific procedures are described below.

5.2.1 Surface Preparation

Prior to surface etching, the zinc sulphide structures as supplied were cleaned for several hours in boiling isopropyl alcohol in a Soxhlet refluxing system to ensure thorough degreasing. Because of their small size these samples were mounted using 'Lacomit' onto degreased glass microscope slides. 'Lacomit' was also used to protect the surface ohmic contacts. The samples were then etched for 2 minutes in a 2% solution of bromine in methanol, stirred gently. After diluting this solution down to pure methanol in stages, the samples were rinsed in carbon disulphide for

about 10 minutes to remove surface residues left by the bromine. Finally, before film deposition the samples were washed in absolute ethanol for another ten minutes.

5.2.2 LB Film Deposition

Immediately after surface preparation, merocyanine LB films were deposited upon the samples using the techniques described in Chapter 4. For both dyes NK2684 and SC58497 deposition conditions were identical - a dipping speed of 2.5 mmmin^{-1} at a surface pressure of 25 mNm^{-1}. The subphase, at a pH of 5.7±0.2 and temperature 18±2°C, contained approximately 2.5x10^{-4}M cadmium chloride. Both dyes were deposited mixed with arachidic acid at a molar ratio of 1:1. The choice of these deposition conditions is discussed in Chapter 6.

5.3. MIS DEVICE FABRICATION

The standards of cleanliness described in the previous section were also applied to the preparation of these devices.

5.3.1 Ohmic Contacts

The ZnSeS samples as received were initially cleaned for several hours in a Soxhlet system. If necessary, they were cut into smaller pieces using a diamond tipped scribe. Small (~1mm diameter) preformed contacts of 99.999% pure indium wire (Koch-Light) were attached to the rear face of the GaAs using a Weller variable temperature soldering iron set at 250°C. These contacts were annealed by heating the samples

to 275°C for 15 minutes in a nitrogen ambient. At least two contacts were made to each sample so that they could be checked for ohmicity using a transistor curve tracer.

5.3.2 Surface Preparation

Surface preparation of samples was identical to that for the zinc sulphide crystals, save that they were only etched for 30 seconds in a 1% solution of bromine in methanol. It was estimated that this would remove <1μm of ZnSeS from the surface of the sample. Where near-ideal Schottky barrier structures were being fabricated for comparison with MIS, top electrodes were immediately evaporated as described in 5.3.4.

5.3.3 LB Film Deposition

Immediately after etching, LB films of the asymmetrically substituted copper phthalocyanine were deposited using the 'auto' mode technique described in Chapter 4. Films were deposited at 2.5 mmmin^{-1} at a surface pressure of 30mNm^{-1}. The subphase was at a pH of 8.0±1.0 and temperature of 18±2°C, and contained ~5% absolute ethanol. These conditions are currently believed to be the optimum for the deposition of this material(7). Immediately after film deposition the substrates were stored for two days under a low pressure of dry nitrogen to aid the removal of any residual water or organic solvents.

5.3.4 Electrode Deposition

Top electrodes were made by evaporating 99.999% pure gold (Johnson-Matthey) from a molybdenum boat at a pressure <10^{-6} torr in an Edwards 306 evaporation system. The rate of

evaporation and thickness of deposited material was monitored using a quartz crystal thickness monitor. A total thickness of 15nm of gold was deposited in steps of 1nm at a rate of ~0.5nmmin^{-1}. Steps were deposited at least 30 minutes apart, and between steps the sample was shielded from the metal source by a shutter. These precautions were aimed at limiting the heat damage to the LB films. Electrodes were defined by affixing the substrates to brass contact masks - these had accurately drilled apertures of diameter 0.5mm or 1mm.

5.4 MEROCYANINE-SEMICONDUCTOR DEVICE CHARACTERISATION

The structures used for this investigation were of the form shown in Figure 5.2. Enamelled copper wires were connected to the ohmic contacts using conducting silver paste (Electrodag 915), and these flying leads soldered to terminals as appropriate for electrical measurements. The sample was kept mounted on a glass microscope slide to aid handling.

5.4.1 Film Characterisation

All optical characterisation of merocyanine LB films was carried out with the films deposited upon glass slides. Optical absorption spectra of films and their parent solutions were compared using a Cary 2300 UV-VIS-NIR spectrophotometer. Fluorescence spectra of films, both emission and excitation, were measured using a Spex system at RSRE, Malvern.

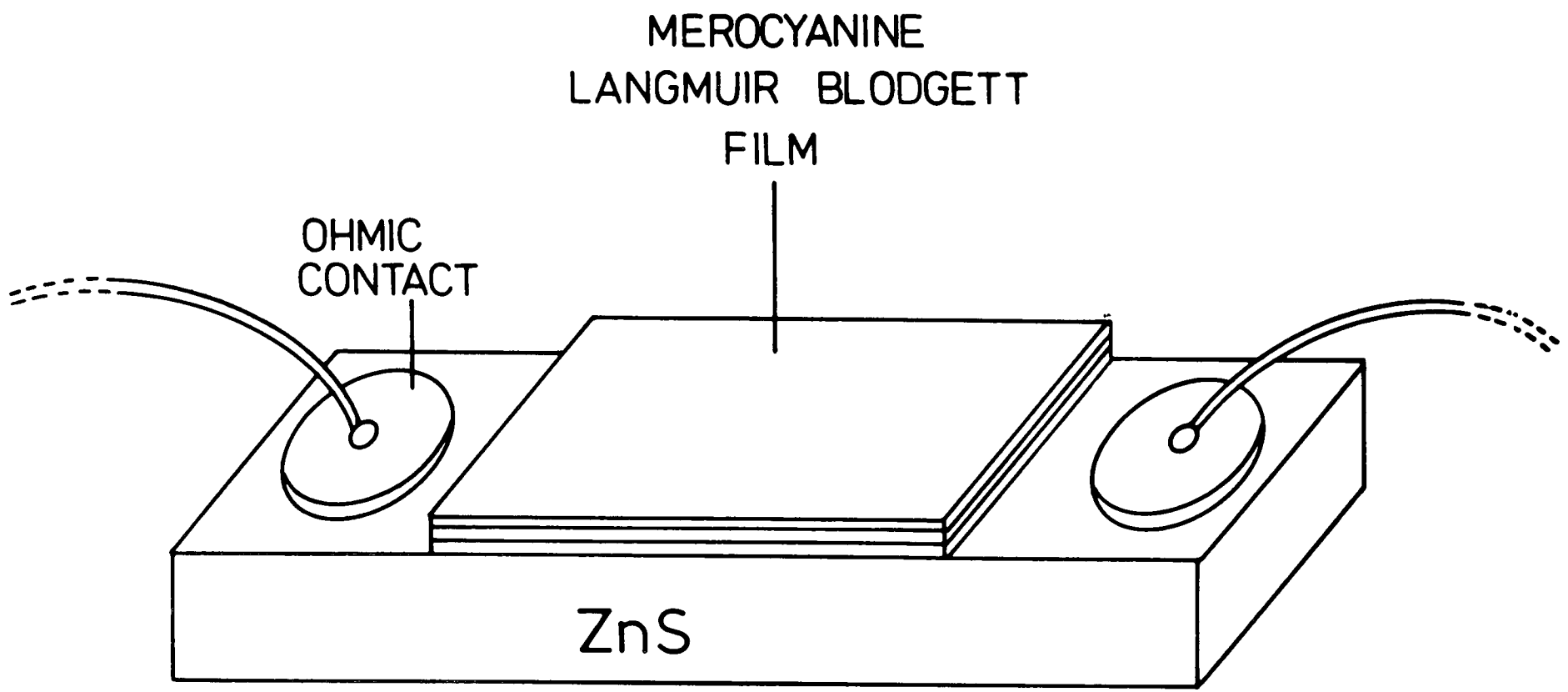

Figure 5.2 Schematic diagram of the device geometry used for dye-sensitisation studies.

5.4.2 Photoconductivity Measurements

For dc photoconductivity measurements the sample was mounted in an Oxford Instruments DF 704 cryostat, and the flying leads soldered to terminals which allowed remote electrical access. The sample was connected to a Time Electronics 2003S dc voltage calibrator and a Keithley 410A picoammeter to allow measurement of conductivity at different biases. It was illuminated through the window of the cryostat by a Bausch and Lomb (33-86-02) high intensity (250W) tungsten source and monochromator. The spectral response of the system was taken into account by calibration with an Oriel 3810 thermopile and a Keithley 181 naovoltmeter. Second order effects were eliminated by using Optics Technology high pass optical filters. Measurements could be made at temperatures down to 77K by evacuating the cryostat with a two-stage vacuum pump, and feeding liquid nitrogen via a supply tube to a copper heat exchanger. A chosen temperature was maintained by an Oxford Instruments DTC2 temperature controller.

5.5 MIS DEVICE CHARACTERISATION

The structures investigated were as shown schematically in figure 5.3. For each film thickness all measurements were made for a number of contacts (at least six) to assess the reproducibility of results.

5.5.1 Electrical Measurements

Most measurements were made in a sealable brass sample chamber, which eliminated the effects of light and electrical interference. Samples were mounted onto a perspex block to

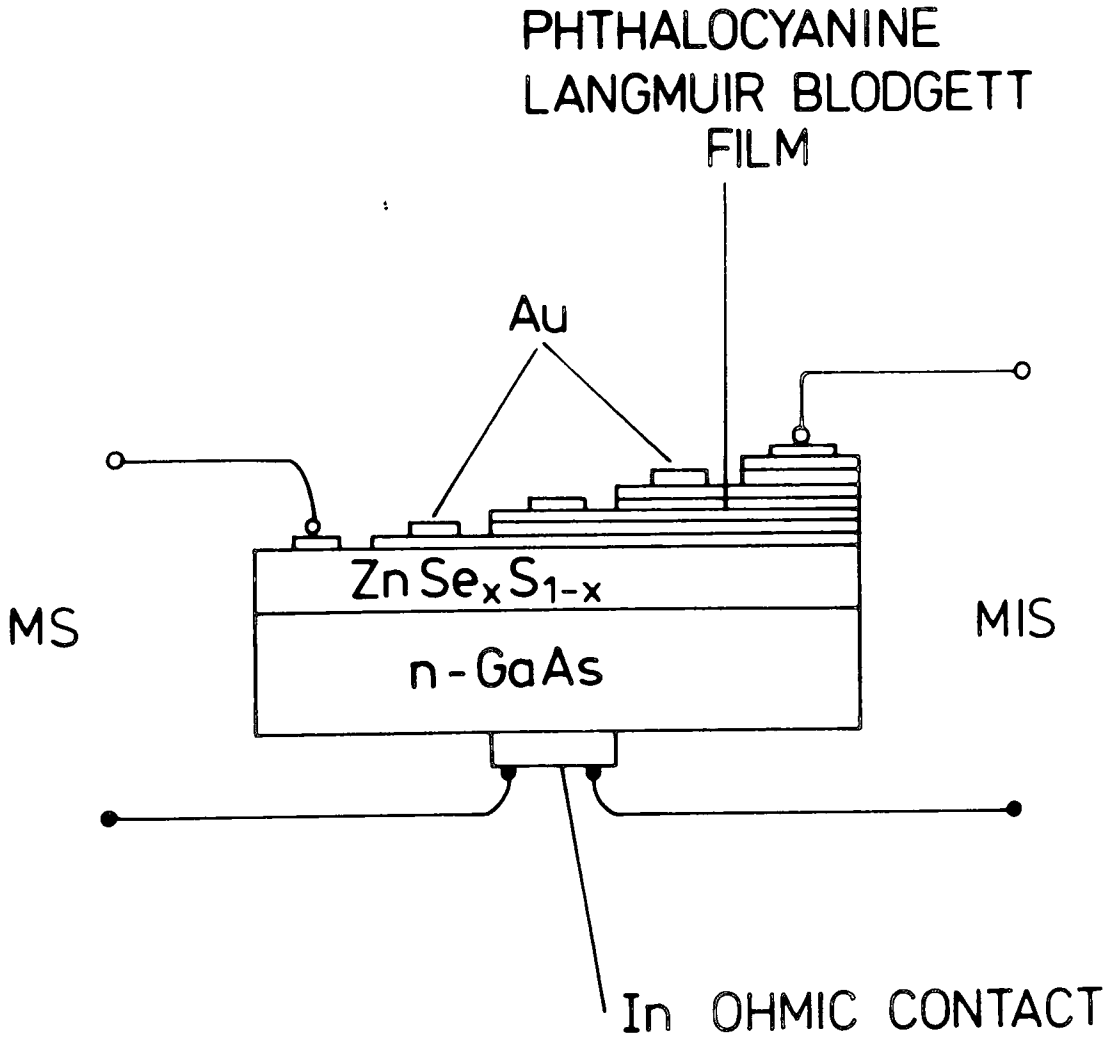

Figure 5.3 Schematic diagram of the device geometry used for studying MIS electroluminescent devices.

which was screwed a metal tag. Enamelled copper wire was soldered to this and connected to an ohmic contact with conducting silver paste. A crocodile clip could be attached to the tag to allow remote access to the back contact. Top contacts were made with a micromanipulator attached to a thin gold wire. The end of the wire was fused into a spherical contact <0.5mm diameter. This was lowered onto the chosen top electrode to make contact.

Bias voltages were set using a Time Electronics 2003S dc voltage calibrator. Currents were measured using a Keithley 410A picoammeter - this had an analogue voltage output which was connected to an X-t chart recorder to ensure equilibrium values were being attained. Capacitance was measured with a Boonton 72BD capacitance meter - this used a 1MHz measuring signal, and a dc bias could be applied to its terminals to facilitate capacitance vs voltage measurements. For drive currents beyond the range of the 2003S, a Keithley 220 programmable constant current source was used and bias voltages monitored with the Keithley 181 nanovoltmeter. Photoresponse measurements were made by directing light from the high intensity monochromator down an optical fibre light pipe onto the device being studied. This was again calibrated with the thermopile.

5.5.2 Optical Measurements

Electroluminescent spectra were recorded by directing light from devices, via the optical fibre link, to a Hilger and Watts D330 motor driven monochromator. The output from the monochromator was monitored with an EMI 9558QC photomultiplier tube, via the analogue output of a

picoammeter to an X-t chart recorder. Intensity and efficiency measurements were made by affixing the sample to a small purpose-built mounting adjacent to the photomultiplier tube window.

CHAPTER 6

RESULTS AND DISCUSSION

MEROCYANINE LB FILMS AND DYE-SENSITISATION

6.1 INTRODUCTION

This chapter is an account of attempts to find and develop a merocyanine dye for use as a novel LB film material. The intention of the research was to show that it is possible to deposit such an LB film onto a semiconductor to achieve dye-sensitisation, i.e increase its photoresponse to light with photon energies less than its bandgap energy. The principles of dye-sensitisation have been discussed in Chapter 2. The results of this research have been partially successful, inasmuch as a novel material has been selected by screening and been shown to be capable, with optimised conditions, of forming good quality, fairly stable LB films. The failure to obtain a wholly suitable semiconductor material to some extent thwarted attempts to demonstrate dye-sensitisation, though some success was achieved through the observation of a relatively small change in the photoconductivity of zinc sulphide.

The chapter consists of three sections: the screening and characterisation of materials for use as LB films, the deposition of dyes and their properties in LB film form, and finally the results of the work on dye-sensitisation.

6.2 CHARACTERISATION OF DYES AS LB FILMS

The required properties of a material for it to form

good LB films have been discussed in some detail in Chapter 4. However, deducing these properties from the molecular structure of a material is currently still a largely empirical process. Hence, to isolate suitable materials from those available requires a screening procedure, as has been previously described. It is to be hoped that as the properties of organic monolayers become better understood, this difficult and time-consuming work will be reduced or even eliminated. This section presents the results of such a procedure.

6.2.1 Pressure-Area Isotherms

An isotherm with distinct phases in its structure, that of stearic acid, has been shown in Figure 4.6a. If a material forms a monolayer when spread on the water surface of a Langmuir trough, plotting an isotherm (as it is compressed) gives clues to its behaviour compared to that of an ideal material. Figure 6.1 shows an isotherm for the material NK2684. It is clear that even though the molecule has a long hydrocarbon chain and distinct hydrophobic and hydrophilic regions, the shape of the curve lacks the structure seen with stearic acid. The gentle slope with increasing pressure is an indication that the molecules are probably lying nearly flat on the water surface when uncompressed, and only gradually altering their orientation such that the hydrocarbon chain points vertically upwards. Only at pressures $>30mNm^{-1}$ does the film appear to be entering a quasi-solid phase region characterised by increasing steepness of the curve. This material and many other dyes with similar amphiphilic substitutions have been

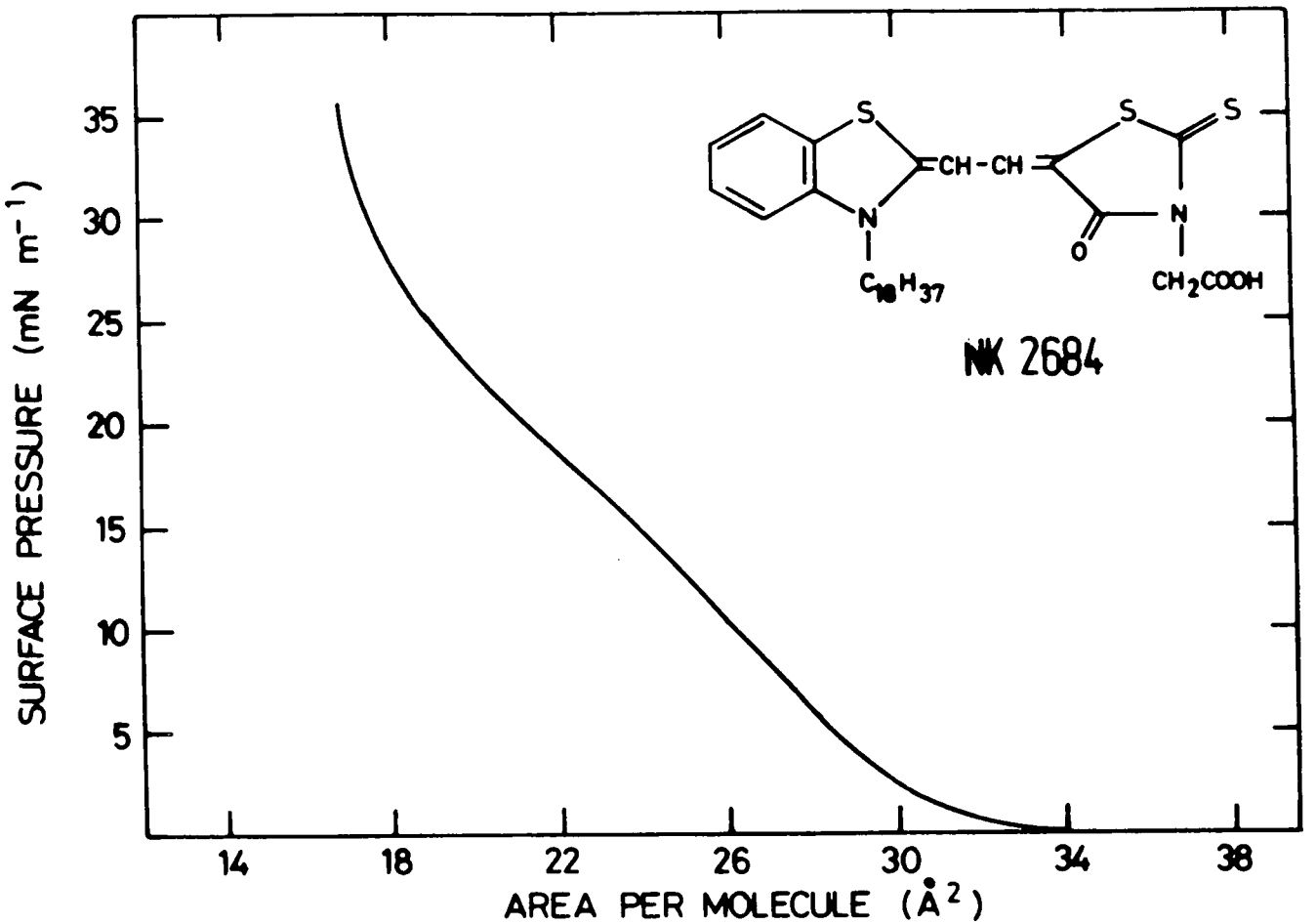

Figure 6.1 Pressure-area isotherm for a film of merocyanine dye NK2684.

used by other workers studying dye LB films(1). Invariably they report the necessity of forming a mixed monolayer with arachidic or stearic acid in order to produce good quality LB films. These mixtures are of a molecular ratio acid:dye of at least 2:1, though for some dyes the ratio is 10:1 or even higher(2).

The desire to develop a merocyanine LB film without long-chain substitutions, and their consequent dilution of the electrical and optical properties of the dye's constituent ring structures, was a primary aim of this research. To this end, samples of twenty-four unsubstituted merocyanine dyes were obtained from ICI Organics Division for screening. This initial stage of this process was to study the relative polarity of substituents incorporated in their molecular structure. From this it was possible to rank the materials in order of their probable relative solubility at the air-water interface. For each material a solution of concentration ~1mgcm^{-3} was made in an organic solvent (usually chloroform). A small amount of this solution was spread over the water surface of the Langmuir trough as described in Chapter 4. The majority of the dyes spread performed very poorly as Langmuir films under compression, causing only minimal changes in the surface pressure as they collapsed, and dissolving rapidly into the subphase. The properties of films of the eight dyes which performed best are summarised in Tables 6.1 and 6.2. Listed by their ICI code numbers. The colours referred to are those of the spreading solutions. Where a film is referred to as 'blotchy' or 'flaky' this implies that it has visibly failed to spread evenly over the surface of the water, and will

SC 19095

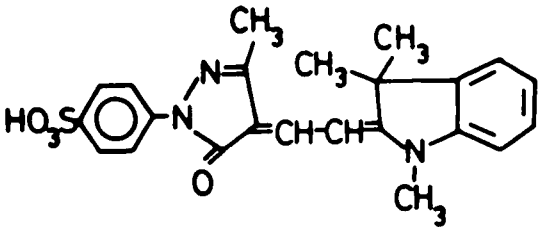

SC 20075

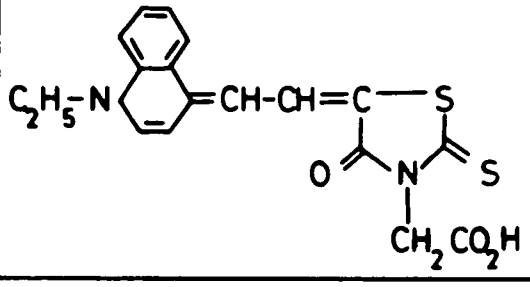

SC 25424

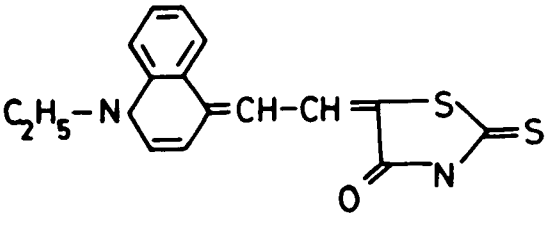

SC 61714

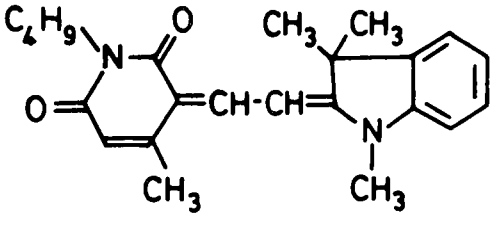

SC 68781

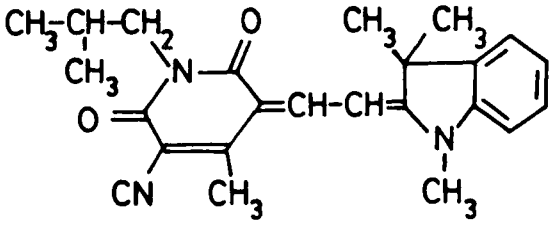

SC 58497

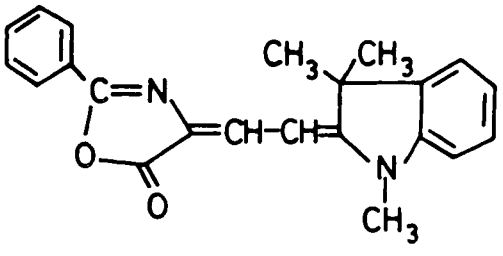

SC 24887

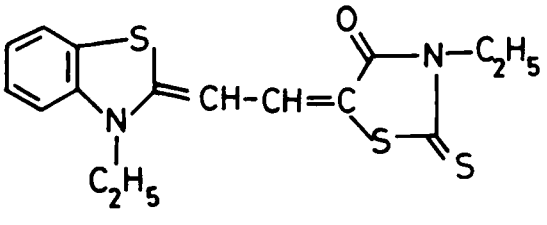

SC 11748

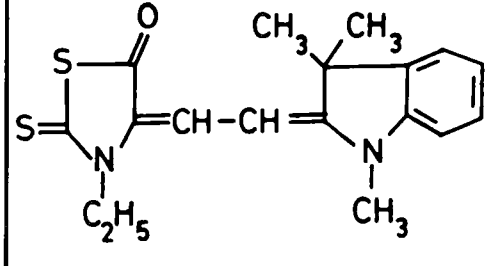

Table 6.1 Structural formulae of merocyanine dyes selected for screening as LB film materials.

Dye	Solubility	Colour	Film Quality	Stability
SC 19095	Readily in $CHCl_3$	Yellow	Poor (Flaky)	Poor (dissolved rapidly)
SC 20075	Readily in acetone. Deposited in 50/50 acetone/$CHCl_3$ mixture	Blue	-	Highly soluble in subphase
*SC 25424	Very readily in $CHCl_3$	Purple	Visible-promising isotherm	Broke up under pressure of 40 dyn/cm - collapse rate $\sim$ 15 cm^2/minute
*SC 61714	Readily in $CHCl_3$	Bright Red	Visible - reasonable isotherm	Collapse rate $\sim$ 4.5 cm^2/minute @ 40 dyn/cm
*SC 68781	Fairly in $CHCl_3$	Red	Visible - reasonable isotherm	Collapse rate $\sim$ 15 cm^2/minute @ 40 dyn/cm
*SC 58497	Readily in $CHCl_3$	Orange	Visible - very promising isotherm (n.b. film appears pink)	Collapse rate $\sim$ 6 cm^2/minute @ 40 dyn/cm
SC 24887	Readily in $CHCl_3$	Magenta	Faint and blotchy - poor	-
SC 11748	Readily in $CHCl_3$	Red/Orange	Very poor (blotchy)	-

Table 6.2 Performance of merocyanine dyes as Langmuir films.

certainly not be forming a monolayer. The approximate collapse rates referred to are from an initial surface area $\approx 600 cm^2$ (n.b 1 dyn/cm = 1 mNm^{-1}).

Isotherms for the best four of the dyes listed in the table (indicated with an asterisk) are shown in Figures 6.2 to 6.5. The areas per molecule are calculated using a simple relationship. The abscissa of an isotherm as recorded is calibrated against the water surface area (A) enclosed by the trough barriers. If the concentration of the spreading solution (C) is known accurately through careful weighing, the volume (V) of solution spread is measured and the molecular weight (M_m) of the molecule obtained, the molecular area can be calculated as

$$A_m = AM_m/CVN_A \qquad (6.1)$$

where N_A = Avogadro's number. For this to be the surface area occupied by one molecule does of course require that the spread film be one molecule thick. It is conventional with Langmuir films to assign an area per molecule in the solid phase by extrapolating the steep, linear, high-pressure region of the isotherm to zero pressure. Two of the problems when making this calculation in practice are that some of the material spread may have dissolved into the subphase and that there is no proof that the film exists as a monolayer. These are demonstrated by the isotherms for dye SC61714 shown in Figure 6.2. Curve (a) results from an initial compression and curve (b) from a subsequent recompression soon afterwards. The lower steepening parts of the characteristics can be assigned to compression of the molecules lying lengthways on the water surface, followed by a process as the pressure passes ~20mNm^{-1} where the molecules

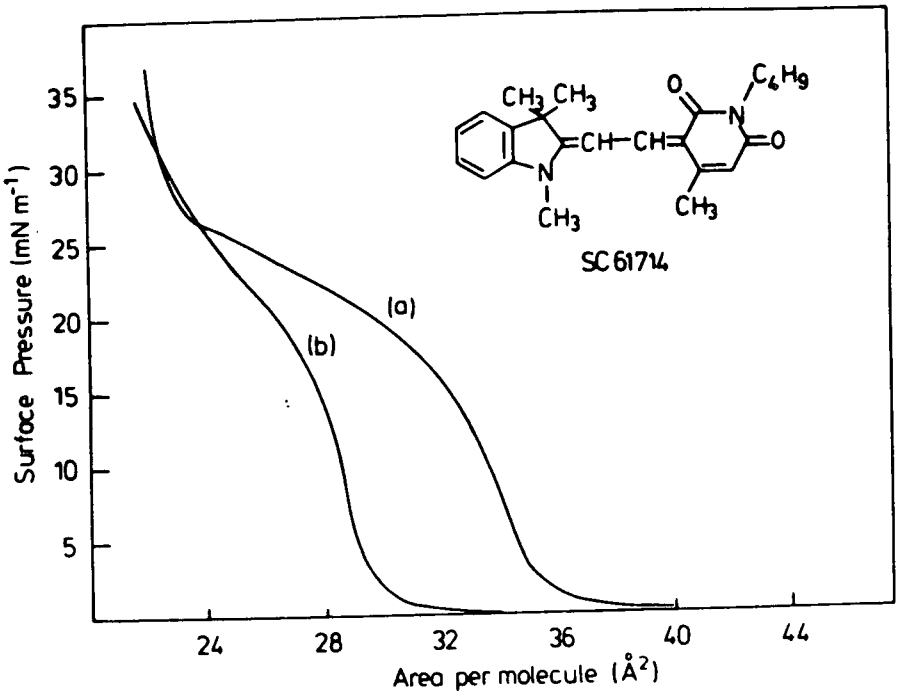

Figure 6.2 Pressure-area isotherm for a film of merocyanine dye SC61714. (a) first compression. (b) subsequent compression.

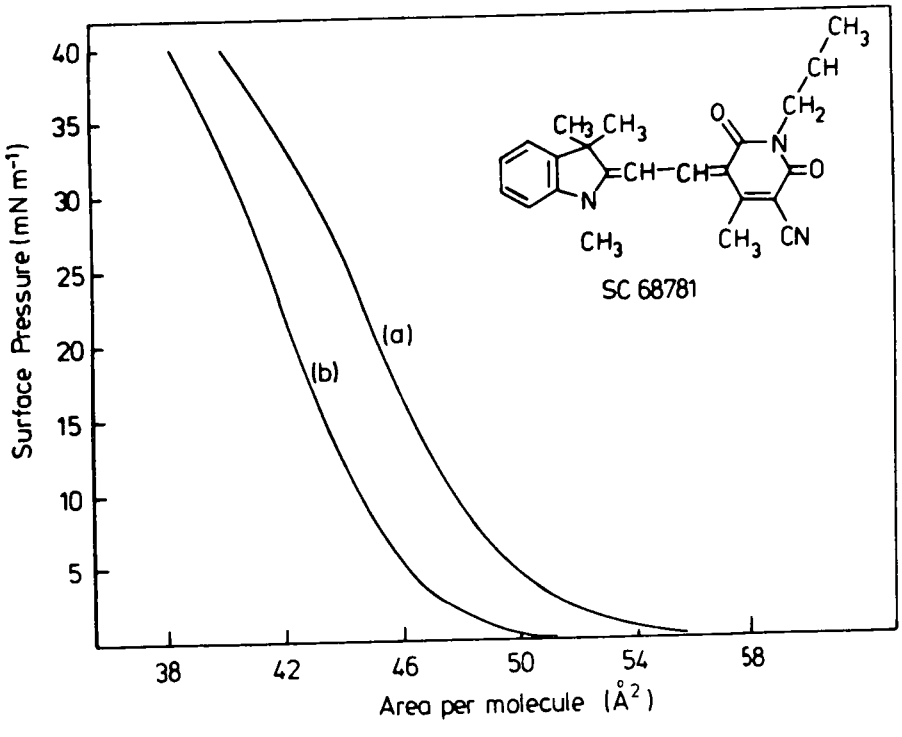

Figure 6.3 Pressure-area isotherm for a film of merocyanine dye SC68781. (a) first compression. (b) subsequent compression.

turn to stand vertically (i.e with the methine link perpendicular to the water surface). Further compression shows the beginning of a clearer solid phase region. The shift between the two curves is primarily caused by the loss of material as it dissolves into the subphase. Since this dissolution will commence from the time the film is spread, molecular areas calculated in terms of the amount of dye solution deposited will be somewhat lower than the true value.

The isotherms for dye SC69781 (Figure 6.3a and b) have been interpreted in a similar fashion. In view of the molecular areas calculated and the relatively gentle slope of the curves up to a surface pressure of $40mNm^{-1}$ the molecules are thought to remain lying lengthways on the water surface. At this pressure the rate of dissolution of the dye is too high to make it convenient for LB film deposition.

The isotherm for dye SC25424 (Figure 6.4) behaves well at low surface pressures ($<20mNm^{-1}$) but degrades badly as surface pressure is increased. The deviation of the curve here is assigned to the structure of the film breaking up (i.e molecules piling up on each other). At a pressure of $40mNm^{-1}$ striations were visible in the film, i.e dark lines of dye material parallel to the moving edges of the barrier). It is possible that the lack of many side groups on the molecules limit the cohesion between them in a monolayer.

The best isotherm obtained for any of the materials screened was that of dye SC58497 (Figure 6.5). Although lacking the clear breakpoints between phases of an ideal material, it shows a very steep condensed phase region for surface pressures $\gtrsim 5mNm^{-1}$. The calculated molecular area

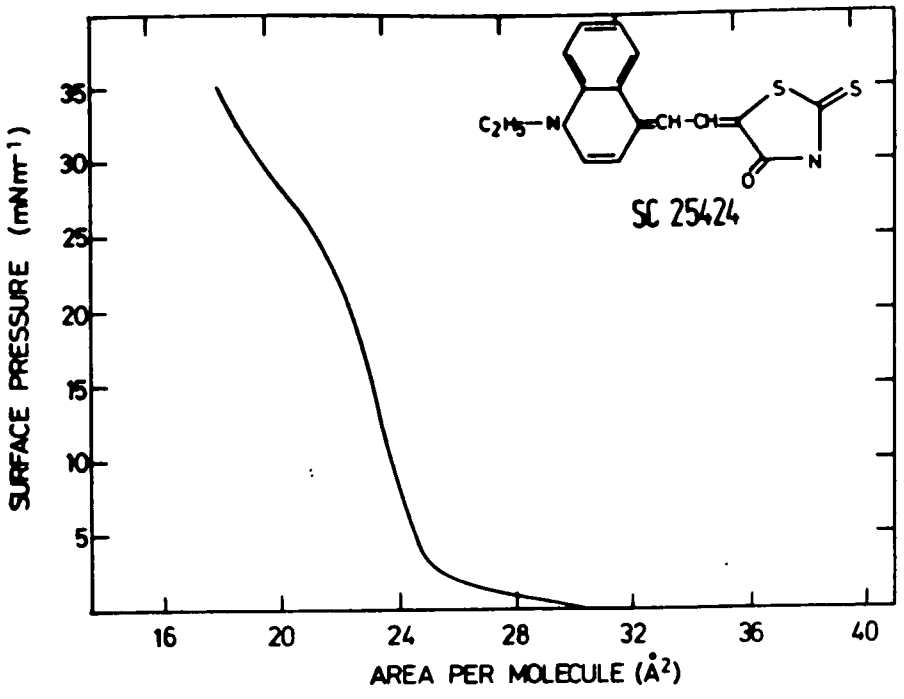

Figure 6.4 Pressure-area isotherm for a film of merocyanine dye SC25424.

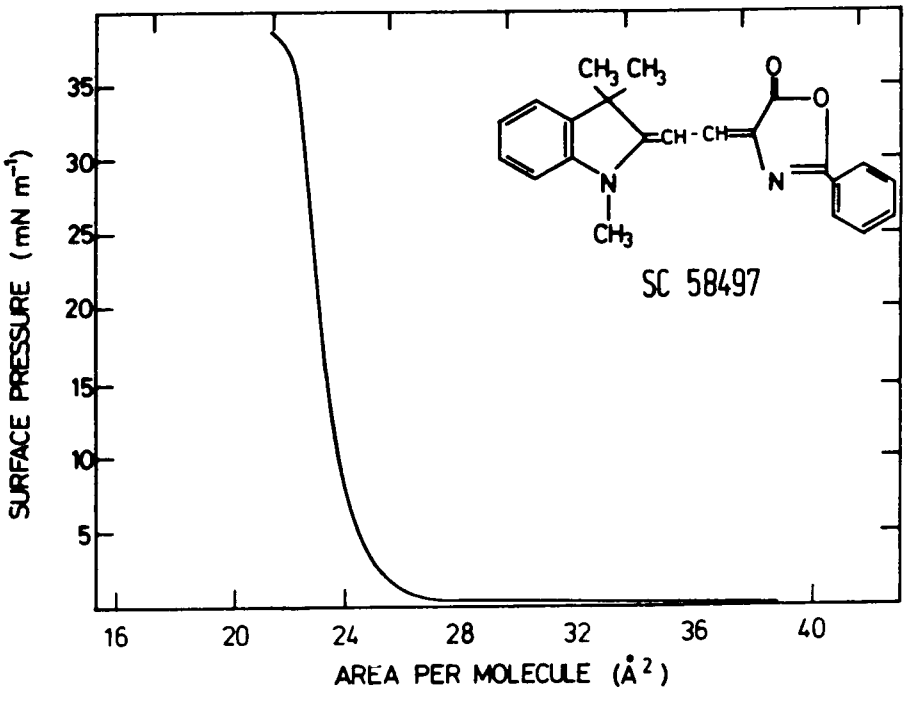

Figure 6.5 Pressure-area isotherm for a film of merocyanine dye SC58497.

seems to indicate the molecules are standing vertically immediately the film is compressed. The dye did not have the lowest collapse rate of those screened at high pressures, but this was measured beyond the pressure at which the film begins to break up ($\sim 35 mNm^{-1}$), as the top end of the characteristic shows. At lower pressures the film was far more stable, the collapse rate reduced by almost an order of magnitude at $25 mNm^{-1}$. In view of these superior qualities, subsequent film characterisation was devoted to this material.

6.2.2 Molecular Arrangement

Having chosen to concentrate upon the dye SC58497, it was necessary to establish that the above speculations regarding its behaviour on the water surface could be further justified. To this end a computer model of the dye molecule was generated using the program package PLUTO, available through the NUMAC computer system at Durham University. Relative atomic coordinates were calculated from standard bond angles and distances(3), to produce diagrams of the form shown in Figure 6.6. These diagrams of the molecule, which could be presented at any angle, allowed its dimensions to be established as shown. They gave a far clearer picture of the true shape of the molecule than the simple structural chemical formula. Although the overall height (10Å) and width (6Å) of the molecule seem to contrast with the experimentally measured area of $25 Å^2$, its effective dimensions are clearly reduced by allowing for close packing of a continuum of molecules in a monolayer. In order to demonstrate this close packing, space-filling Corey-Pauling

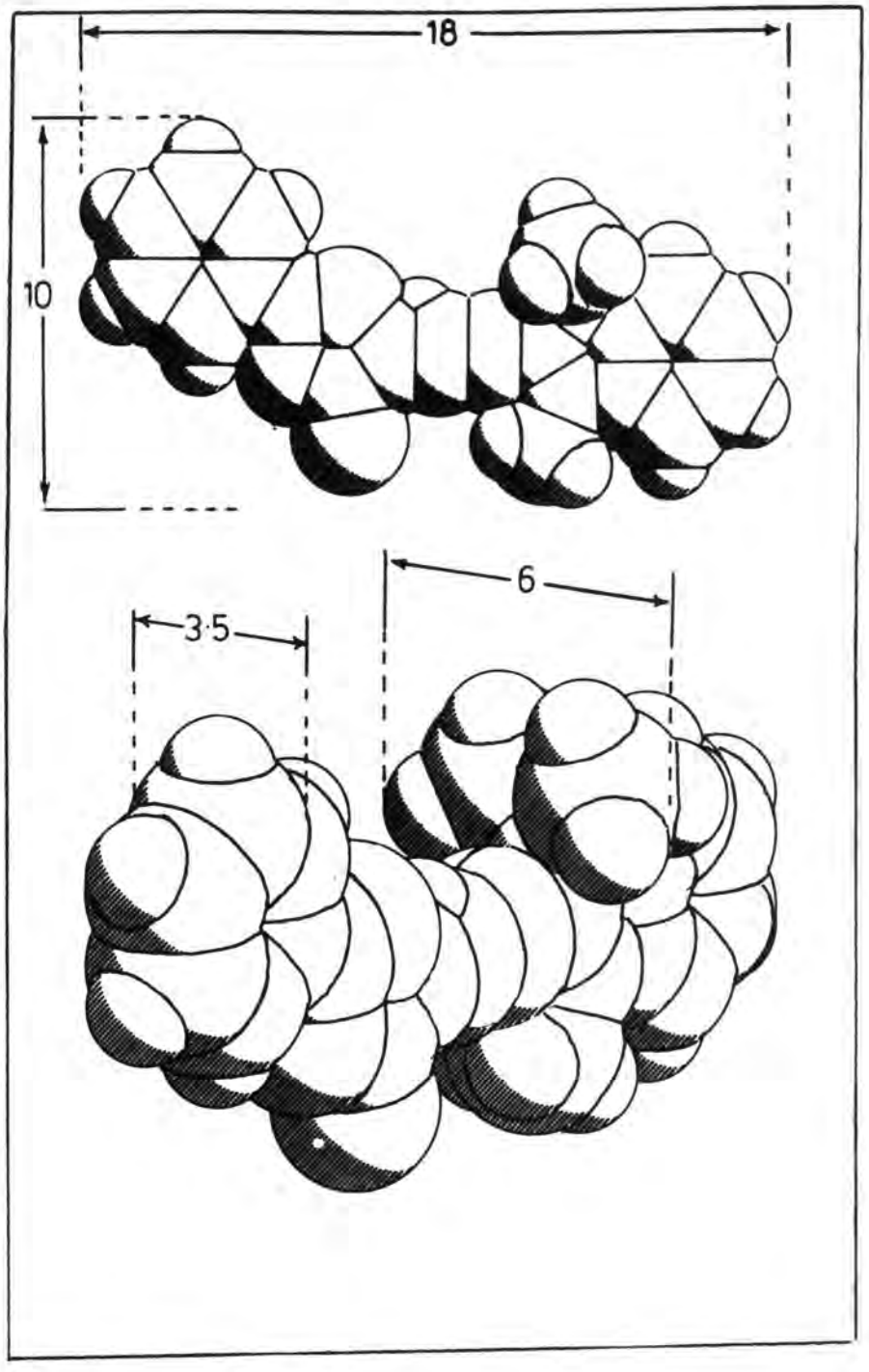

Figure 6.6 Computer generated diagrams of merocyanine dye SC58497 showing molecular dimensions in Angstrom units.

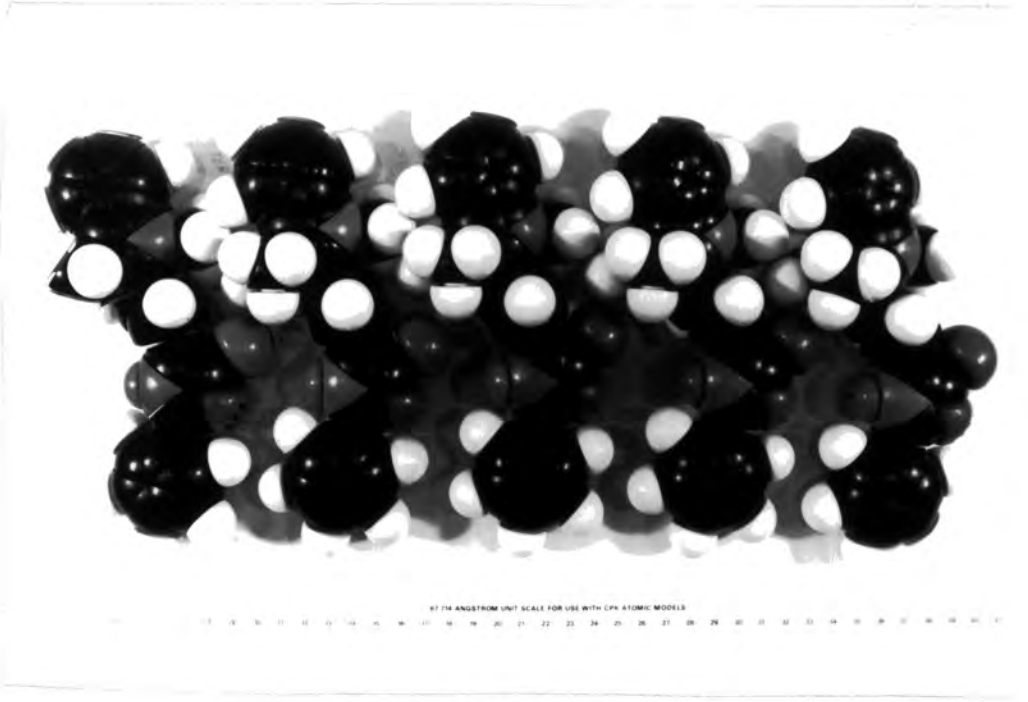

(A)

(B)

Figure 6.7 Space-filling molecular models of merocyanine dye SC58497 showing a possible stacking arrangement, (a) plan view, (b) angled view.

molecular models (Ealing Ltd) were assembled and stacked together. Figures 6.7a and b are photographs of these models. As stacked, the molecules would occupy an area 7Å x 4Å, a molecular area of 28Å^2. This seems to confirm the experimentally determined value when allowance is made in for the error in that due to film collapse.

6.2.3 Collapse Mechanisms

The rate of collapse of films of dye SC58497 was not considered fast enough to hinder its deposition as an LB film. However, it was considered worthwhile investigating the rate of dissolution as a function of the conditions in the water subphase, in case optimisation of these conditions were possible. Although temperature may have some effect, only the pH of the water can conveniently be varied with the Langmuir trough used for this work. It has previously been reported that the solubility of Langmuir films of lightly substituted anthracene is much reduced at low values of pH(4). With other factors (temperature, compression rate, etc) kept as uniform as possible, the change in film area with time was plotted for various values of pH (Figure 6.8). The collapse process in each case can be seen to commence with relatively rapid dissolution, followed by a process obeying equation 4.1, i.e $\ln(N) = -kT + C$. It was apparent that decreasing the pH of the subphase was more likely to accelerate film collapse; an increase had no detectable effect. Thus the subphase was subsequently maintained at the standard dipping pH = 5.7±0.2 when using this material.

Although films of this dye were adequately stable on the water surface, to be useful as LB films they must be

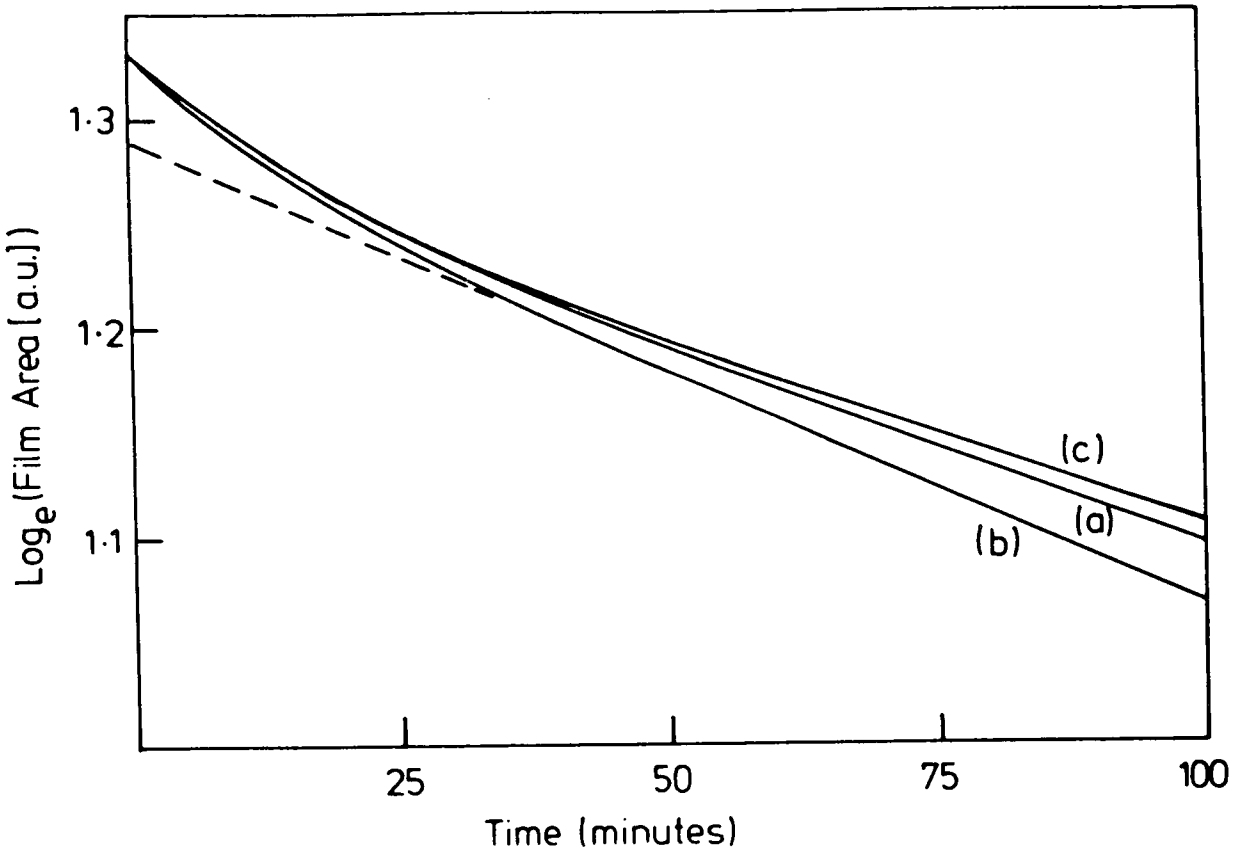

Figure 6.8 Collapse of a Langmuir film of SC58497 with time. Subphase at (a) pH = 4.1. (b) pH = 4.5 and (c) pH = 5.5 or 7.3.

transferred to a substrate. The deposition system used requires that the film as a whole responds rapidly to the removal of material from the film. Using the 'suction test' films were found to respond poorly, behaving almost like a rigid sheet. A useful parallel is that of a thick sheet of ice on water. A good LB film material must be far more mobile, more like a flexible, floating carpet. A number of mixing agents were tried to improve the film responsivity, but many of these were themselves poor as film materials. For example, the alkane nearest in size to SC58497, dodecane, did not even register a molecular area when a mixed solution was spread. The best mixing agents were, not surprisingly, long chain fatty acids. A mixture with a 1:1 molecular ratio of arachidic acid to dye was found to respond to pressure changes sufficiently quickly for dipping to be undertaken at normal speeds. This mixture was used throughout the subsequent investigations of LB films.

6.3 LB FILMS OF MEROCYANINE DYES

This section presents the results of measurements made on deposited LB films. After describing the dipping properties of the dyes SC58497 and NK2684, the optical characteristics of multilayers of these are discussed. To conclude, the stability of the films is considered.

6.3.1 Deposition Conditions

Initially attempts were made to deposit films of SC58497 spread and compressed under the conditions as chosen in the previous section. The substrates used were plain and aluminised (i.e vacuum evaporated) glass microscope slides

(Chance-Propper Ltd). These had been washed in chloroform followed by 'Decon 90' detergent and purified water, then refluxed for several hours in boiling isopropyl alcohol. Even at slow deposition speeds ($\sim 2.5 mm min^{-1}$) deposition records showed that pickup of the film was only partial, and deteriorated further after the first two or three layers. A visible sign of poor film adhesion was the presence of an irregular meniscus against the substrate as it moved through the air-water interface. It was observed that the performance of NK2684 in a similar molecular mixture was only slightly better.

It is well established for classical LB film materials that the addition of $CdCl_2$ to the water subphase improves film cohesion by partly converting it to a bimolecular cadmium salt(e.g ref 4). Upon addition of $CdCl_2$ at a concentration 2.5×10^{-4} M (that widely accepted as the optimum for stearic and arachidic acid) it was found that deposition of both types of dye film improved markedly. If a slow dipping speed ($\sim 2.5 mm min^{-1}$) was maintained, the meniscus along the substrates was regular and followed its movements both upwards and downwards. This is an indication of Y-type deposition, and was confirmed by dipping records which were estimated to indicate deposition ratios close to 100%. Such a record for the deposition of SC58497 is shown in Figure 6.9. This differs slightly from the ideal record of Figure 4.8b since there is a continual additional decrease in the surface area due to dissolution of the film. Also, the presence of the meniscus has the effect in introducing a small offset between the relative positions at which the substrate enters and leaves the subphase.

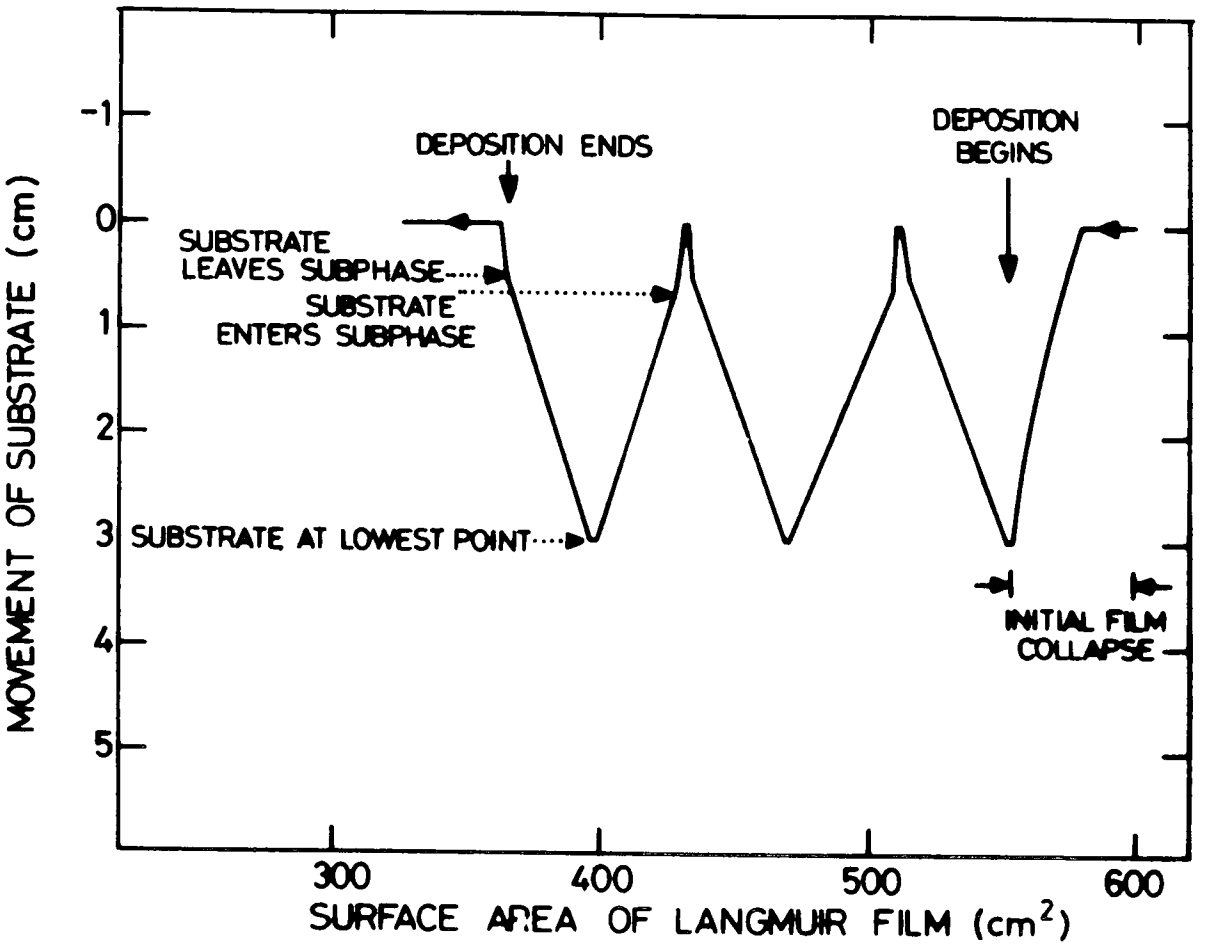

Figure 6.9 Typical LB film deposition record for a 1:1 mixture of SC58497 and $CdAr_2$ onto glass.

6.3.2 Optical Properties of Deposited LB Films

Figure 6.10 and 6.11 contrast the optical absorption spectra of multilayer LB films of the two merocyanine dyes with those in solution. The solution spectrum of NK2684 shows a peak absorption at 523nm, corresponding to electron transitions of energy 2.37eV, with associated vibrational structure manifested by a 'knee' in the characteristic at ~495nm (~2.5eV). In the absorption spectrum of the LB film these two features are red-shifted to 538nm (2.30eV) and ~510nm (~2.4eV) respectively, and an new absorption band is developing at 595nm (2.1eV). The shift in wavelength can be attributed to the way in which molecules pack in the film. The extent of this shift will be dictated by the angle between the planes of the dye molecules and the lines through their centres(5). The additional transitions in the film, leading to the extra absorption band, can be qualitatively explained by assuming the presence of some dimeric structure, and that the two molecules of each dimer interact through dipole-dipole coupling. Clearly the spectrum is far less sharply structured than it was for the solution. The changes are a result of the increased intermolecular interactions which occur in the solid state where molecules are only a few Angstroms apart, held together by van der Waal forces. The greater coupling between electron orbitals in the molecules will allow electrons to occupy states in a broader continuum of energy levels.

The same explanation applies to the absorption characteristics of SC58497. Two electron transitions located at 500nm (2.47eV) and ~475nm (~2.6eV) in the solution spectrum are red-shifted to 540nm (2.29eV) and 500nm (2.47eV)

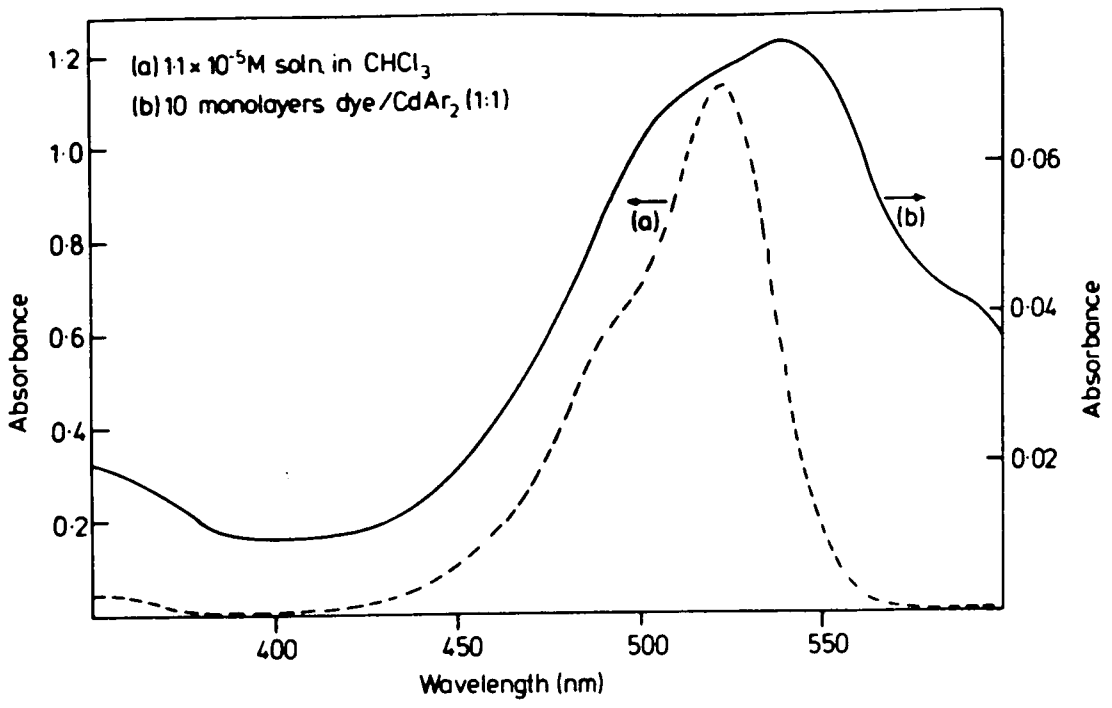

Figure 6.10 Optical absorption spectra of NK2684 (a) in solution and (b) in LB film form.

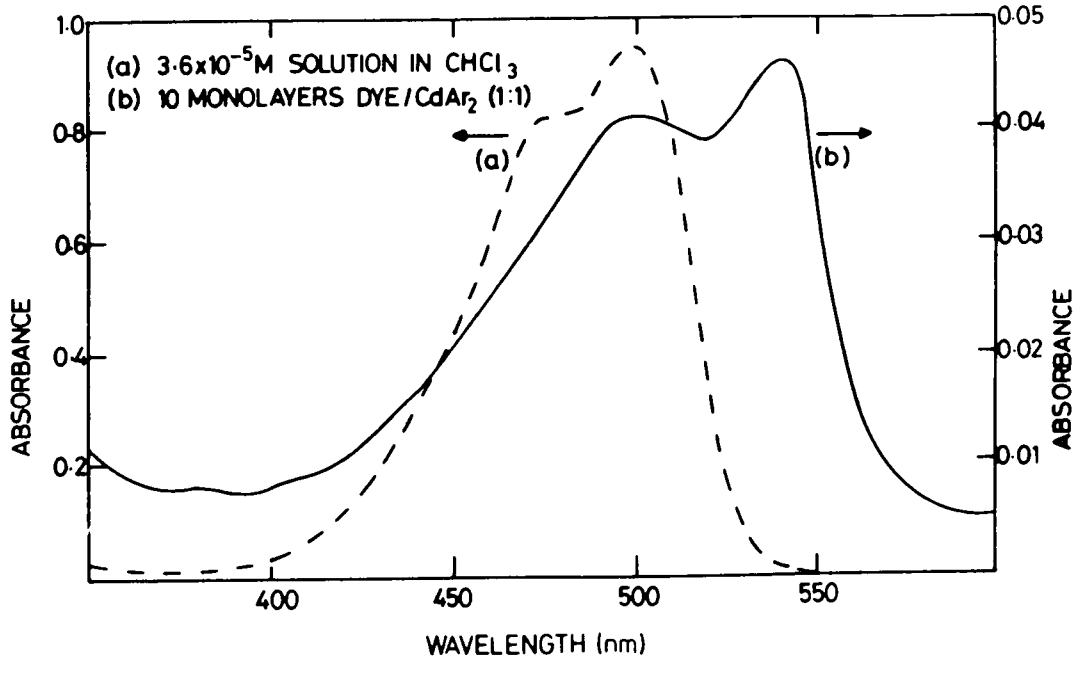

Figure 6.11 Optical absorption spectra of SC58497 (a) in solution and (b) in LB film form.

respectively. However, in this case there is no indication of dimeric structure from the film absorption spectrum. It is interesting to note that by calculating the molar extinction coefficient for the dye solution, and assuming the density of the deposited film to be ~1gcm^{-3}, an order of magnitude estimate of the film thickness may be obtained. Comparing the absorbance of the LB films with those of the solutions suggests for both that the dye LB films have a monolayer thickness ~2nm. It is unwise to attempt a precise calculation using this method because of the differences in the absorption processes for the solutions and the LB films, and the added complication of the dilution of the dye films with cadmium arachidate.

The absorbances of the dyes as a function of the number of deposited layers are plotted in Figures 6.12 and 6.13. The absorbance measurements were made at 540nm since this was where peak absorption occurred for both dye films. Both types of film obey the Beer-Lambert law to a good approximation, the law being expressed as

$$\log(I_o/I_T) = \alpha N d_{lb} \qquad (6.2)$$

where I_o and I_T are the incident and transmitted light intensity, α the absorption coefficient of the dyes, N the number of layers, and d_{lb} the thickness of each layer. The multiple beam interference effects(6) which have been observed with multilayers of cadmium arachidate and some other LB films are not apparent here. There was little change in the shape of the absorption characteristics of the dyes with increasing film thickness, which allowed good predictions to be made of the absorption by different thicknesses of film.

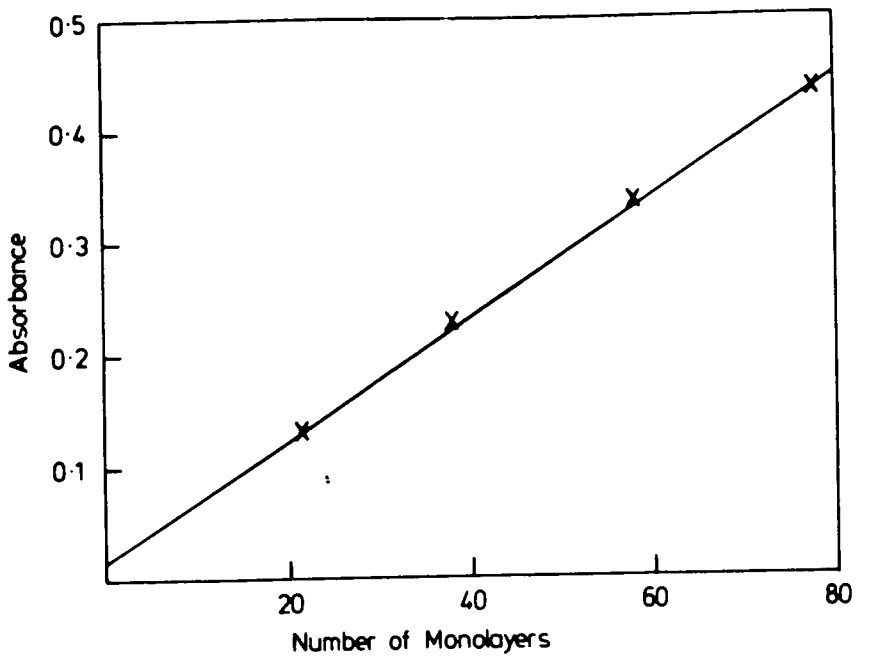

Figure 6.12 Peak optical absorption (λ= 540nm) vs number of monolayers for NK2684/$CdAr_2$(1:1)

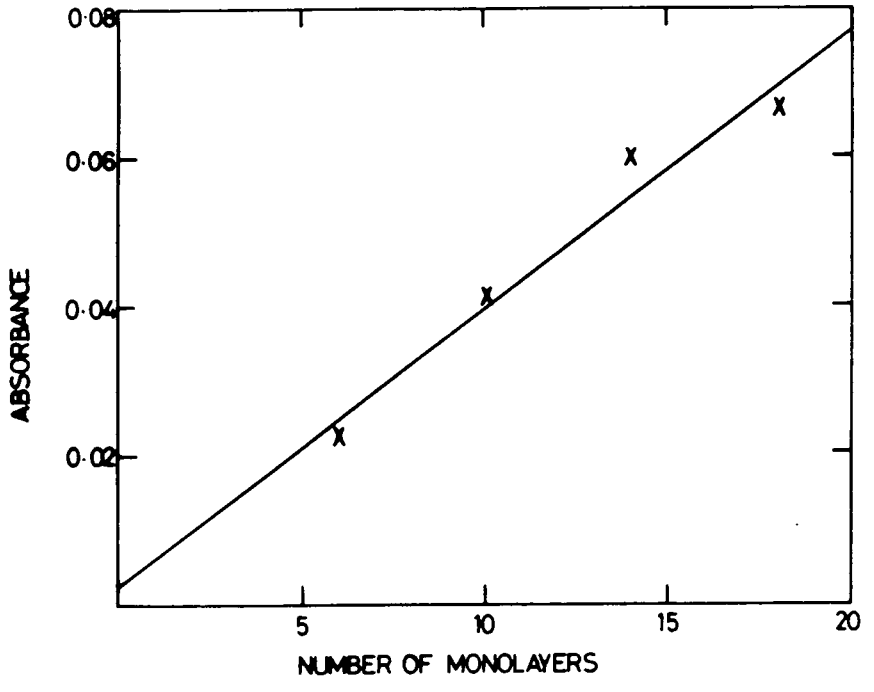

Figure 6.13 Peak optical absorption (λ= 540nm) vs number of monolayers for SC58497/$CdAr_2$(1:1)

Fluorescence measurements, in contrast, showed that changes were taking place in the interactions between dye molecules as film thickness increased. The fluorescence emission spectra of films of the two dyes are shown in Figures 6.14 and 6.15. In both cases the emission was excited by 500nm light. The characteristic of a single monolayer incorporating NK2684 shows the normal molecular fluoresence peaking at about 550nm, i.e close to the wavelength of peak absorption. For five monolayers, however, any molecular fluorescence is swamped by a broad, structureless, red-shifted peak, that associated with excimer emission (section 2.1.3). This peak at 605nm corresponds closely to the developing absorption band at 595nm in Figure 6.10 which was attributed to dimeric structure. The behaviour of SC58497 is somewhat similar though the excimer emission peak is shifted further into the red (640nm), is broader, and the molecular fluorescence is still detectable. The greater overall fluorescent intensity of SC58497 can be attributed to lower internal absorption (the absorptivity of NK2684 being about twice that of SC58497). The small emission bands apparent at even higher wavelength (~660nm for NK2684 and ~695nm for SC58497) are thought to indicate the formation of J bands due to partial aggregation of the dye molecules. The presence of excited dimer states in the emission spectra suggest that there are very weak interactions between substituent chromophores in the ground state, but that significant interaction occurs in the excited state. These fluorescence processes should be quenched where efficient sensitisation of a semiconductor substrate occurs.

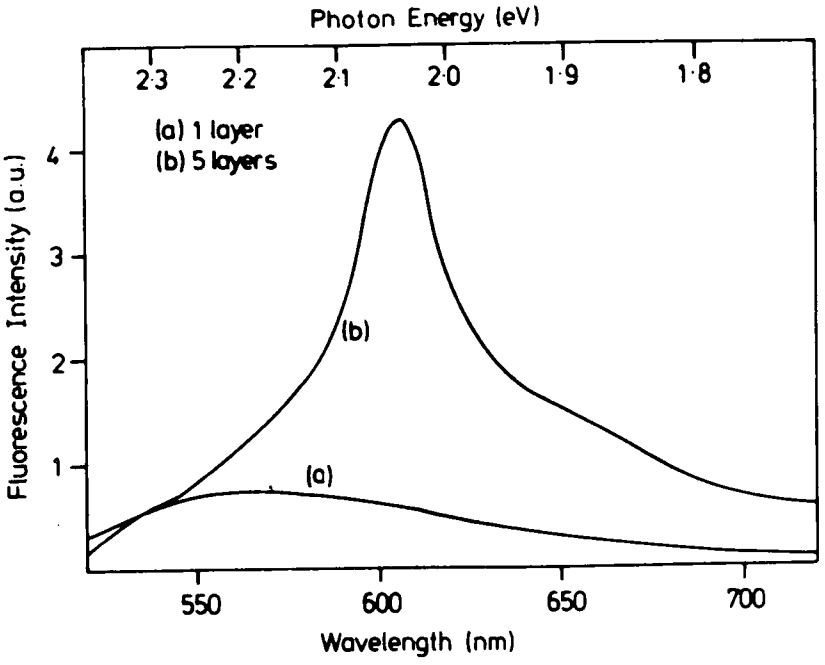

Figure 6.14 Fluorescence emission spectra of LB films of NK2684/$CdAr_2$(1:1) excited by 500nm light. (a) 1 layer. (b) 5 layers.

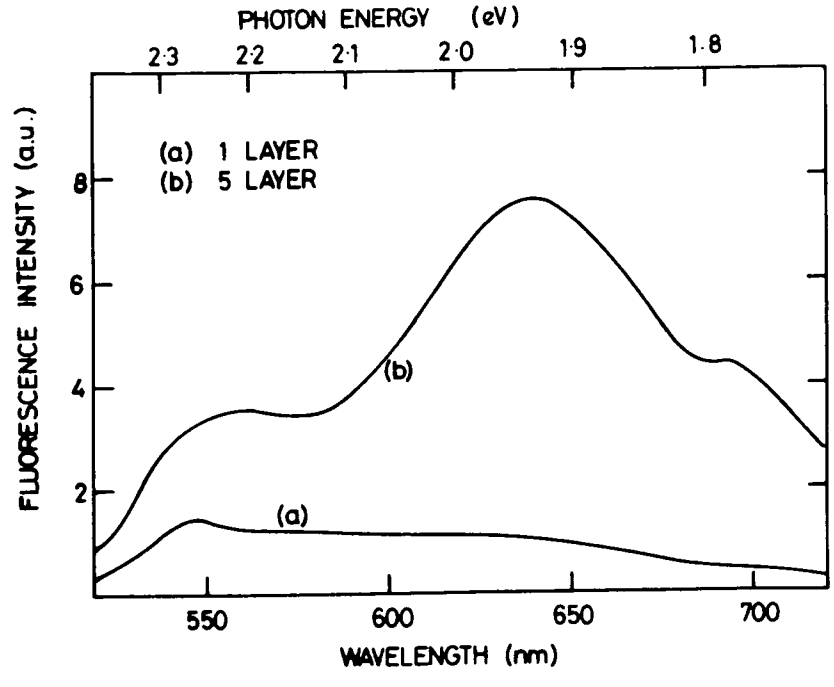

Figure 6.15 Fluorescence emission spectra of LB films of SC58497/$CdAr_2$(1:1) excited by 500nm light. (a) 1 layer. (b) 5 layers.

6.3.3 Stability of Films

It was found that LB films of the dyes on glass were prone to bleaching effects when exposed to strong light (i.e sunlight) for more than a few minutes. When stored in darkness the films showed no deterioration over several months, maintaining their original absorption characteristics. It is very likely that the molecules undergo a photo-oxidation process, though the mechanisms behind such processes in dyes remain uncertain(7). An attempt was made to eliminate the effect by sealing the dye layers with an LB film layer of cadmium 22-tricosenoate, but without success. This suggests the process may be associated with oxygen absorbed into the dye film before or during deposition. It is interesting to note that the change in the photoconductivity of zinc sulphide when coated with a dye LB film, as discussed in the next section, did not diminish after exposure of the sample to strong light. This could imply that excited dye molecules on the semiconductor surface were involved in a charge transfer process with the semiconductor which reduced the effects of photo-oxidation.

6.4 DYE-SENSITISATION STUDIES

Having succeeded in obtaining LB films of merocyanine dyes of reproducible quality, an objective of this research was to incorporate the films in semiconductor devices. It was planned to study the dye-sensitisation effect in wide bandgap semiconductors as a function of the dye coverage of their surfaces. The LB technique clearly offers far finer control than the relatively crude techniques of dye adsorption from solution or vapour, or vacuum evaporation.

This section firstly discusses the difficulties encountered in finding suitable semiconductor substrate materials, and then the results of an investigation of the sensitising effect of LB films of merocyanine dyes on zinc sulphide crystals.

6.4.1 Substrate Materials

Much of the past research into sensitisation of semiconductors using more conventional dye deposition techniques has involved the study of photoeffects in ZnO. As with the silver halides, it has been found that the photoeffect at the sensitisation maximum for ZnO can reach ~80% of the maximum inherent photoconductivity of the semiconductor (the efficiency of the dye-sensitisation process is normally quoted as this ratio). Initial attempts were thus aimed at demonstrating the effect on ZnO single crystals, as had previously been used by several workers (e.g 8,9). Unfortunately all the crystals obtained were too conducting to enable photoconductivity to be detected over the dark conductivity, even at 77K. Conversely, attempts to use sputtered ZnO films or ZnO powder spread in a binder were frustrated by these systems being too resistive to pass any measurable currents. Hoping to emulate the work of Gerischer(10) by sensitising organic crystals, anthracene crystals were obtained. With these it proved impossible to obtain reliable contacts, a failure repeated with C4-anthracene LB films(11) as the substrate. However, polycrystalline zinc sulphide prepared in a low-resistivity form(12) was found to exhibit detectable d.c photoconductivity across the visible spectrum, and hence

allow direct measurement of the change induced by the presence of merocyanine dye films.

6.4.2 LB Films on Zinc Sulphide

The ZnS crystals as supplied (Chapter 5), though regarded as low-resistivity for this material, had a bulk resistivity $\sim 10^{6} \Omega m$ ($10^{8} \Omega cm$). It was nonetheless possible to measure the d.c dark conductivity and photoconductive response of samples with relative ease, using techniques previously described. Figure 6.16a shows the dark conductivity of a sample at room temperature, measured over a wide voltage range, to be fairly linear up to ~1V. The superlinear region of the curve is assumed to be where the ohmic current crosses over to being space charge limited. The dashed lines (b) and (c) were the dark conductivity of the sample after etching and the deposition of LB films of the two merocyanine dyes. Curve (a) was reproducible if the films were removed by washing the sample in chloroform then refluxing in isopropyl alcohol.

The d.c photoresponse of the sample was measured as the increase in current from the dark current as a function of the wavelength of the incident light. By calibrating the incident light power using a thermopile this could be expressed as the number of carriers generated per incident photon, and is plotted as such in Figure 6.17. The response at room temperature is curve (a); that at 100K (b) is shown for comparison. Both responses were measured with a bias of 1V across the sample. This photoresponse may be regarded as an external quantum efficiency of the sample, since strictly it represents only the carriers generated which do not

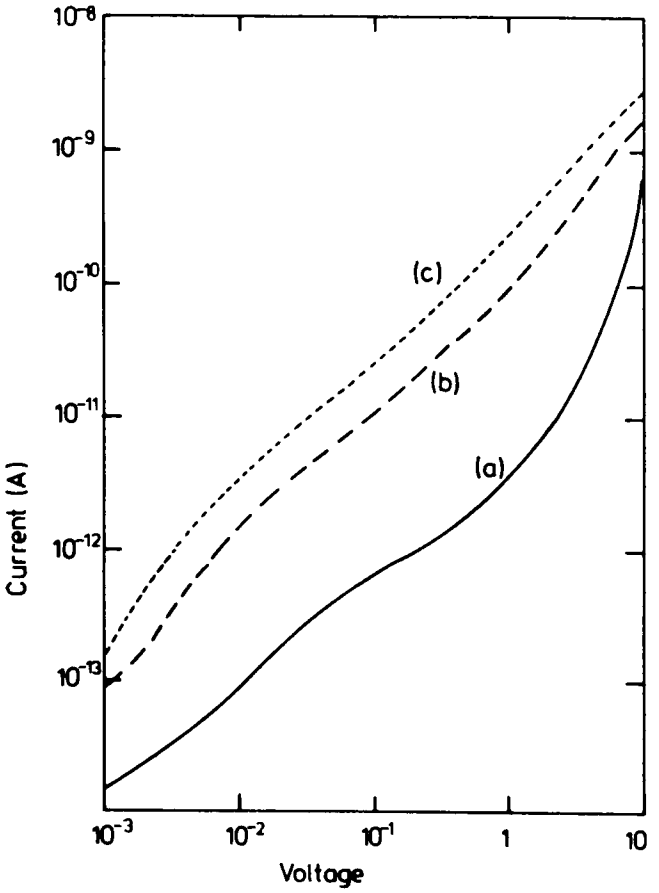

Figure 6.16 Conductivity of zinc sulphide crystal (a) untreated. (b) after deposition of three monolayers of NK2684 $CdAr_2$(1:1). and (c) after deposition of three monolayers of SC58497 $CdAr_2$ (1:1).

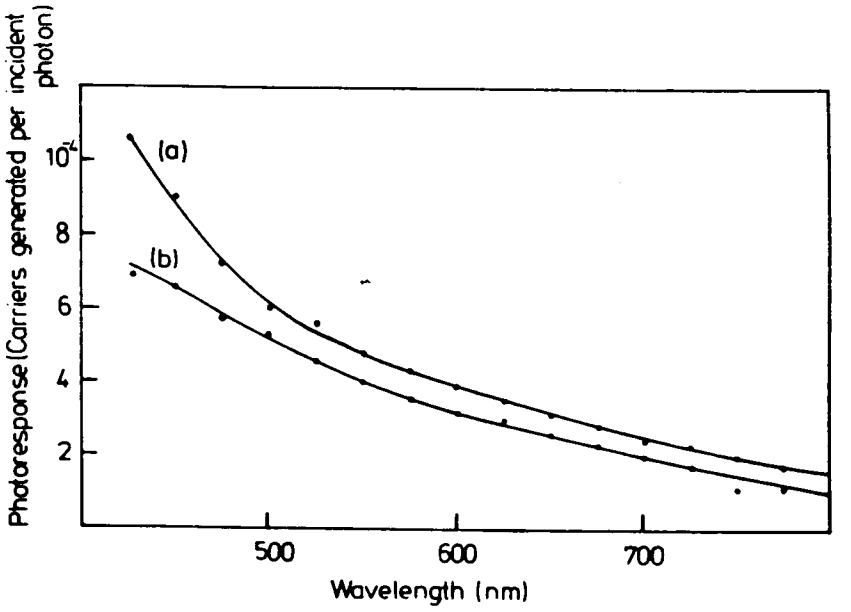

Figure 6.17 Photoconductivity of untreated zinc sulphide crystal at (a) 298K and (b) 100K.

recombine within the sample. At 400nm (the low wavelength limit for reliable measurements with the equipment used) this efficiency was ~10^{-4} for the unsensitised sample, falling to ~$2x10^{-5}$ at 800nm. The energy bandgap of ZnS is ~3.7eV, implying a peak response should occur at ~335nm (n.b the response at 350nm was roughly estimated at ~10^{-3}).

No change in the photoresponse was detectable when a single monolayer of either merocyanine dye was deposited upon the sample. The changes measured due to the presence of three monolayers of dyes NK2684 and SC58497 are shown in Figures 6.18 and 6.19 respectively. The effects of the dye layers are plotted as the relative quantum efficiency, that is the ratio of the photoresponse after deposition of the dye to that before. For five or more monolayers of dye the effect diminished rapidly, barring a small drop in response assumed to be associated with absorption by the dye.

The analysis of these curves can only be qualitative since the changes involved are relatively small, particularly in the case of dye SC58497. The greatest relative quantum efficiency attained at a bias of 1V was 1.5 at a wavelength ~650nm for a film of dye NK2684. This implies (referring to Figure 6.17) that the photoresponse at that wavelength has increased from ~3% to ~4.5% of the maximum inherent photoconductivity of the semiconductor (i.e the sensitisation efficiency). Akimov (13) has reported that dye-sensitisation of the photoeffect in ZnS is not detectable with undoped material, but that sensitisation efficiencies $\gtrsim$50% are observed if there is a concentration of $\gtrsim 10^{17}$ cm^{-3} of shallow donor levels, created by deliberately incorporating impurity halide ions. It was surmised that to obtain effective

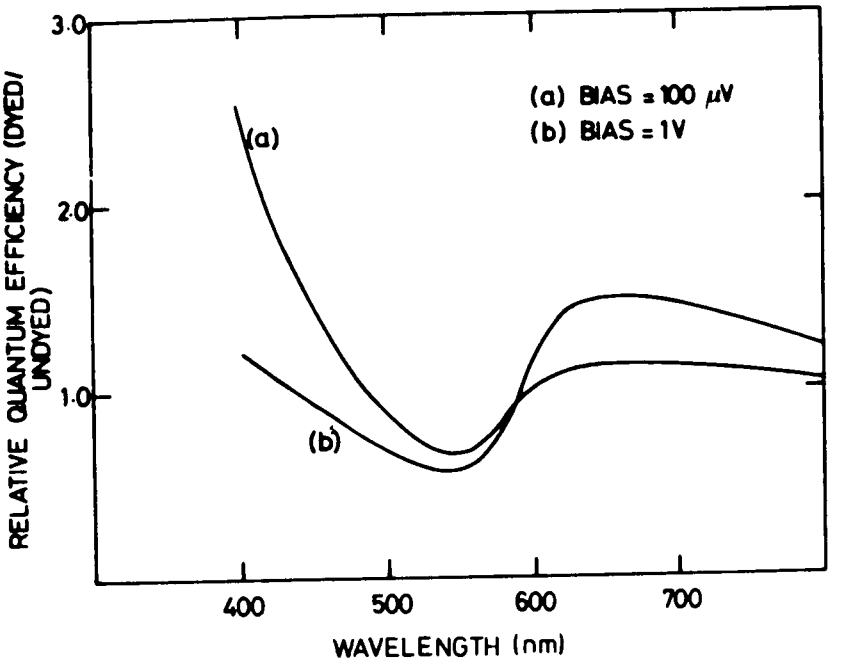

Figure 6.18 Relative desensitisation effect of three monolayers of NK2684/$CdAr_2$ (1:1) on the photoconductivity of zinc sulphide. (a) bias = 100μV, (b) bias = 1V.

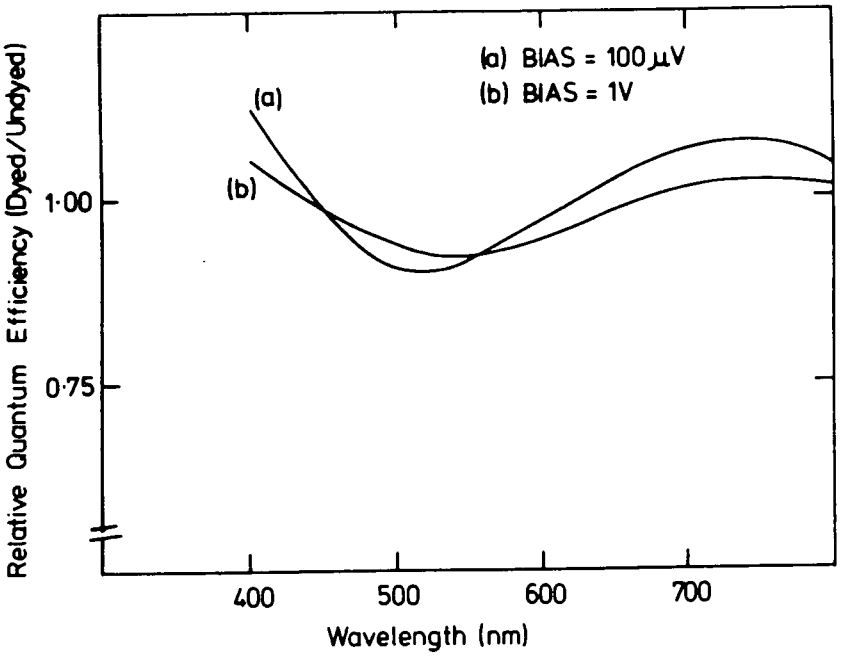

Figure 6.19 Relative desensitisation effect of three monolayers of So58497/$CdAr_2$ (1:1) on the photoconductivity of zinc sulphide. (a) bias = 100μV, (b) bias = 1V.

sensitisation requires the presence of a depletion layer near the surface which causes injected electrons to drift into the semiconductor bulk, rather than recombining with the excited dye. The ZnS used here has had no such treatment, but heating the sample in a melt of zinc and other additives (part of the preparation of the low resistivity form(12)) will have increased the density of shallow donors. The resistivity of the material does, however, imply that this density is much less than 10^{17} cm^{-3}. The fundamental chromophore structure of NK2684 is identical with that of known organic photoconductors which are characterised as p-type semiconductors(14). It is thus possible to consider the dye-semiconductor system as having some of the characteristics of a p-n junction photocell. This aspect of the preferred electron transfer model for sensitisation is consistent with reports that good sensitisers of n-type semiconductors act as desensitisers on p-type materials and vice versa(7).

The spectral characteristics of the relative quantum efficiencies of the structures are similar for both dyes, though considerably smaller in the case of SC58497. In part at least this will be due to the lower absorption of the dye (i.e a lower oscillator strength associated with its electron transitions). It is assumed here that the processes occurring are similar for both dyes since they appear to have broadly similar absorption characteristics in LB film form. The most striking feature of the change in photoresponse is that it has been reduced by the presence of the dye at wavelengths between 430nm and 600nm, with a minimum value of relative quantum efficiency ~0.55 occurring at 540nm, the

wavelength at which maximum absorption by LB films on glass occurred. It might be intuitively surmised that this drop is merely a result of the dye filtering out the incident light, but the effect is far too large for this. Assuming the Beer-Lambert law invoked for Figures 6.12 and 6.13 it is found that three monolayers of dye would only absorb ~4% of the incident light at 540nm - at least 60 layers would be required to reduce the photoconductivity to the level measured. It is far more likely that this is a desensitisation process where dye molecules act as hole injectors. The energy level corresponding to the highest occupied molecular orbital of the dye in its ground state must lie beneath the valence band of the semiconductor (section 2.2). When the dye is excited the generated photohole will be injected into the ZnS, thus promoting electron-hole recombination in the semiconductor and causing the photoconductivity to decrease. The probable mechanism for recovery from such a process is thought(5) to be the transfer of the excited electron to an intermediate level of similar energy in the semiconductor (i.e a trap). This desensitisation process by itself does not explain the rise in quantum efficiency at other wavelengths. Perhaps at wavelengths where the desensitisation process is not dominant the carriers generated by the intrinsic photoconductivity of the ZnS are transported between the electrodes more efficiently. This would be consistent with the increase in dark conductivity shown in Figure 6.16. It is true, however, that such a process would be expected to lead to a similar increase in the photoconductivity of the sample incorporating SC58497. This effect was not evident.

It is wise to consider whether the maximum absorption of light is actually occurring at 540nm. As discussed in Chapter 2, the absorption characteristics of a dye may be strongly influenced by the crystal structure of a substrate onto which it is adsorbed. Unfortunately, it was impractical to measure the absorption characteristics of the dyes on ZnS because of the small sample size. As a demonstration of the effect, however, Figure 6.20 shows the reflectance of a sample of single crystal silicon before and after the deposition of three monolayers of SC58497. In this case it is clear that the dye film is absorbing most strongly (i.e reflecting least) at 430nm, with lesser structure at ~470nm and ~510nm. The lattice constants of ZnS (5.41Å) and Si (5.43Å) are fairly close, so it is possible the absorption characteristics of the dye layers behave similarly on both materials. We could then be observing a true sensitisation process at 430nm, i.e the transfer of excited dye electrons into the conduction band of the semiconductor. If this is true, however, it is difficult to explain the drop in the characteristic at 540nm. Until more detailed measurements are made on a more convenient version of this structure, it is a matter for speculation which process is occurring.

6.5 SUMMARY

This chapter has presented the results of an investigation of the properties of novel LB films of a merocyanine dye, and of the use of merocyanine LB films to sensitise the photoresponse of zinc sulphide. These results and the conclusions drawn from them are summarised as follows:

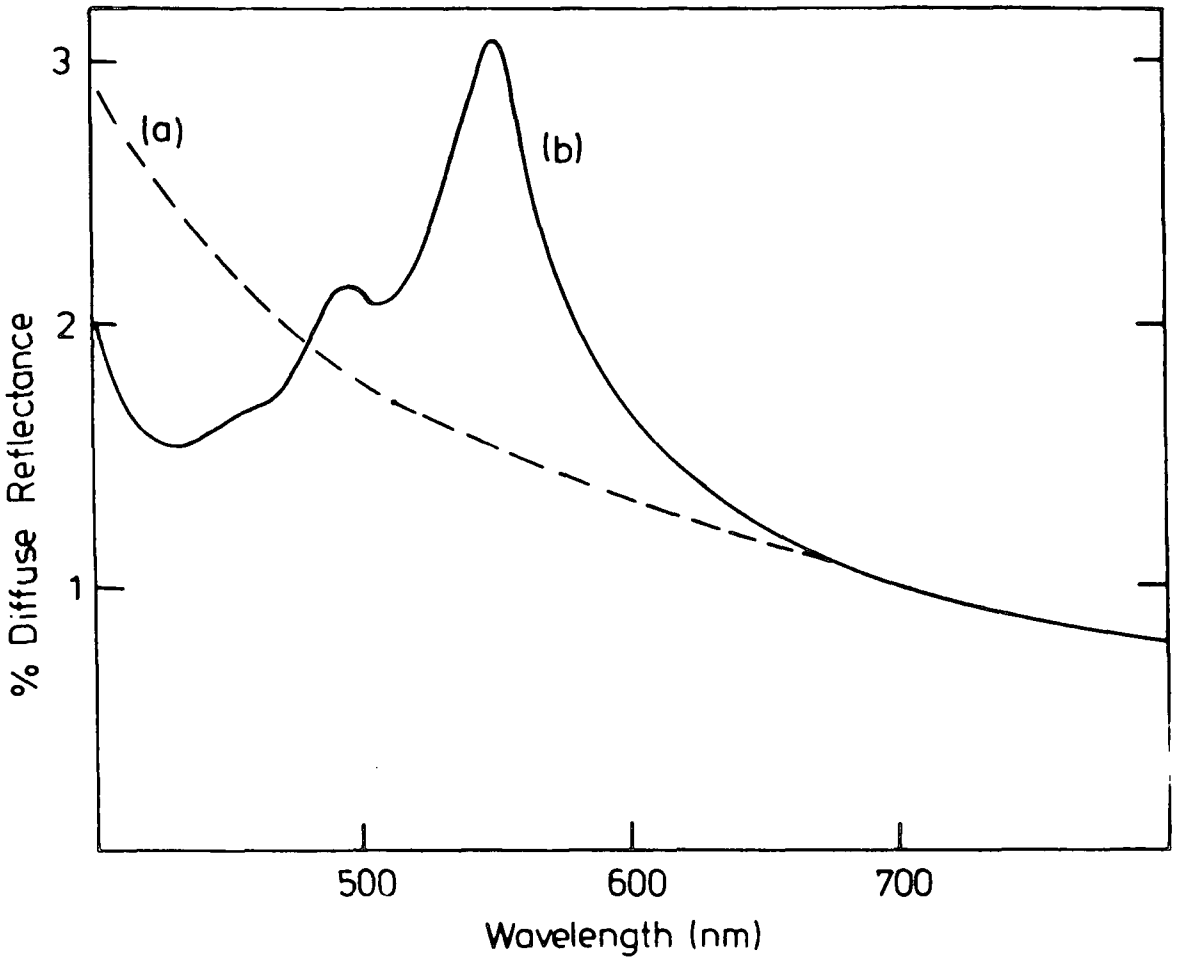

Figure 6.20 Diffuse reflectance of single crystal silicon (a) before and (b) after deposition of three monolayers of SC58497 $CdAr_2$ (1:1).

(i) A number of merocyanine dyes, without the hydrophilic and hydrophobic substitutions traditionally associated with LB film materials, were screened to assess their suitability as such films. One of these dyes, denoted as SC58497, was found to exhibit the behaviour associated with good LB films when spread in solution on the surface of a Langmuir trough.

(ii) Pressure-area plots for this material suggested it was forming a layer one molecule thick on the water surface. These data were supported by molecular modelling. The slow dissolution into the subphase of compressed films was found to be accelerated at low values of pH, but remained constant as pH was increased from the level used when dipping classical LB film materials.

(iii) Films of the pure dye were too rigid for deposition in LB film form, but improved markedly in quality when mixed at a 1:1 molar ratio with arachidic acid. Transfer of the films to substrates was enhanced by the incorporation of $CdCl_2$ in the subphase at a concentration 2.5×10^{-4} M.

(iv) The optical properties of LB films of SC58497 were compared and contrasted with those of LB films of NK2684, a merocyanine dye with distinct hydrophilic and hydrophobic substitutions. For both dyes the optical absorption spectra were broadened and red-shifted from the solution spectra, and in the case of NK2684 suggested the presence of some dimeric structure in the films. The peak absorption of both dyes as a function of the number of deposited layers obeyed the Beer-Lambert law (i.e was linear). Fluorescence spectra of both dye films were dominated by excimer emission, indicating

greater interactions between molecules in their excited state.

(v) Films of the dyes were deposited by the LB technique onto samples of polycrystalline zinc sulphide, and changes in the d.c photoconductivity of the semiconductor were investigated. No change was observed for a single monolayer of either dye, but three monolayers caused small changes. The effect diminished rapidly with more layers. The photoconductivity of the ZnS was found to have dropped over a wavelength range centred at 540nm, but to have increased at higher and lower wavelengths. These changes were far more marked with dye NK2684, presumably because of its higher absorptivity. The spectra of the change in photoconductivity suggested a desensitisation process, explained in terms of hole injection by the dye. However, consideration of the possible effects of the surface lattice structure of the ZnS crystal on the optical properties of the dyes suggested that other processes should not be ruled out.

CHAPTER 7

RESULTS AND DISCUSSION

ZnSeS ELECTROLUMINESCENT STRUCTURES

7.1 INTRODUCTION

Attempting to understand and explain the performance of the MIS devices developed in this research is considerably hindered by the limited current knowledge of the electrical and structural properties of phthalocyanine LB films. Indeed the semiconductor substrates themselves are relatively novel, and have yet to be fully characterised. Against this background it is important to note that the analysis of electrical properties presented here relies on explaining data in terms of previously established models for similar systems. The most relevant past work is that of Batey et al (1-4) with electroluminescent MIS structures made by depositing LB films on GaP substrates. GaP is amphoteric, and hence p-n junction LEDs with high injection efficiencies are already attainable with it. However, as a well characterised material it served as the basis of a 'model' system for investigation, extended to II-VI compounds by this research. The results of the work on GaP are summarised in section 7.3, following a brief discussion of electroluminescence in ZnSe.

In the remainder of this chapter the electrical and optical characterisation of ZnSeS Schottky barrier and MIS devices is presented and discussed. Initially electrical data for the simple Au/ZnSeS structure are studied. These

are then contrasted with the electrical properties of devices where multilayers of phthalocyanine have been incorporated as an insulating layer. There follow the results of the effect of the thickness of the LB film insulating layer on the electrical and EL properties of the devices. These results are interpreted in the form of a model of the energy band structure of the MIS device. The proposed model is used as a basis for explaining the electroluminescent characteristics of the devices, and in particular the dependence of their efficiency upon insulator thickness. The measurement techniques for all the results presented in this chapter have been described in Chapter 5.

7.2. ELECTROLUMINESCENCE IN ZnSe

Interest in the EL properties of II-VI semiconducting materials reflects the desire to utilise their very high internal luminescent efficiencies, apparent from photo- and cathodoluminescence measurements. In these direct bandgap materials radiative processes compete with the non-radiative far more efficiently than in the indirect gap III-V semiconductors. However, all II-VI materials exhibit the phenomenon of self-compensation, which makes it very difficult (if not impossible) to prepare them in a low-resistivity p-type form necessary for the formation of the pn homojunctions conventionally used for exciting EL (an exception is CdTe, but its bandgap of 1.5 eV is of no use for visible EL). Efforts to produce efficient EL devices using the alternative device structures described in Chapter 3 are not yet expected to compete with the well-established technology of III-V EL devices at lower wavelengths (e.g

GaAsP red LEDs). However, there is great potential in the green and blue regions of the visible spectrum (λ<540nm) where efficient carrier injection could give devices with a luminance (brightness) >1000Cdm^{-2} for a power dissipation of only 1Wcm^{-2}.

The near bandgap luminescence of II-VI materials to some extent dictates their usefulness. ZnTe (~550nm) is in direct competition with GaAsP, as is CdS (~520nm) which is anyway inefficient at room temperature. ZnS (~340nm) requires careful control of doping to obtain visible (>400nm) luminescence from deep centres. This leaves ZnSe (~460nm) and ZnSeS alloys as arguably the most likely candidates for producing an efficient II-VI LED.

Much research has been aimed at determining the mechanisms responsible for luminescence in these materials, and several reviews of the field have been written (5,6). There are essentially two forms of mechanism, edge emission and emission from deep centres.

7.2.1. Edge Emission

Edge emission describes radiative recombination mechanisms occurring close to the band edges (i.e within a few kT). In ZnSe these processes are attributed to free exciton, bound exciton and distant pair recombination as discussed in 3.2.2. Edge emission is difficult to obtain in a device - band to band radiation is clearly absorbed very strongly by the semiconductor, and the presence of impurities leads to the spectral output being dominated by broad bands of lower energy.

7.2.2. Deep Centre Emission

This can be further broken down into localised and non-localised processes. Localised emission can occur when impact ionisation of impurities themselves occurs, usually in reverse bias (see 3.2.1.). Considerable research has been undertaken of this impurity effect, particularly for manganese centres, but it is not directly relevant to the carrier injection studies here. Non-localised emission involves the transition of carriers from bands to levels associated with impurities. The role of impurities such as copper, aluminium and chlorine has been investigated, as well as that of intrinsic defects in the semiconductor lattice (e.g vacancy complexes). The spectral characteristics of luminescence are highly dependent upon impurity levels and hence upon growth conditions. This is one reason for continuing interest in ZnS, since the desirable blue emission is at a considerably lower energy than edge emission.

7.3 GaP MIS STRUCTURES

Batey et al undertook a comprehensive study of the effect of the insertion of films of cadmium stearate and cadmium 22-tricosenoate into the gold/n-type GaP system. Devices incorporating phthalocyanine LB films were also investigated. They found that the presence of an insulator increased the effective barrier height to electrons in the device, and that the minority carrier injection ratio (γ) and EL efficiency were increased. The change in effective barrier height proved to be independent of film thickness, but the EL efficiency showed an optimum at a thickness ~27nm for both types of fatty acid LB film(2). This thickness was

well beyond that associated with direct quantum mechanical tunnelling, and an alternative mechanism for traversal of the insulator by minority carriers was proposed. It was assumed that up to the optimum thickness the flow of minority carriers is primarily limited by their diffusion in the semiconductor bulk, and that they cross the insulator via traps in its energy bandgap. This could be by a Poole-Frenkel process or a 'hopping' process, which has been suggested as the dominant bulk conduction mechanism in insulating LB films(7). As the insulator thickness is increased from one monolayer the barrier to majority carriers remains effectively constant, but the increasing ability of the insulator to support a voltage allows an increasing degree of band realignment to occur between the semiconductor valence band edge and the metal Fermi level. Hence γ increases with insulator thickness (section 3.6) until the hole current is primarily limited by the insulator. Broadly similar results were obtained with devices incorporating phthalocyanine films(3), but in this case an optimum EL efficiency was found for an insulator thickness ~5.6nm (seven monolayers). Such a thickness corresponds closely to that expected from conventional tunnel injection theory.

Throughout this chapter comparisons are drawn where thought relevant with the results of Batey et al. In particular, results presented here cast some doubt on whether the optimum thickness of phthalocyanine reported by these workers was truly of tunnellable dimensions.

7.4 NEAR-IDEAL SCHOTTKY DIODES

This section considers the electrical properties of

near-ideal Schottky diode structures of Au/ZnSeS, prepared as described in section 5.2.2.

7.4.1 Conductivity Data

The current density as a function of voltage for a typical Au/ZnSeS Schottky diode is shown in Figure 7.1. The reverse bias characteristic does not show a clear current saturation, but the linear region of the forward characteristic is well-described by equation 3.22 from the thermionic emission theory, i.e $J = J_o \exp(eV/nkT)$. It should be noted that for a forward bias greater than ~0.5V these devices underwent a catastrophic breakdown, predictable in view of the very large current density being passed. No electroluminescence could be detected before failure occurred.

From the measured value of $J_o = 5.6 \times 10^{-4}\ Am^{-2}$, a value for the barrier height to electrons $\phi_{bn} = 0.81eV$ may be deduced using equations 3.17 and 3.18. This assumes an electron effective mass $m_e^* = 0.17m_e$, as reported for ZnSe(6). However, the ideality factor, n, for 7.1a is 1.5. Card and Rhoderick's analysis, described in 3.6.1, suggests that this is indicative of the presence of an interfacial layer. If so, the calculated value of ϕ_{bn} can only be regarded as an upper limit, since the effective barrier will include a contribution due to the insulator (equation 3.29). Using data for the $Si-SiO_2$ interface(8) to approximate the effect of this layer, the increase in effective barrier height with thickness would be: δ = 1nm, $\Delta\phi_{bn} \sim 0.046eV$; δ = 2nm, $\Delta\phi_{bn} \sim 0.18eV$; δ = 3nm, $\Delta\phi_{bn} \sim 0.41eV$. Without an independent measurement δ can only be estimated, but for a

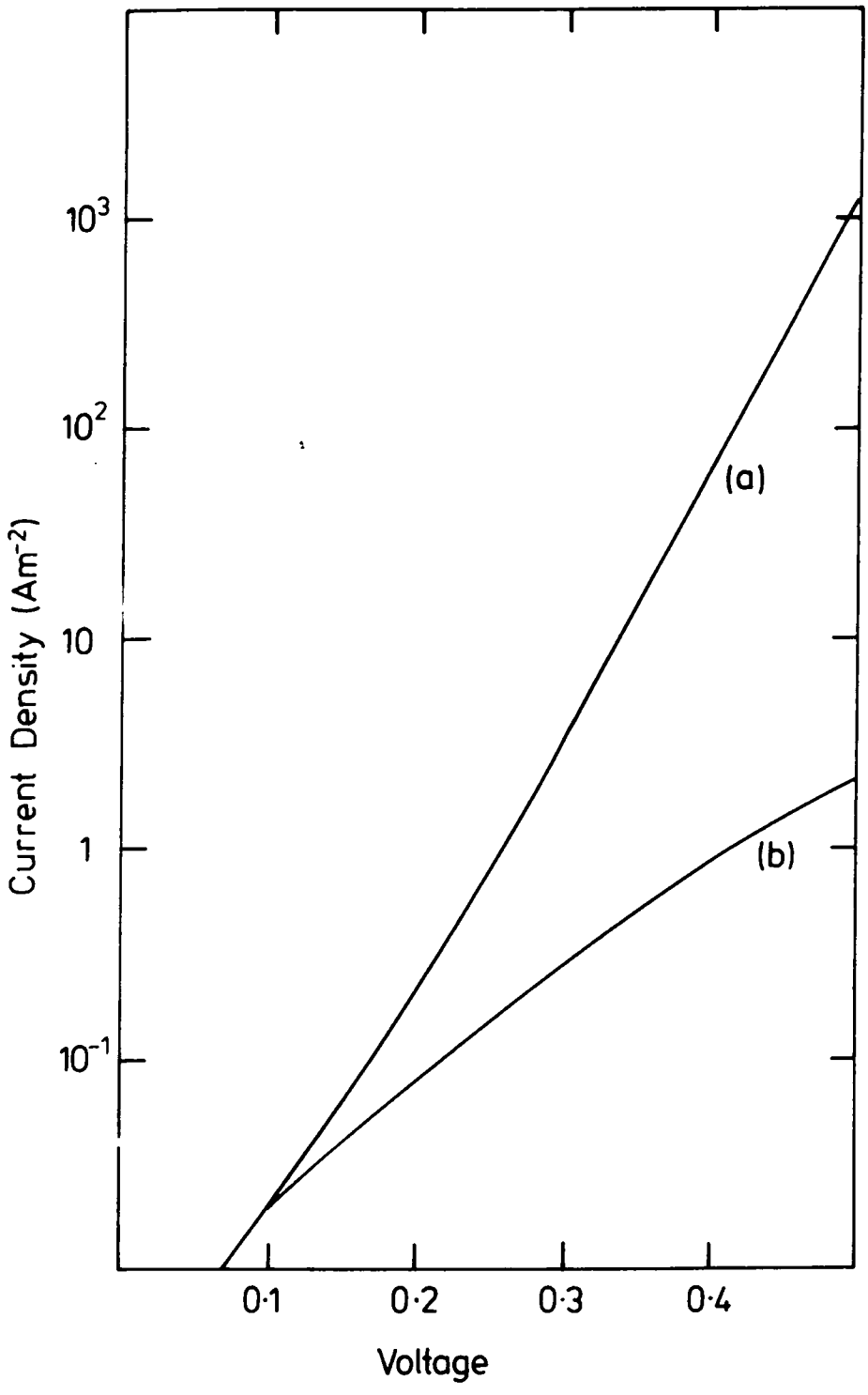

Figure 7.1 Conductivity data for a Au/ZnSeS Schottky diode (a) under forward bias and (b) under reverse bias.

freshly etched semiconductor surface it would be expected that $\delta \sim$ 1nm (e.g ref 5). This value has been assumed here, suggesting the true barrier height to electrons is still ~0.8eV. To justify the value found for n under these conditions requires an estimate of the density of surface states associated with the interface. The capacitance data presented next are required to make this estimate.

7.4.2 Capacitance Data

Figure 7.2 shows the inverse capacitance squared vs voltage characteristic of the Schottky diode structures. The error bars show the standard deviation of values measured over a number of contacts. The slope of this plot suggests a donor density in the semiconductor, $N_d = 1.53 \times 10^{18}$ cm^{-3}. The intercept with the voltage axis would imply a barrier height to electrons >1.0eV if this were assumed to be an ideal Schottky barrier (equation 3.25). However, an upper limit of $\phi_{bn} = 0.81$eV has already been established. It is proposed that the disparity with the value obtained from conductivity data is the result of the presence of interface states associated with the interfacial layer. The data are analysed using the Cowley(9) model for a structure incorporating an insulator (equation 3.32), assuming a case which is within the limitations imposed by Fonash(10). It is assumed that the true barrier height is $\phi_{bn} = 0.8$eV and that most interface states are in equilibrium with the metal, i.e $\alpha_1 >> \alpha_2$, which gives a linear relationship in equation 3.32 with the same slope as for an ideal Schottky diode.

Firstly it is necessary to consider the modification to the ideality factor due to the presence of interface states.

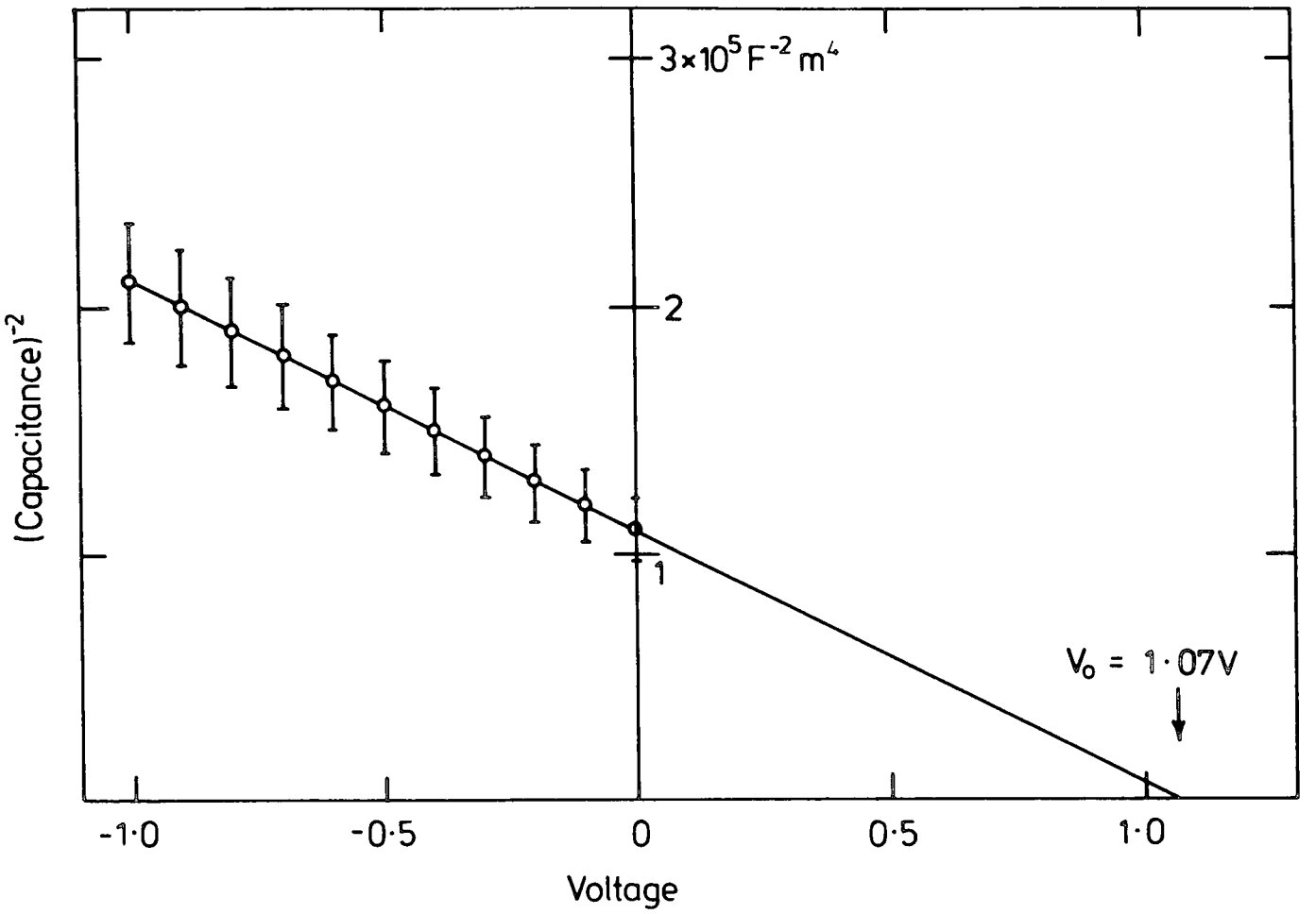

Figure 7.2 Inverse capacitance squared vs voltage plot for a Au/ZnSeS Schottky diode.

A more general form of equation 3.30 is(8)

$$n = 1 + \{(\delta/\varepsilon_i)(\varepsilon_s/W + eD_{sb})\}/\{1 + (\delta/\varepsilon_i)eD_{sa}\} \qquad (7.1)$$

$$= 1 + \delta\varepsilon_s/W(\varepsilon_i + \delta eD_{sa}) \qquad \text{for} \quad \alpha_1 >> \alpha_2$$

$$W = (2\varepsilon_s V_{do}/eN_d)^{1/2} \qquad (7.2)$$

Hence a value can be determined for $D_{sa} = 3.3\text{x}10^{16}\ m^{-2}eV^{-1}$ (δ = 1nm, $\varepsilon_i \sim 2\varepsilon_o$, ε_s = 9.2(ref 6), V_{do} = 0.8V, $N_d = 1.5\text{x}10^{24}\ m^{-3}$). These values can be used to determine the variables α_1 and V_1, as featured in equation 3.32 (α_1 = 0.30, V_1 = 0.13V) which prove to be consistent with a diffusion voltage $V_{do} \sim$ 0.8V. Although at best an order of magnitude estimate, this value for D_{sa} is comparable with that found for the interface of the near-ideal Au/GaP system by Batey et al(4). Using Cowley and Sze's(11) analysis in terms of the Bardeen model, in which surface states were assumed to be uniformly distributed over an energy interval in the bandgap, equation 3.12 gives a value for $E_g - \phi_o \sim$ 0.1eV. This implies that ϕ_o is above the semiconductor Fermi level, and hence that a net positive charge will be present at the interface.

7.4.3 Photoresponse Data

Figure 7.3 shows the photoresponse of a typical Au/ZnSeS Schottky diode in the form of a Fowler plot, as described in section 3.5.3. This diagram demonstrates the problem in trying to make such a measurement without a much thicker top electrode. Any generation of photoexcited electrons in the gold is swamped by the excitation of carriers in the semiconductor as the incident light reaches band gap energy ($\sim$2.73eV for $ZnSe_{0.94}S_{0.06}$). Even at the lower light energies corresponding to the barrier height estimated here

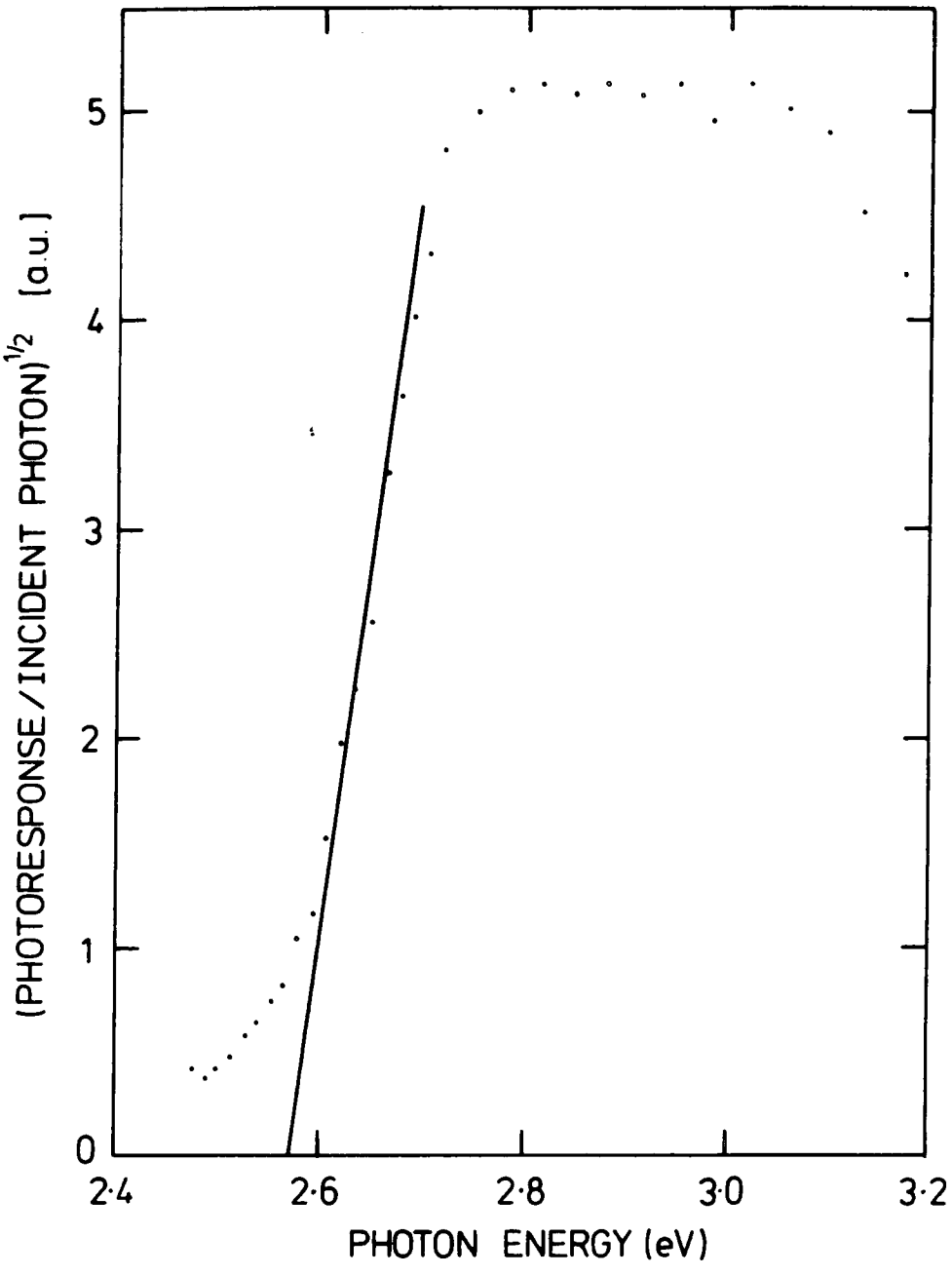

Figure 7.3 Fowler plot of the photoresponse of a Au/ZnSeS Schottky diode.

the metal-semiconductor photoresponse could not be distinguished. Consequently, this technique has not been used further in this work.

7.4.4 Energy Band Diagram

The value for ϕ_{bn} quoted here, 0.8eV as obtained from conductivity data, is appreciably lower than that predicted for an ideal diode by the Schottky-Mott theory of equation 3.10, which would give ϕ_{bn} = 1.01eV. This suggests that a net positive charge at interface states influences the barrier height, as proposed by the Bardeen model of section 3.5. The consequent pinning of the Fermi level relative to the band edges at the interface allows little change with bias to the difference in barrier heights for holes and electrons, ϕ_{bp} and ϕ_{bn} as were shown in Figure 3.6. Thus the minority carrier injection ratio will remain very low for these devices, allowing only very low levels of electroluminescence, as has been seen to be the case. In the model proposed for these Au/ZnSeS Schottky diodes the parameters are as shown in Figure 7.4. These assume a metal work function ϕ_m = 5.1eV and a bulk semiconductor electron affinity of 4.09eV (that reported for ZnSe(6)).

It is clear from the preceding results that there are good grounds for hoping to improve the performance of these structures as electroluminescent devices by the incorporation of a thin insulating layer. Initially it was necessary to establish that LB films of phthalocyanine could be used for this purpose. The next section describes initial measurements made on devices incorporating such films.

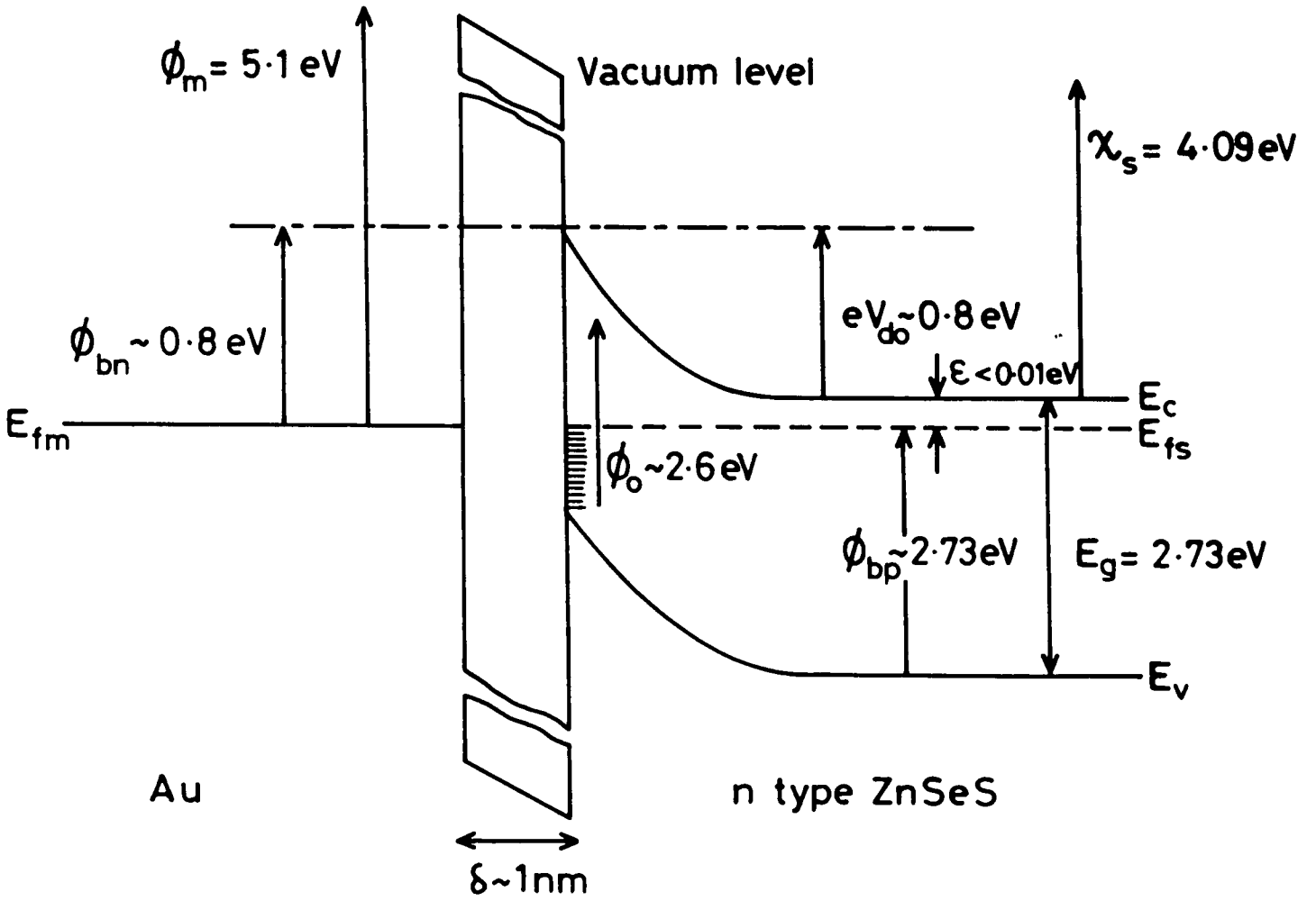

Figure 7.4 Proposed energy band diagram for the near-ideal Au/ZnSeS Schottky diodes.

7.5 NON-IDEAL SCHOTTKY DIODES AND MIS STRUCTURES

This section recounts electrical properties of devices on a single semiconductor substrate, half of which was coated with ten monolayers of phthalocyanine before the evaporation of gold top contacts. Preparation was as described in section 5.3, but it should be noted that the devices not incorporating the LB film were not expected to match the near-ideal Schottky diodes just described. The prolonged exposure of the uncoated region of the substrate to the aqueous environment of the Langmuir trough after etching made the build up of some significant interfacial layer inevitable.

7.5.1 Conductivity Data

Figures 7.5 and 7.6 show current-voltage characteristics of the two types of device. The effect of the insulating layer is readily apparent, particularly at lower biases. Clear evidence for the presence of a significant interfacial layer in the non-film devices is the current limiting which occurs at higher voltages, and allowed the diodes to be operated at a bias >10V before failure occurred. The reverse bias characteristic shows a clearer current saturation than that of the near-ideal Schottky diodes. Both types of device show a region apparently conforming to thermionic emission theory, but with ideality factors of 1.9 for the non-film structure and 3.5 for the devices incorporating the LB film. If the equations describing the thermionic emission theory were assumed valid, the characteristics of the devices would indicate barriers to electrons of height 0.86eV and 0.89eV respectively. The excess conductivity apparent in the lower

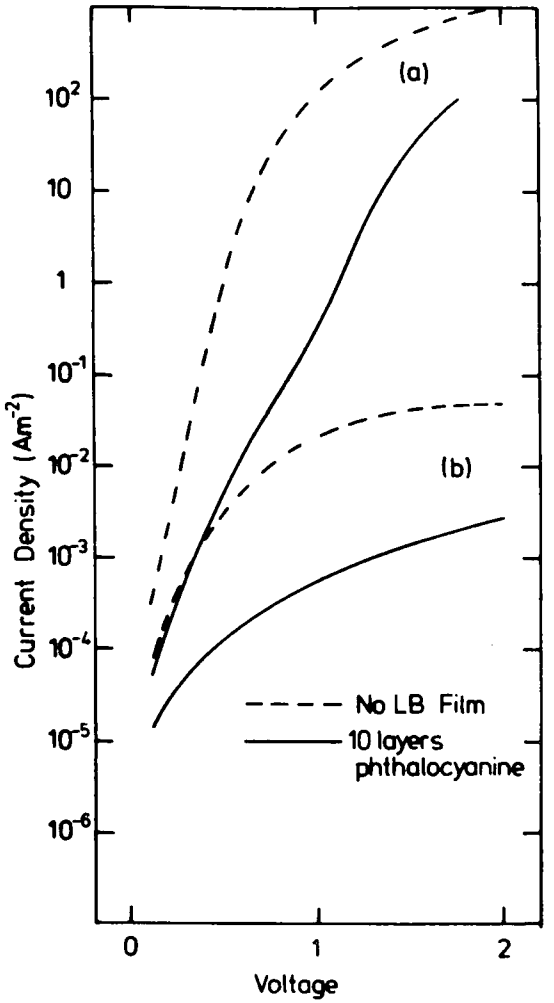

Figure 7.5 Conductivity data showing the effect of the incorporation of phthalocyanine multilayers into a Au ZnSeS diode. (a) under forward bias and (b) under reverse bias.

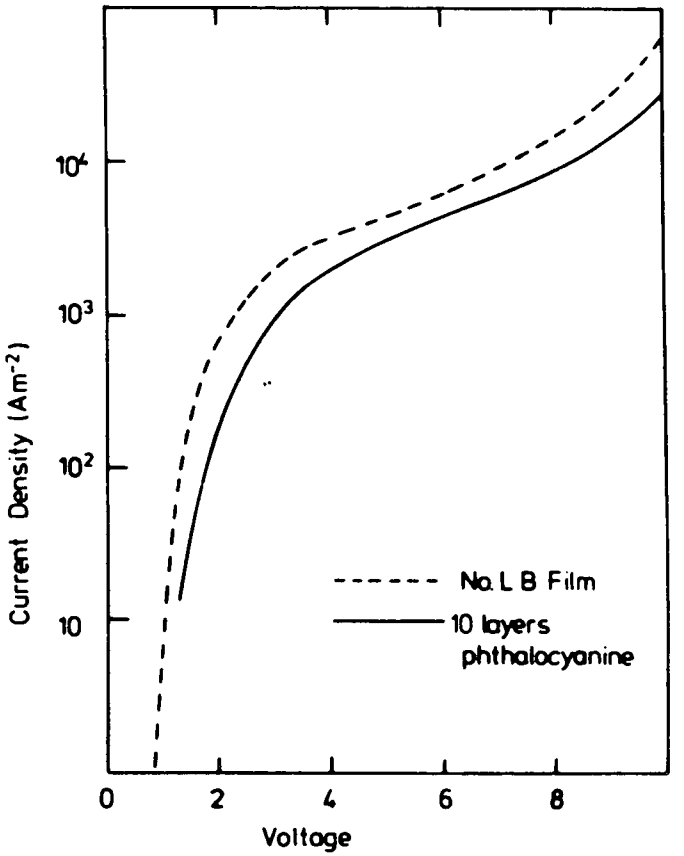

Figure 7.6 Higher field conductivity of the devices in Figure 7.5.

region of the forward bias characteristic of the LB film device is of uncertain origin. One possibility is that it is associated with a charge trapping effect at the interface, presumably due to the presence of the phthalocyanine film. Electrons from the semiconductor conduction band could be recombining in interface states then tunnelling through the insulator to the metal. However, this effect is not readily apparent in all of the MIS conductivity characteristics presented later. For both structures it is clear from Figure 7.6 that for $V \gtrsim 3V$ the current is no longer barrier limited but rather limited by the series resistance present. The characteristics indicate a resistivity of 2Ωm probably associated with the interface between the ZnSeS and the GaAs, since this value is rather high for the semiconductor components alone. Both structures exhibited detectable electroluminescence, in the case of the film-incorporating devices at forward biases as low as ~1V. The light output of devices is discussed in section 7.7.

7.5.2 Capacitance Data

The inverse capacitance squared vs voltage characteristics, averaged over a number of contacts on the two structures, are shown in Figure 7.7. Both are highly linear, but differ considerably from that of the Schottky diode structure in Figure 7.2. In each case the slope is over twice that for the Schottky barrier, though the semiconductor substrates were of near identical donor concentration. The intercepts with the voltage axis are much larger, and it is clearly unreasonable to attempt to analyse them in terms of equation 3.25, i.e that for the near-ideal

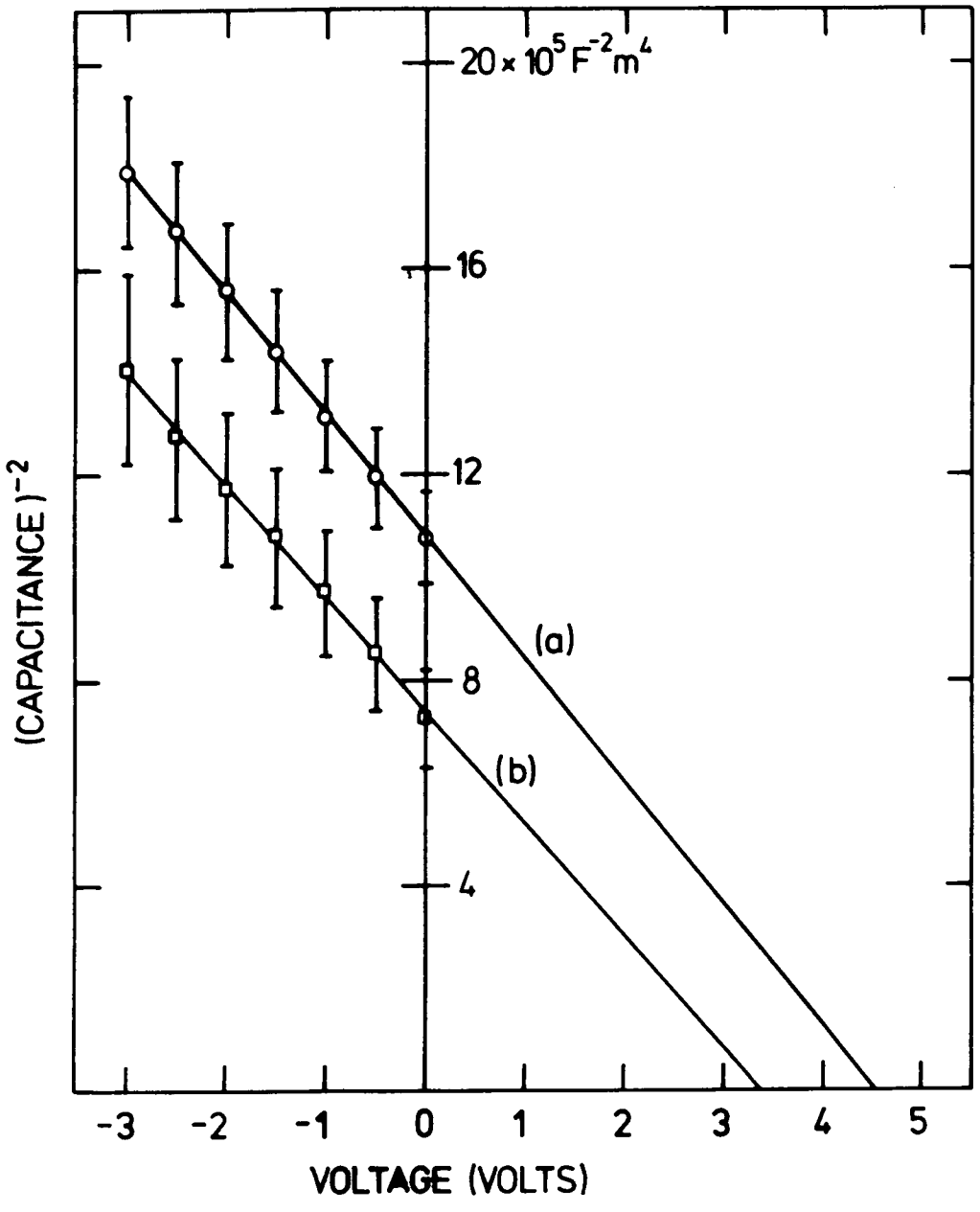

Figure 7.7 Inverse capacitance squared vs voltage plots for (a) Au/ZnSeS diodes incorporating 10 monolayers of phthalocyanine and (b) non-ideal Au/ZnSeS Schottky diodes.

Schottky barrier. It is, however, possible to explain the characteristics qualitatively in terms of Cowley's model for the metal-thin insulator-semiconductor diode. Although Fonash(10) has pointed out imperfections in the model, it does predict the change in slope and intercept in terms of the dielectric properties of the insulating layer and the concentration of surface states. Data can also be interpreted quantitatively to a limited extent. This is done in section 7.6, where the electrical properties of MIS diodes are investigated as a function of insulator thickness.

The growth of an interfacial layer when the etched semiconductor surface is exposed to the local environment for a prolonged period has a clear effect. It is highly probable that such a layer also exists beneath deposited LB films, hence the importance of minimising its growth by etching immediately before LB film deposition.

7.6 MIS DIODES WITH VARYING INSULATOR THICKNESS: ELECTRICAL CHARACTERISATION

This section deals with the electrical data for a series of Au/phthalocyanine/ZnSeS MIS structures with insulator thicknesses of 2, 4, 6 and 8 monolayers of phthalocyanine. The devices were constructed on semiconductor substrates identical to those used in sections 7.4 and 7.5. Their properties are contrasted with those of the near-ideal Schottky diode structures.

7.6.1 Conductivity Data

The conductivity of typical devices up to forward and reverse biases of 0.5V is shown in Figures 7.8 and 7.9

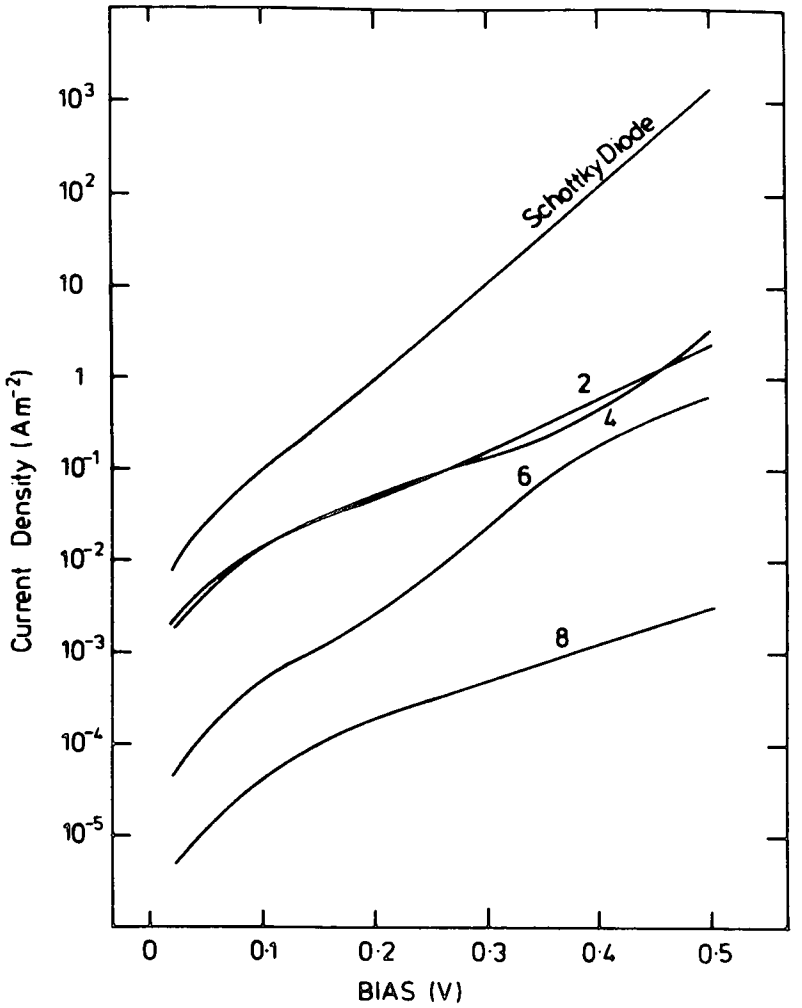

Figure 7.8 Forward bias conductivity data for Au LB film ZnSeS MIS diodes incorporating 2. 4. 6 and 8 monolayers of phthalocyanine.

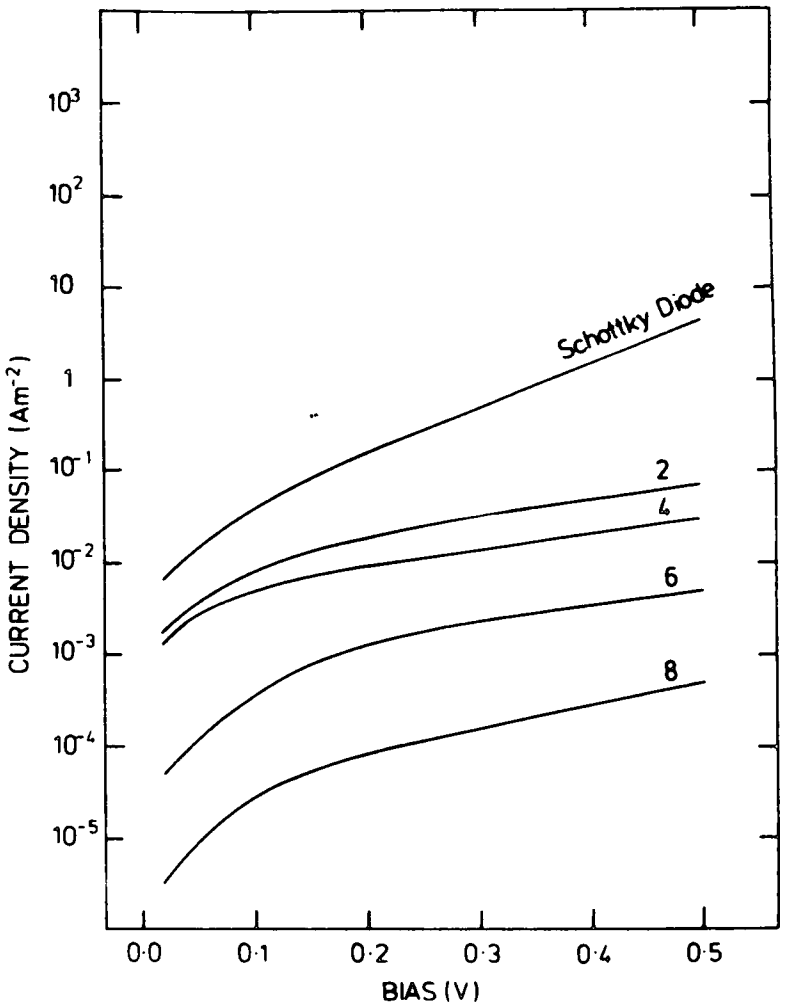

Figure 7.9 Reverse bias conductivity data for Au LB film ZnSeS MIS diodes incorporating 2. 4. 6 and 8 monolayers of phthalocyanine.

respectively. The devices all act as diodes inasmuch as their forward current increases more rapidly with bias than reverse current, though the characteristics are far from ideal. There is an overall trend for decreasing conductivity with increasing film thickness, and also a decrease in the value of J_o. The ideality factor increases from ~1.5 for the Schottky diode devices to ~8.6 for MIS devices incorporating 8 monolayers of phthalocyanine. Though there are some deviations, the ln(J) vs V characteristics are all fairly linear for V>3kT/e (i.e $\gtrsim$0.075V). The reason for the close similarity between the forward bias characteristics for 2 and 4 film layers remain uncertain. One arguable possibility is that 2 layers do not seal off the semiconductor surface sufficiently to prevent further formation of an interfacial layer there. There is a marked contrast between these results and those of Batey et al(4) for the low bias conductivity of GaP MIS diodes incorporating cadmium stearate films. Their devices showed ideality factors close to one even with several LB film layers. A single monolayer reduced J_o by about four orders of magnitude, but subsequent layers had relatively little further effect. However, their GaP MIS diodes incorporating phthalocyanine showed a decrease in ideality factor and J_o with film thickness. It thus seems likely this effect is associated with the properties of the phthalocyanine itself.

It is possible to qualitatively justify the characteristics presented here in terms of the analysis by Card and Rhoderick(8) as in section 3.6.1. They showed that the presence of an insulator will reduce J_o, primarily as a result of the increase in the effective barrier height to

electrons. This increase is a consequence of the barrier to current flow constituted by the energy gap of the insulator. The ideality factor will increase with the associated change in interface state charge density. However, this analysis can really only be applied to small changes in the ideality factor. It seems far more plausible that the limiting of conductivity is related to conduction through the phthalocyanine. One possibility is that the characteristics are indicative of the relationship $\ln(J) \propto V^{1/2}$, that associated with the Poole-Frenkel process proposed for other LB films(7).

7.6.2 Capacitance Data

Figure 7.10 shows the inverse capacitance squared vs voltage characteristics of the different structures averaged over a number of devices (error bars representing standard deviation have been excluded to simplify the diagram, but were typically ~10%). The plots are fairly linear, though some deviation is seen for thicker insulators. The overall trend apparent is that the slopes and intercepts of the plotted data both increase with film thickness. As with the conductivity data the characteristic for two layers of phthalocyanine appears anomalous. The voltage axis intercept V_o is greater than that for 4 layers, again suggesting that the growth of an interfacial layer at the semiconductor surface may be contributing to the insulator thickness. However, there is no obvious explanation for the decrease in slope which occurs.

Before attempting to further analyse the capacitance data, it is interesting to refer to the results of Batey et

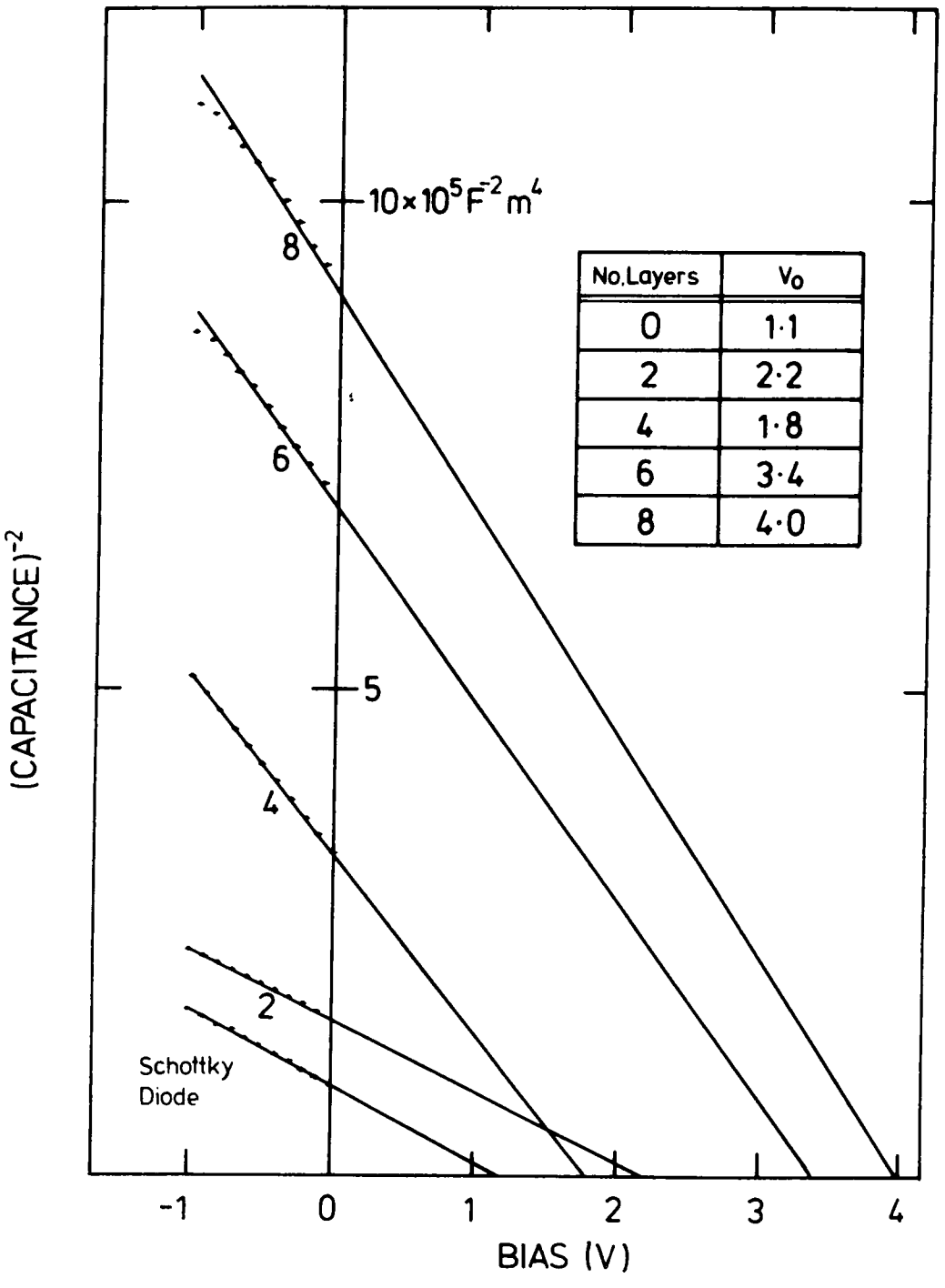

Figure 7.10 Inverse capacitance squared vs voltage plot for Au/LB film/ZnSeS MS diodes incorporating 2, 4, 6 and 8 monolayers of phthalocyanine.

al(4). Their capacitance plots showed the same general trend with insulator thickness as that observed above. Arguing in terms of the Cowley model as represented by equation 3.32 they reasoned that the increase in slope was indicative of the increasing relative effect of interface states at the semiconductor-insulator boundary. This would be manifested as an increase in the term α_2 (or more accurately an increase in the ratio $(1 + \alpha_1 + \alpha_2)/(1 + \alpha_1)$). Since this increase also affects the voltage axis intercept it is clearly impossible to derive a value for the diffusion voltage directly. However, by plotting the reciprocal zero bias capacitance as a function of the insulator thickness (as reproduced in Figure 7.11) they had grounds to propose that the diffusion voltage was independent of the presence of LB films. The device was modelled by three capacitances in series; that due to the LB film (C_{lb}), that due to any interfacial layer (C_i), and that associated with the semiconductor depletion region (C_{sc}) at zero bias (C_{sc} is of course voltage dependent). The zero bias capacitance of the device was then given by

$$1/C = 1/C_{lb} + 1/C_i + 1/C_{sc} \qquad (7.3)$$

$$= Nd_{lb}/\varepsilon_o\varepsilon_{lb} + \delta_i/\varepsilon_i + 1/C_{sc}$$

where N is the number of monolayers, d_{lb} and ε_{lb} the LB film monolayer thickness and relative permittivity, and δ_i and ε_i the thickness and permittivity of the interfacial layer. The high linearity of Figure 7.11, coupled with the fact that the slope corresponded closely with the dielectric thickness of cadmium stearate films as measured elsewhere(12), implied that the depletion region capacitance and hence the diffusion voltage V_{do} remain constant.

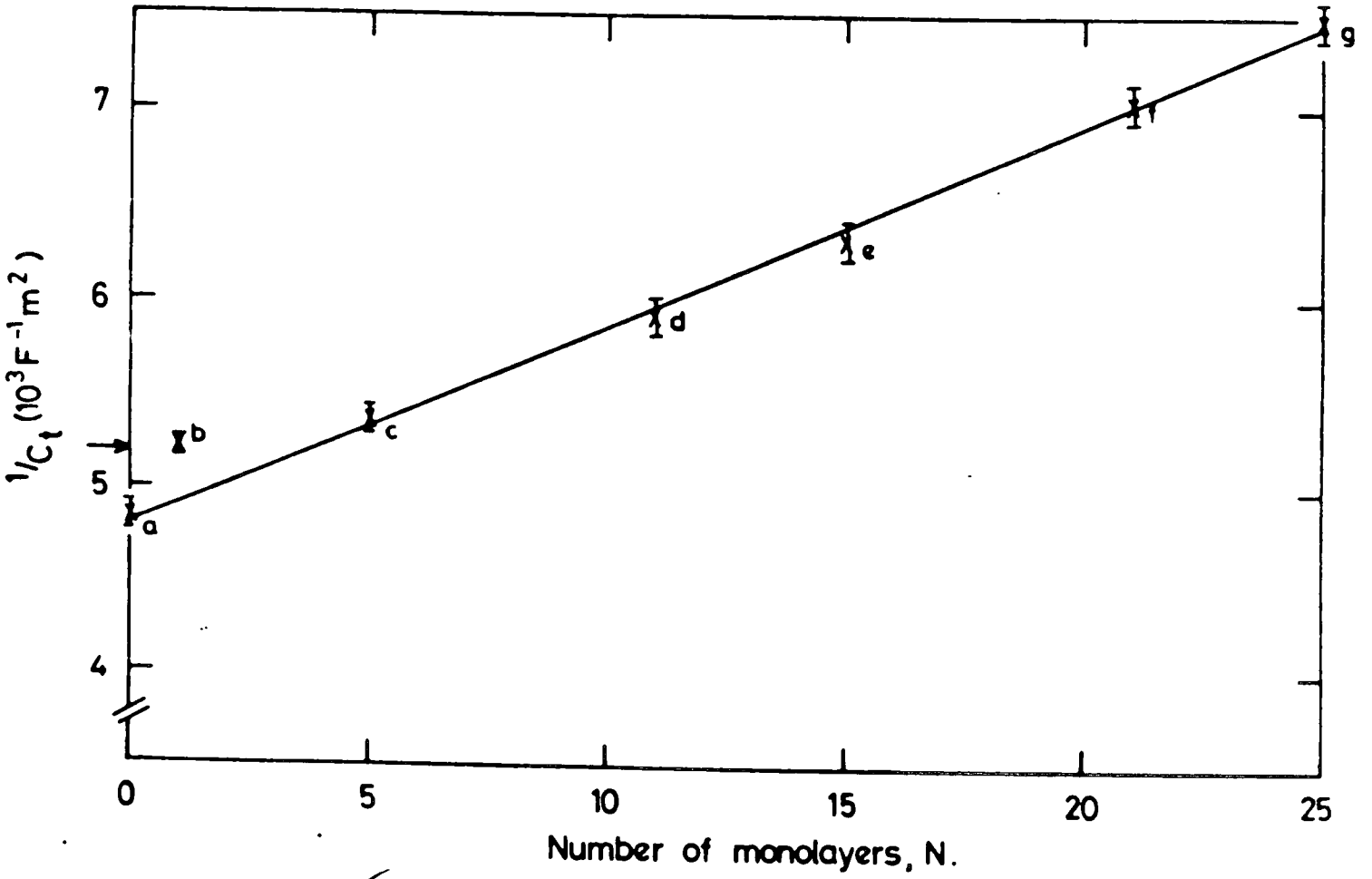

Figure 7.11 Reciprocal capacitance vs number of monolayers for GaP MIS diodes incorporating a range of thicknesses of cadmium stearate. (After Batey(4)).

An equivalent inverse capacitance plot for the devices studied here is shown in Figure 7.12. Again it is linear, but the dielectric thickness calculated from the slope is 0.75nm, compared with 0.25nm reported by Baker et al(13). This would indicate a film thickness of 2.25nm per layer (taking the dielectric constant of single crystal phthalocyanine as 3.0(14)). In view of a value ~2.4nm per layer found with recent preliminary ellipsometry measurements(15), and the fact that this thickness is still consistent with areas per molecule calculated for phthalocyanine films(16), it is thought reasonable to assume that the value obtained here is correct (this is claimed as the thickness per deposited layer - these are not necessarily monolayers). It is thus proposed that the diffusion voltage, and hence the height of the barrier to electrons presented by the semiconductor depletion region alone, is unaltered by the presence of phthalocyanine LB films. The model suggested for the system with this criterion is discussed in section 7.8.

The effect of an interfacial layer on this type of characteristic has been considered in terms of the Cowley model in 7.4.2. It has been found here that the data presented in Figure 7.12 can be satisfactorily analysed using Cowley's equation 3.32, even though it is known to be slightly in error. It can be seen from this equation that to increase the slope and intercept as has been found requires an increase in the relative value of α_2, and hence the number of surface states which are in equilibrium with the semiconductor rather than the metal. This is a logical progression as the thickness of the insulator between metal and semiconductor is increased. If it is assumed that the

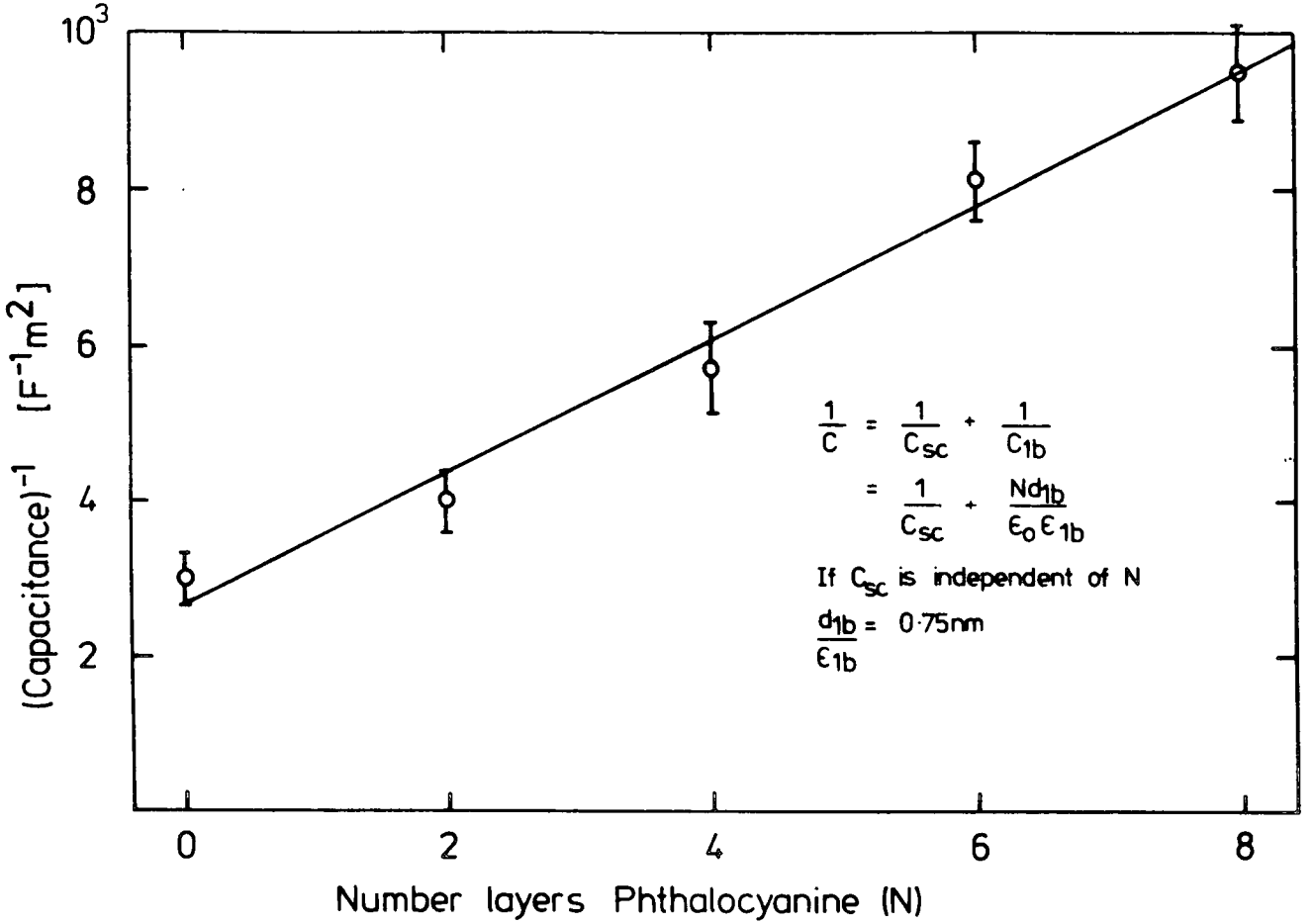

Figure 7.12 Reciprocal zero bias capacitance of Au/LB film/ZnSeS MIS diodes vs number of incorporated layers of phthalocyanine.

diffusion voltage ($V_{do} \sim 0.8V$) and donor concentration ($N_d \sim 1.5x10^{24} m^{-3}$) obtained from the near-ideal Schottky diode structures are correct, interface densities can be deduced. If the change in slope from the Schottky diode case is denoted by

$$x = (1 + \alpha_1 + \alpha_2)/(1 + \alpha_1) \qquad (7.4)$$

the voltage axis intercept from equation 3.32 can be rewritten

$$V_o = V_i/4x(1 + \alpha_1)^2 + V_i^{1/2}V_{do}^{1/2}/(1 + \alpha_1) + V_{do}x \qquad (7.5)$$

This is a quadratic in $1/(1 + \alpha_1)$ which can be solved

$$1/(1 + \alpha_1) = (-V_i^{1/2}V_{do}^{1/2} \pm \{V_i V_{do} + V_i(V_o - V_{do}x)/x\})/(V_i/2x)$$
$$= 2\{(V_o x)^{1/2} - (V_{do})^{1/2}x\}/V_i^{1/2} \qquad (7.6)$$

The capacitance data were analysed using this equation. Values of V_i were estimated using a single layer thickness for phthalocyanine of 2.25nm, and assuming an interfacial layer beneath the LB film identical to that for the near-ideal Schottky diodes. The results of this analysis are presented in Table 7.1. Note that the anomalous slope for 2 layers of phthalocyanine is not considered.

Although the interface state densities obtained must only be regarded as order of magnitude estimates, the ratios $D_{sa}:D_{sb}$ may be taken as fairly realistic. These display a trend for an increasing proportion of the interface states being in equilibrium with the semiconductor as the insulator thickness grows, as would be expected. D_{sa} does not drop significantly for film thicknesses beyond that normally associated with quantum mechanical tunnelling ($\delta \lesssim 10nm$). This suggests that communication between the metal and the semiconductor is by other processes (e.g Poole-Frenkel

Number of Monolayers	x	V_0 (Volts)	V_1 (Volts)	α_1	α_2	D_{sa} (m^{-2} eV^{-1})	D_{sb} (m^{-2} eV^{-1})	D_{sa}/D_{sb}
0	1.00	1.07	0.13	0.30	-	3.3×10^{16}	-	-
2	0.72(?)	2.2	2.0	-	-	-	-	-
4	1.81	1.8	6.2	5.7	5.4	9.0×10^{16}	8.6×10^{16}	1.05
6	1.98	3.4	12.7	1.2	2.1	1.3×10^{16}	2.3×10^{16}	0.55
8	2.23	4.0	21.5	1.3	2.9	1.1×10^{16}	2.4×10^{16}	0.47
10	2.35	4.5	32.6	1.5	3.4	1.0×10^{16}	2.3×10^{16}	0.44

TABLE 7.1 : Interface State Densities Deduced from C^{-2} vs V data for Au/phthalocyanine/ZnSeS MIS Diodes.

conduction in the LB film). This is the same conclusion as that drawn by Batey et al for Au/GaP structures incorporating fatty acid LB films(4).

7.7 MIS DIODES WITH VARYING INSULATOR THICKNESS: OPTICAL CHARACTERISATION

This section is concerned with the study made of the EL properties of the MIS diodes discussed in sections 7.5 and 7.6. Light output was measured using the techniques described in Chapter 5.

7.7.1 Spectral Distribution of Electroluminescence

The forward and reverse bias EL spectra of an MIS diode with 10 layers of phthalocyanine incorporated are shown in Figure 7.13. The spectra have been corrected for the responses of the monochromator and photomultiplier tube used in the measurement. The forward bias EL was excited by a drive current of $\sim 5 \times 10^{4}$ Am^{-2} at 5V, and the reverse bias EL by a drive current of $\sim 3 \times 10^{3}$ Am^{-2} at -10V. The diodes were prone to catastrophic failure beyond this reverse bias. Power conversion efficiencies were estimated by intensity comparisons with unencapsulated green-emitting GaP LEDs supplied by Dr.G.Lidgard of Plessey Ltd. The external power conversion efficiencies estimated for both biases under the above conditions were only $\sim 3 \times 10^{-7}$ %, but this figure improved markedly for higher forward bias.

The forward bias EL output peaked in the yellow at 580nm with a half height width of 80nm. Such deep centre emission from ZnSe is well-documented, and temperature dependent studies of photoluminescence have shown it to be a

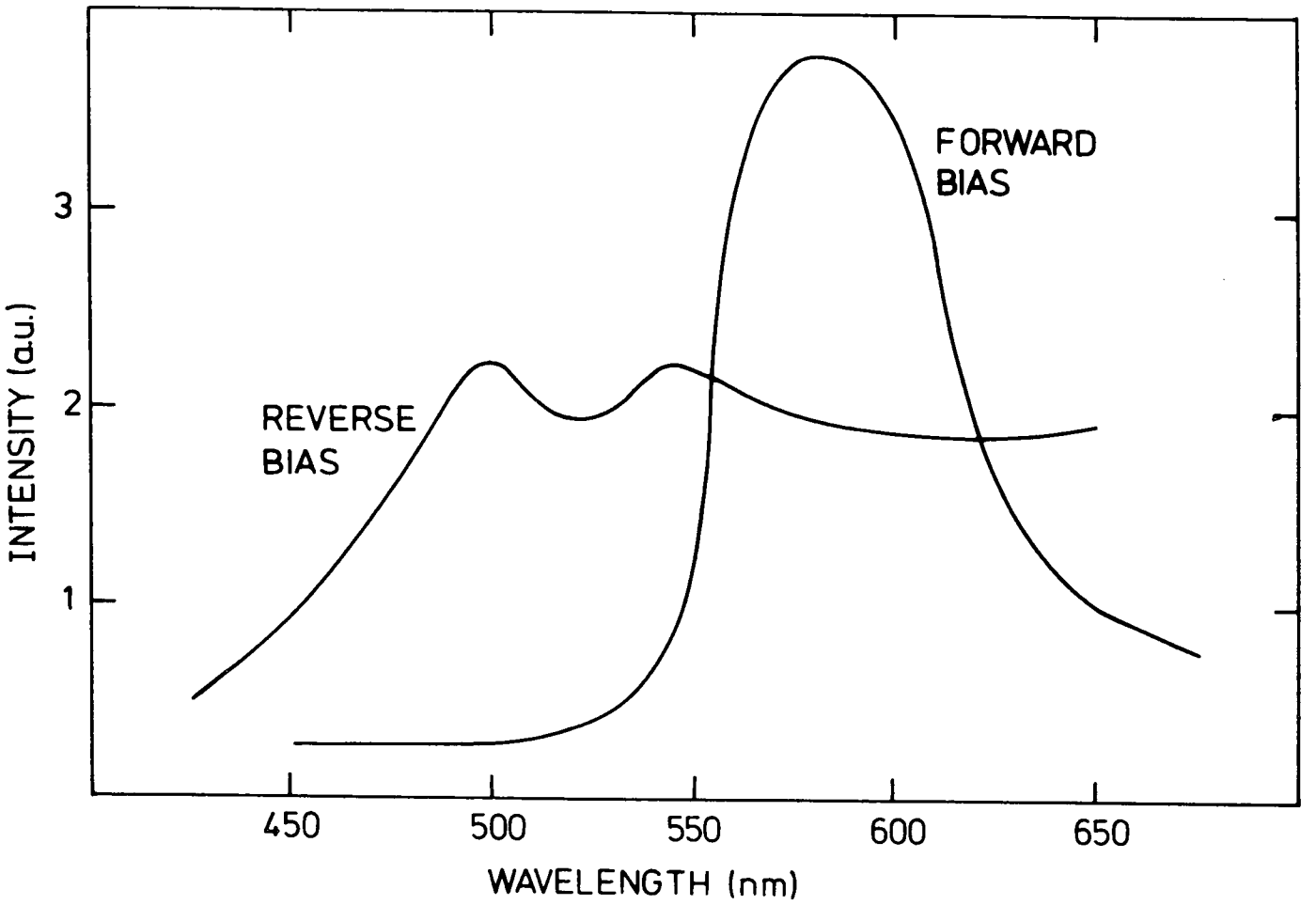

Figure 7.13 Spectral content of light emitted by Au/LB film/ ZnSeS MIS diodes under forward and reverse bias.

self-activated luminescence band arising from localised states of a centre consisting of a Zn vacancy and an Al impurity(6). None of the diodes investigated here showed any measurable band-to-band EL which would be expected to peak in the blue at about 460nm. A past study of the cathodoluminescent properties of ZnSe films grown by MOCVD found that the ratio of photon intensity in the blue to that in the yellow varied between 10^{-2} and 10^{3} over a range of samples(17). It is thought that it should be possible to find an optimum doping density such that the more desirable blue emission will dominate, without excessively reducing the conductivity of the semiconductor structures. Indeed, preliminary work on MOCVD films of ZnSe with a donor density $\sim 10^{17}$ cm^{-3} detected EL output dominated by a narrow band at 469nm(4). The devices studied in that case suffered from high resistivity (and hence required high operating voltages) due to the lattice mismatch between GaAs and relatively pure ZnSe.

Reverse bias EL from the diodes has not been studied in detail since devices were prone to failure at the required operating voltages. However, the spectral distribution of the EL obtained is clearly different from that for the forward bias case. The structure of the characteristic is far more broad band, and shows two distinct peaks at 500nm and 540nm. A band peaking at 545nm has previously been reported for reverse bias EL from crystals of $ZnS_{0.6}Se_{0.4}$, and assigned to impact ionisation of self-activated luminescent centres(18). Here it will suffice to suggest that the emission is a result of one of the high field effects described in section 3.2.1. It should be noted that

(A)

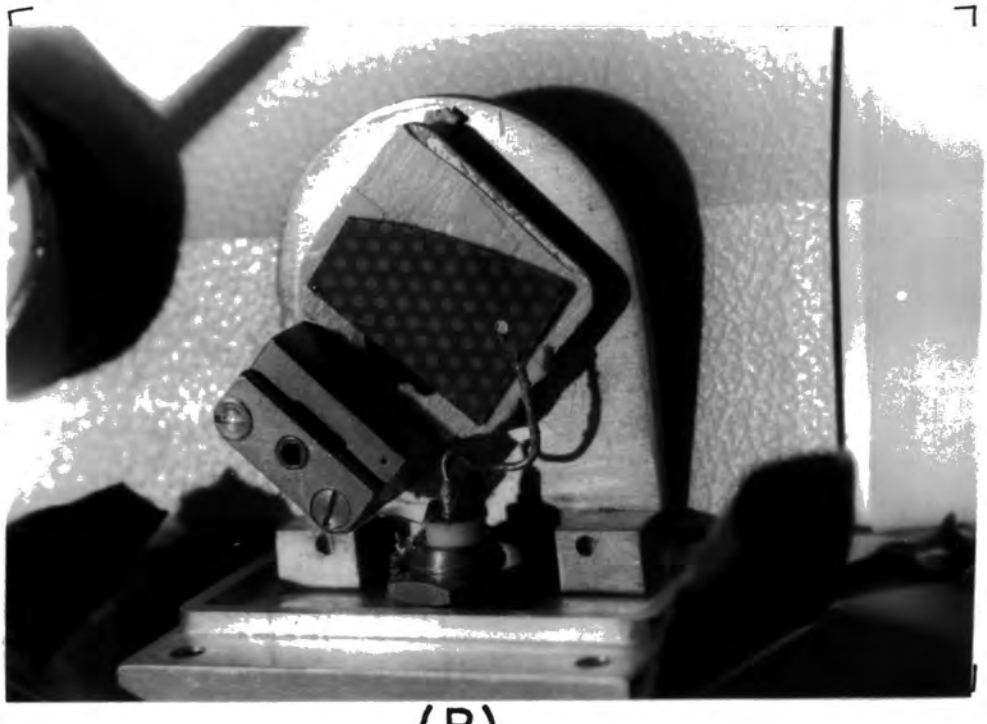

(B)

Figure 7.14 Au/phthalocyanine/ZnSeS MIS diodes operating in (a) forward and (b) reverse bias.

the threshold voltage for detecting EL was invariably 6V in reverse bias, compared with ~1.1V in forward bias.

Figures 7.14a and b are photographs of diodes operating at a forward bias of 10V and a reverse bias of 20V respectively. The gold top electrodes are 1mm in diameter. The forward bias case shows light being emitted through and around the gold top electrode, whereas light was only seen to come through the electrode for reverse bias. A possible explanation is the lower self absorption in the semiconductor of the higher wavelength forward bias EL (Figure 7.15 shows the reflectance spectrum of a ZnSeS/GaAs sample indicating an absorption edge at 455nm). However, there is insufficient difference between the spectral outputs of the two polarities to justify such contrasting behaviour. It is likely that the spreading of light emission is more a consequence of injection effects extending beyond the area of the electrode due to lateral conduction in the phthalocyanine film.

7.7.2 Bias Dependence of EL Output

Figures 7.16 and 7.17 are logarithmic plots of the increase in forward bias EL intensity with voltage and current density respectively (the ordinates are the same in both diagrams). They are typical characteristics of devices incorporating 10 monolayers of phthalocyanine. For lower levels of light output both characteristics obey power law relationships which remain valid up to a current density $\sim 2 \times 10^{4} Am^{-2}$ corresponding to a bias of 8V. As indicated, the EL intensity increases as V^{13} and as $J^{4.3}$. This is somewhat different to the variation reported for ZnSe MIS diodes by other workers where the relationship took the form I

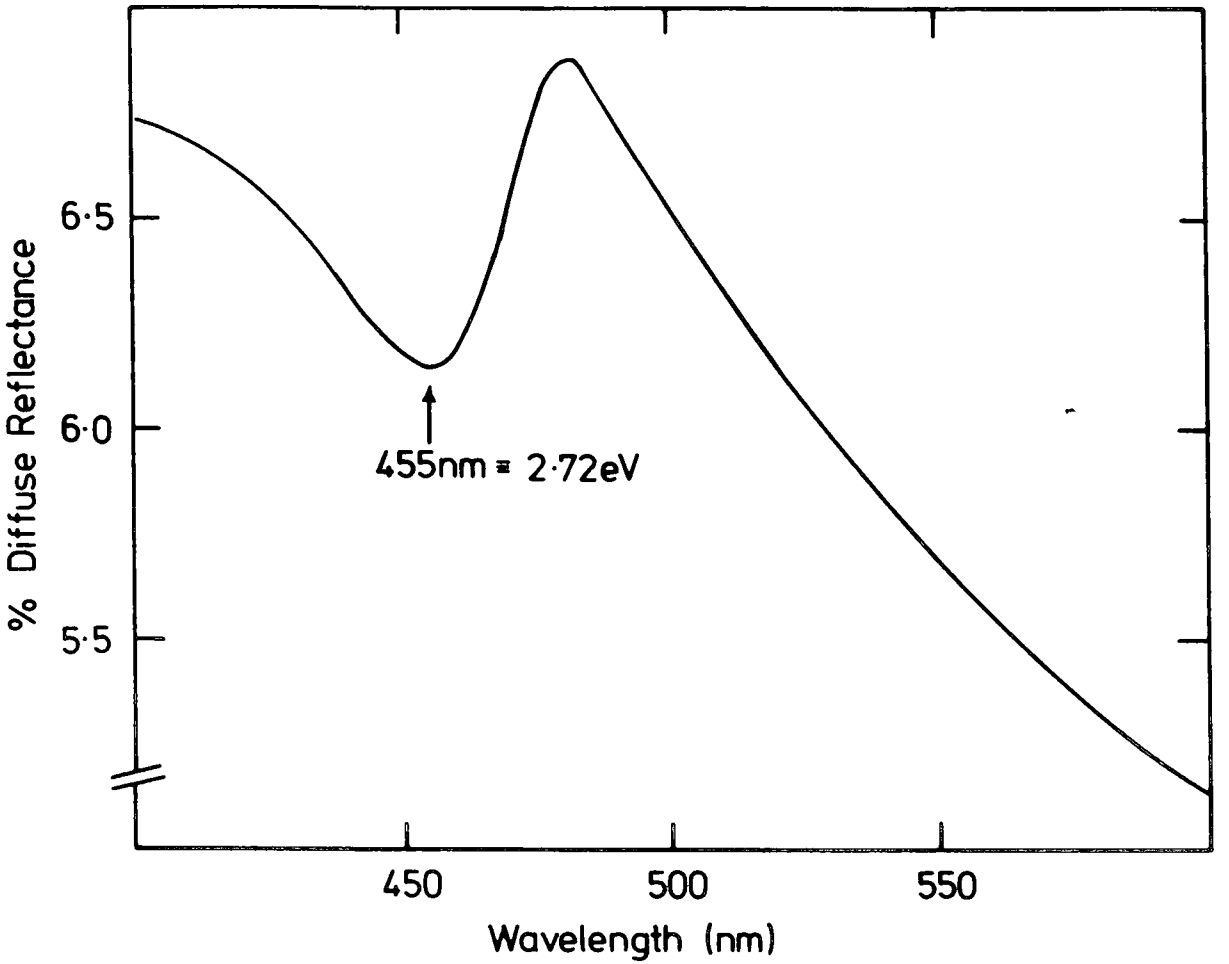

Figure 7.15 Optical reflectance spectrum for ZnSeS grown by MOCVD onto GaAs.

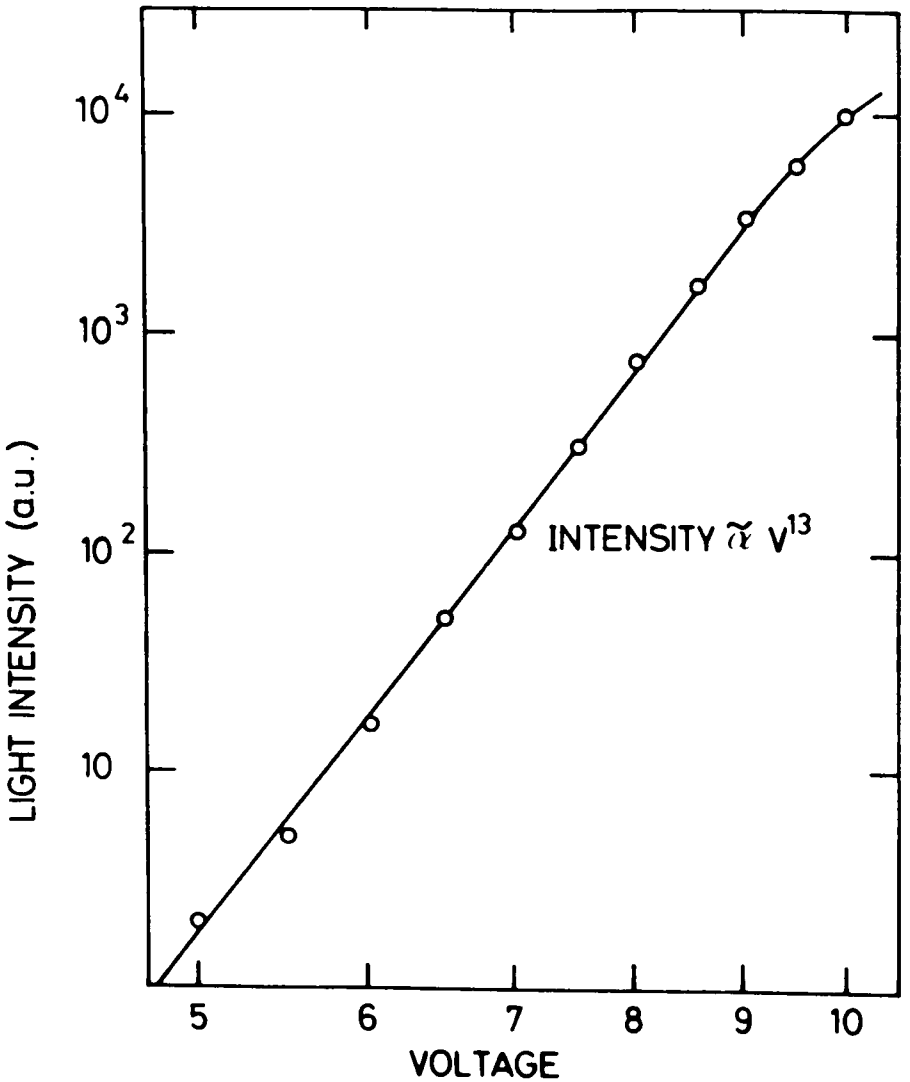

Figure 7.16 Output light intensity vs voltage (log scale) of a Au LB film ZnSeS diode under forward bias.

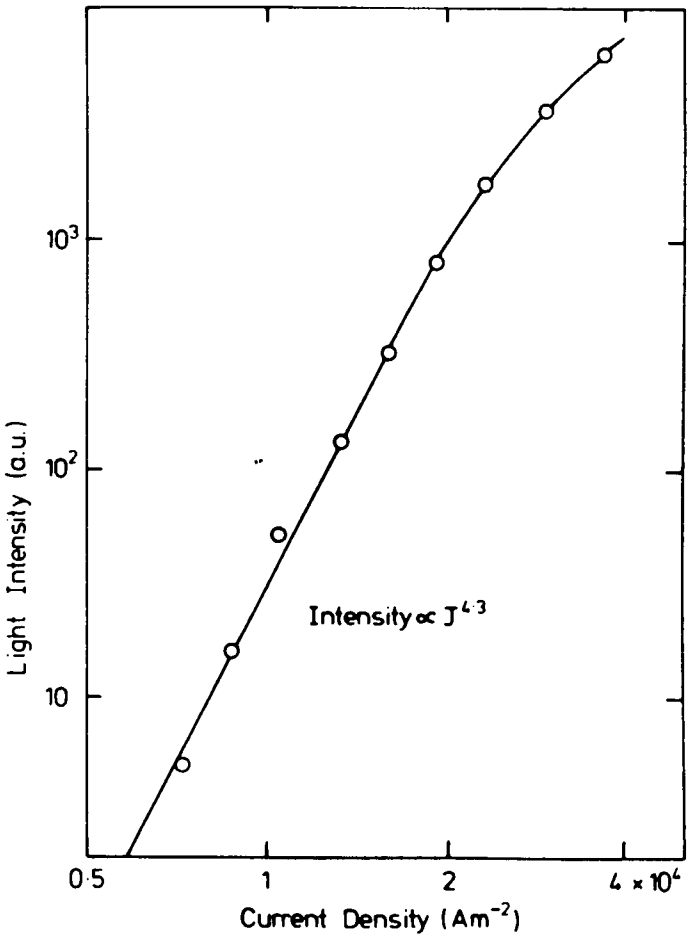

Figure 7.17 Output light intensity vs current density (log scale) for the same device as Figure 7.16.

(intensity) $\propto J^n$, with $n \sim 2$ for low current levels ($J < 10^2 Am^{-2}$) and $n \sim 1$ for higher current levels(19,20). A linear dependence of emission intensity on device current has often been observed for radiative recombination associated with a high-field impact-ionisation process(6). The more rapid rise here is thought to indicate that the voltage drop across the insulator is continuing to raise the semiconductor valence band edge towards the metal Fermi level. The minority carrier injection ratio and hence the efficiency of the device will rise exponentially with the decrease in the difference in barrier heights to electrons and holes. That this degree of band bending has not been achieved at a lower bias may be an indication that a substantial proportion of the voltage applied is being dropped at the interface between the ZnSeS and the GaAs substrate. It is certainly clear from the conductivity data of Figure 7.6 that some series resistance effect is dominating the characteristics for voltages greater than ~5V. This would help explain the rather low external efficiencies attained with the devices. The maximum power conversion efficiency estimated for a typical diode incorporating 10 monolayers of phthalocyanine was $\sim 2 \times 10^{-4}$ % at a bias of 10V and a current density $\sim 5 \times 10^4 Am^{-2}$, close to the reliable operating limits of the devices.

7.7.3 Variation of EL Efficiency

Figures 7.18 a and b show the variation in the estimated EL power conversion efficiencies of Au/LB film/ZnSeS diodes with the number of incorporated monolayers. In each case the devices were driven by a current density of $5 \times 10^4 Am^{-2}$.

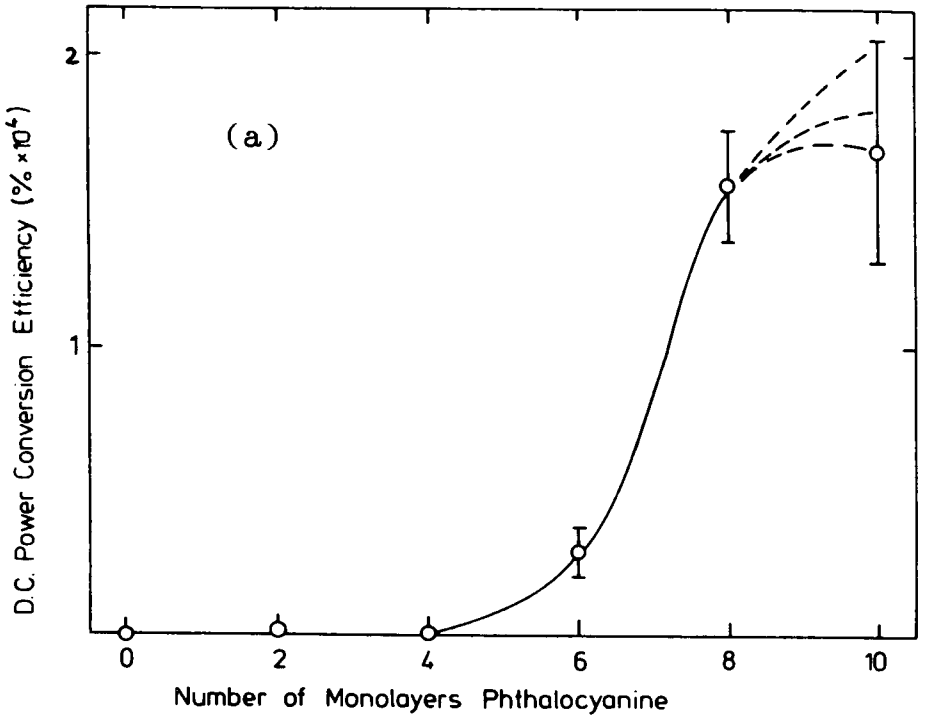

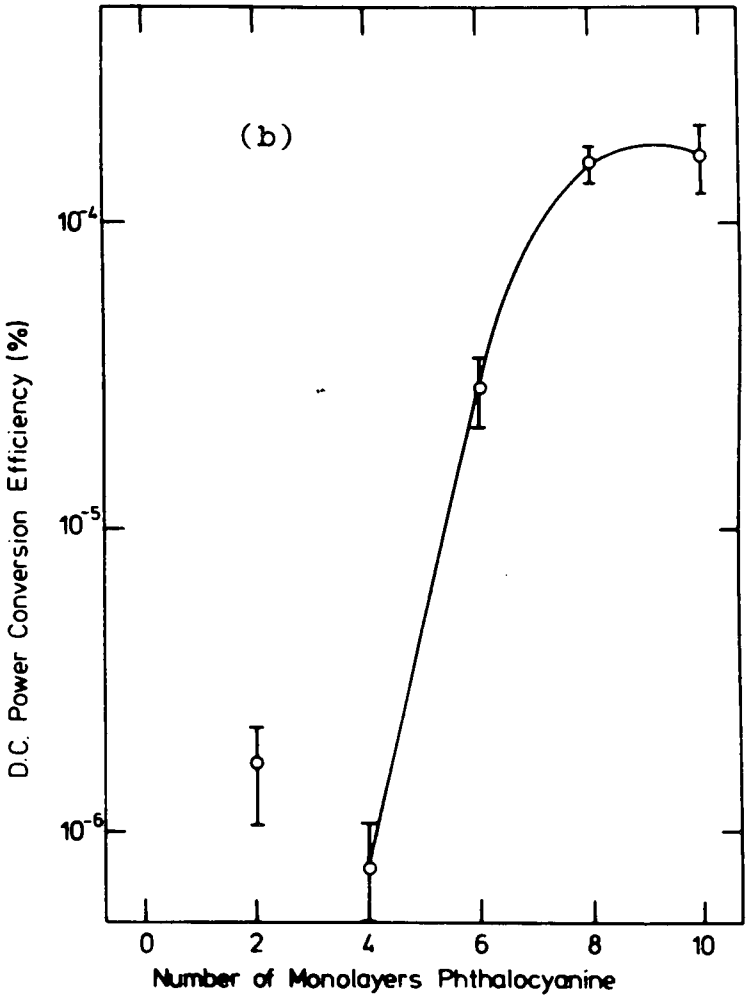

Figure 7.18 External electroluminescent dc power conversion efficiency of Au/LB film/ZnSeS MIS diodes vs number of incorporated phthalocyanine monolayers. (a) linear plot, (b) semi-logarithmic plot.

Figure 7.18b is a semi-logarithmic plot which shows more clearly the lower efficiencies obtained for devices incorporating 2 and 4 monolayers of phthalocyanine. Once again it can be seen that the result obtained with 2 monolayers appears anomalous.

It is not realistic on the basis of these results to claim that an optimum insulator thickness has been determined. Diodes with insulator thicknesses greater than 10 monolayers were not available due to difficulties yet to be overcome in the deposition of thicker LB films of phthalocyanine. Nonetheless, an increase in EL efficiency of over two orders of magnitude between diodes incorporating 4 and 8 monolayers contrasts clearly with the very small change between 8 and 10 monolayers. Thus it seems likely that the characteristic has at least reached a plateau if not an optimum. If the thickness of 10 monolayers is taken to be ~23nm (as claimed in section 7.6.2), this result can be compared with those reported by other workers. The only related data for phthalocyanine LB films are those of Batey et al for GaP MIS diodes(3), reproduced in Figure 7.19 (note that it is suggested here that the optimum thickness δ_{opt} was actually ~16nm). Although there are obvious similarities between the characteristics, the far greater relative increase in EL efficiency reported here makes direct comparison difficult. However, the results of Livingstone et al(19) (reproduced in Figure 7.20) appear more closely related. They claimed an increase in efficiency of over four orders of magnitude with increasing insulator thickness up to ~25nm, and little subsequent change up to 180nm. In their work the insulator was a native oxide grown on Mn doped ZnSe,

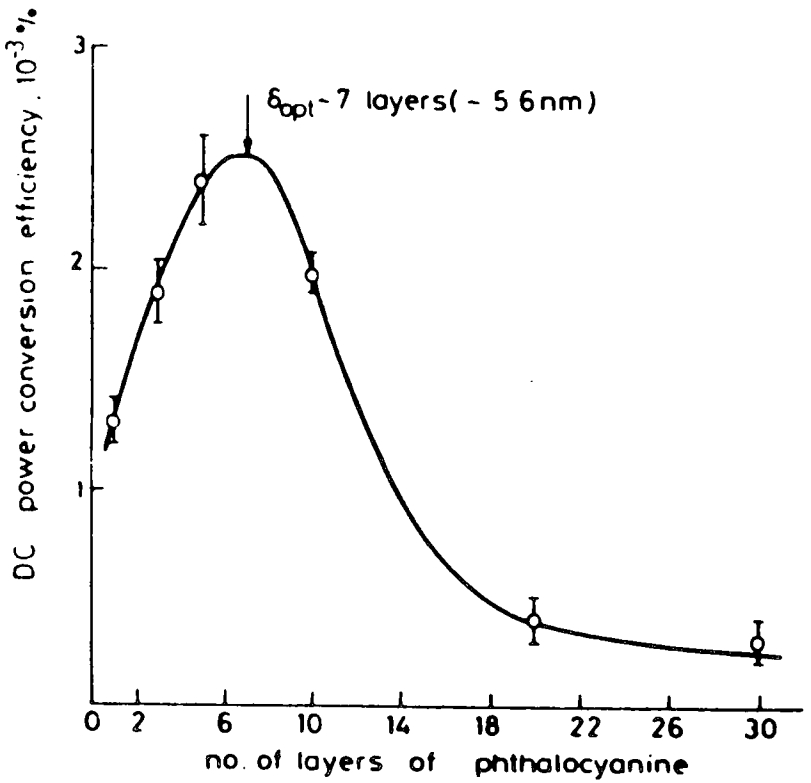

Figure 7.19 DC power conversion efficiency against number of layers of phthalocyanine for GaP MIS diodes. (After Batey et al(3)).

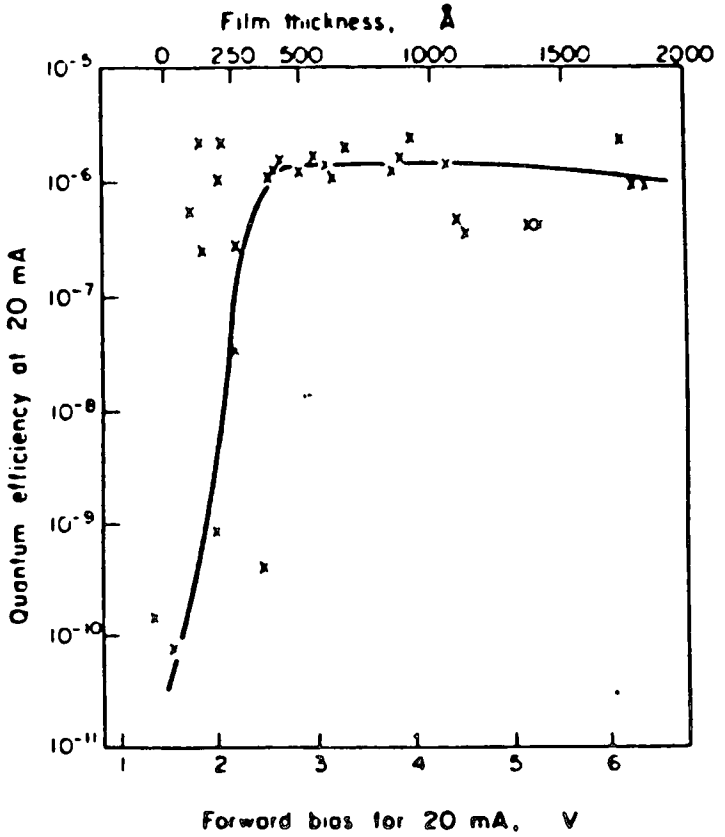

Figure 7.20 Quantum efficiency of ZnSe:Mn diodes measured at 20mA against estimated film thickness. (After Livingstone et al(19)).

and thickness was estimated from conductivity and capacitance measurements. Broadly similar results have been obtained by Watanabe et al(20) using vacuum deposited ZnSe films as an insulator. In all these cases maximum efficiency was obtained for insulator thicknesses well beyond those at which tunnelling of carriers between metal and semiconductor would play a significant role. One favoured explanation of the characteristics is a two-stage Auger recombination process first proposed by Fischer(21). This and other possible processes occurring in the Au/LB film/ZnSeS diodes are discussed in section 7.8.

7.7.4 Device Degradation

If LB film insulators are ever to form the basis of a commercial device it is important that they maintain their properties under the operating conditions associated with EL. Phthalocyanine LB films were used in this research because they have been found to be far more mechanically and thermally stable than classical materials. The EL intensity as a function of time for a diode incorporating 10 monolayers of phthalocyanine is shown in Figure 7.21. The device was run at a continuous current density of $5 \times 10^{4} Am^{-2}$ using a constant current source. The steep curve (a) was the initial degradation of the device from switch on; (b) shows its behaviour after being switched off and allowed to recover for ~30 minutes; and (c) after being run for 15 hours followed by a 30 minute recovery time. The characteristics indicate that a fairly rapid deterioration in performance occurs, but that EL output stabilises at about 20% of its initial value. The output did not drop significantly from this value even after

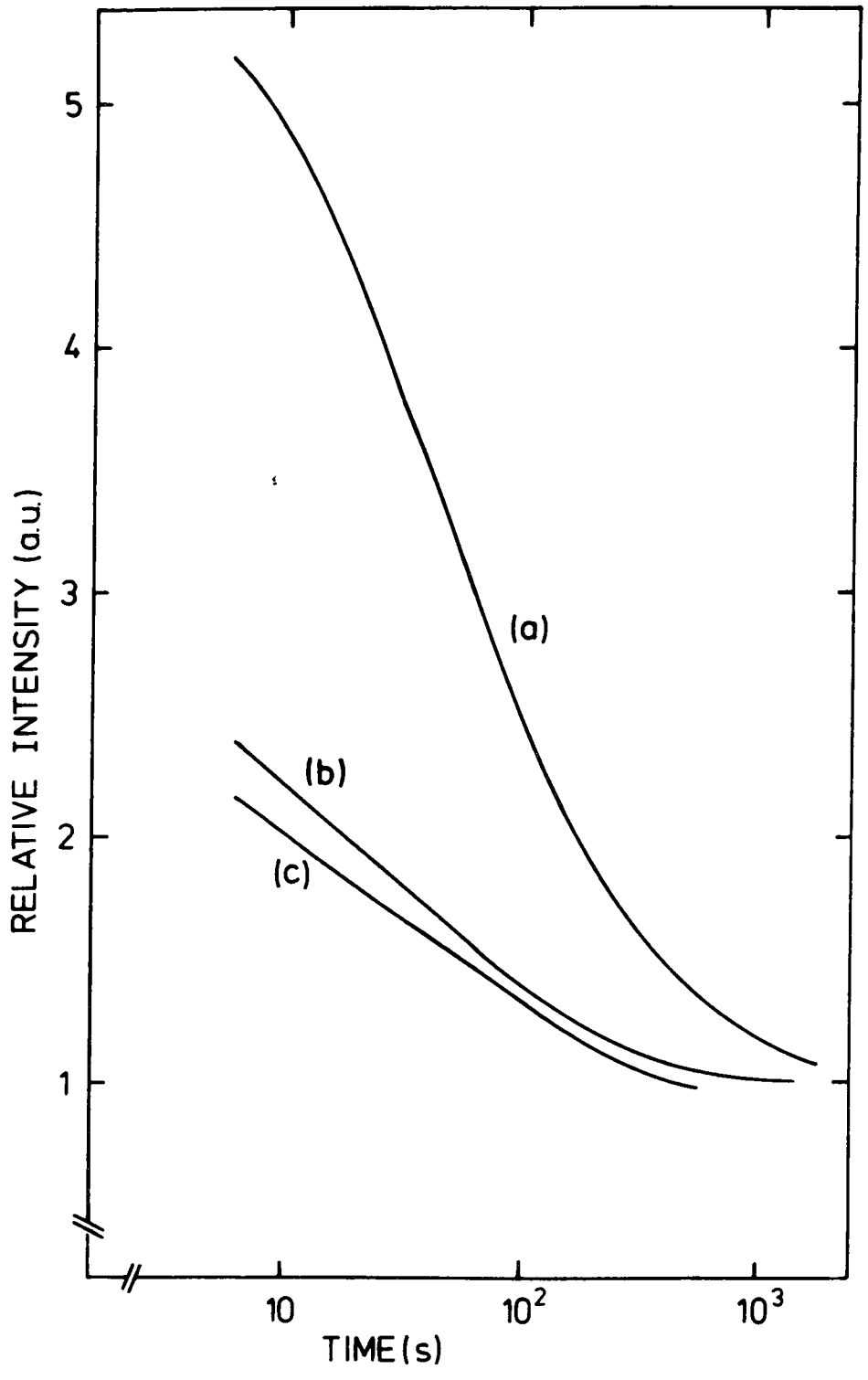

Figure 7.21 Device degradation characteristics of electroluminescence from Au/LB film/ZnSeS MIS diodes. (a) From first switch on, (b) after 30 minutes recovery, (c) after 15 hours operation and 30 minutes recovery.

15 hours continuous operation. The conductivity was noted to have nearly doubled after this time, hence the power conversion efficiency was at ~40% of its initial value. The partial recovery of the device suggests that an increase in conductivity due to heating effects, associated with the fairly high current density, may be a contributory factor. The effect may be reducible if the diodes were pulse driven. However, the irreversible drop to about 40% of the initial intensity is probably associated with changes in the conductivity of the phthalocyanine film. If future research leads to devices with the high efficiencies required for commercial development, the mechanisms responsible for this degradation will need to be studied in depth.

7.8 PROPOSED MODEL FOR MIS DEVICES

An energy band model for the MIS devices studied in this resarch must justify their observed properties. The relevant properties are an estimated barrier height due to the depletion region of ~0.8eV, a threshold for observed EL ~1V, a rapid rise in EL output up to a forward bias of ~10V, and a reduced rate of increase beyond this. Figure 7.22 represents the energy bands in a device under forward bias (cf Figure 3.7). For bias voltages below the threshold ($V \lesssim 1V$) case (a) applies. The most resistive part of the device is the depletion region, and the primary effect of the forward bias is to raise the Fermi level in the semiconductor to cause a levelling out of the energy bands. There is little change to the difference in barrier heights to electrons and holes , and consequently γ remains low. Beyond the threshold voltage (b) a significant part of the applied bias is dropped across

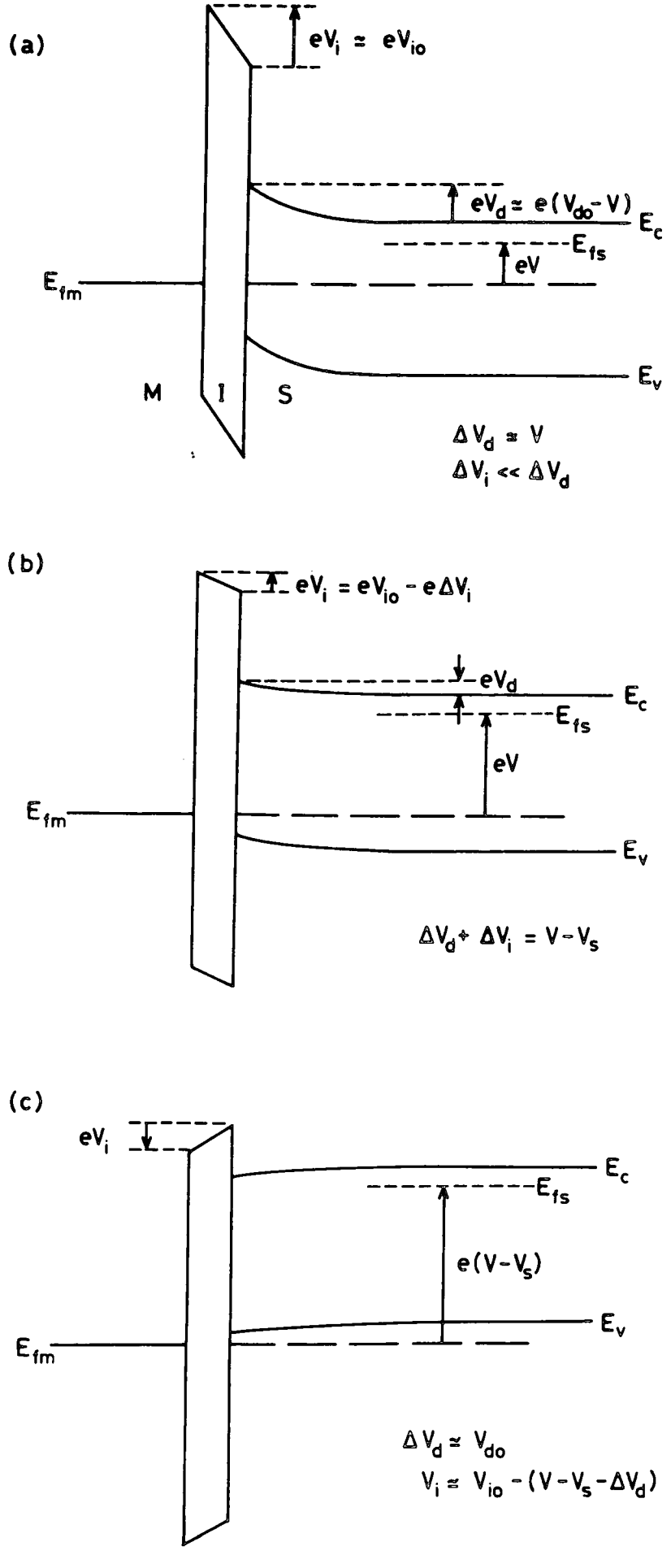

Figure 7.22 Proposed energy band diagrams for Au/phthalocyanine/ZnSeS devices: (a) $V \lesssim 1V$ (below threshold); (b) $1V \lesssim V \lesssim 10V$ (above threshold); and (c) $V \gtrsim 10V$.

the insulator, and E_{fm} is able to descend on the band diagram towards the semiconductor valence band E_v. The reduction in the semiconductor barrier height for holes leads to an increase in γ and hence EL output, as an increased population of electron hole pairs becomes available for radiative recombination. γ will increase exponentially with ΔV_i. As V is increased the total current through the device is limited by series resistance effects and the associated voltage drop V_s becomes a significant fraction of V. Figure 7.6 showed that voltage starts to be dropped across the series resistance at ~2V forward bias. Thus it is not until V $\gtrsim$ 10V that the metal Fermi level is below the semiconductor valence band edge (Figure 7.22c). At this bias and above the increase in the number of valence band states contributing to the hole current will have a relatively weak dependence on ΔV_i. This effect is manifested as a reduced rate of increase in the EL output with bias. The model which has been described here is simply an adaptation of that used in conventional tunnel injection theory(22). The theory also predicts, for a fixed total current density, that γ will initially increase with increasing insulator thickness (δ) since ΔV_i is larger, until the case where $E_{fm} \sim E_v$ after which the hole current grows less rapidly with δ. At some thickness the insulator will have a greater limiting effect on carrier transport than diffusion processes in the semiconductor bulk, and the hole current will begin to fall. For an ideal insulator this thickness will be dictated by the limits for quantum mechanical tunnelling, and indeed Card and Smith(22) reported an optimum insulator thickness of ~4.0nm for GaP MIS devices incorporating SiO_2. The results reported

here, and, for example, those of Batey et al(1,2,4) and Livingstone et al(19), have indicated that γ can increase with δ well beyond the limit for tunnelling ($\delta \sim 10$nm). Clearly an alternative minority carrier injection mechanism must be responsible.

Fischer(21) proposed a two-stage Auger recombination process, shown schematically in Figure 7.23. Electrons coming over the barrier presented by the insulator will enter the metal with kinetic energies given by $E_{fm} + \phi_b$ ①, and some may excite deep-lying electrons to states close to the Fermi level by an Auger recombination process. If the holes produced are sufficiently energetic they may surmount the hole barrier presented by the insulator ② and recombine radiatively in the semiconductor. This mechanism is believed to be inherently inefficient, which could explain the low EL efficiencies obtained here and elsewhere. The rate of injection of holes will depend critically on the band structure of the insulator, and the barriers it presents to electrons and holes. The process by which carriers traverse the insulator remain uncertain, and alternative mechanisms such as holes moving via trapping levels in the insulator bandgap cannot be ruled out.

7.9 SUMMARY

This chapter has presented the results of an investigation of electrical and optical characteristics of Au/phthalocyanine LB film/ZnSeS electroluminescent MIS diodes. These results and some of the conclusions drawn from them may be summarised as follows:

(i) Au/ZnSeS structures were shown to behave as

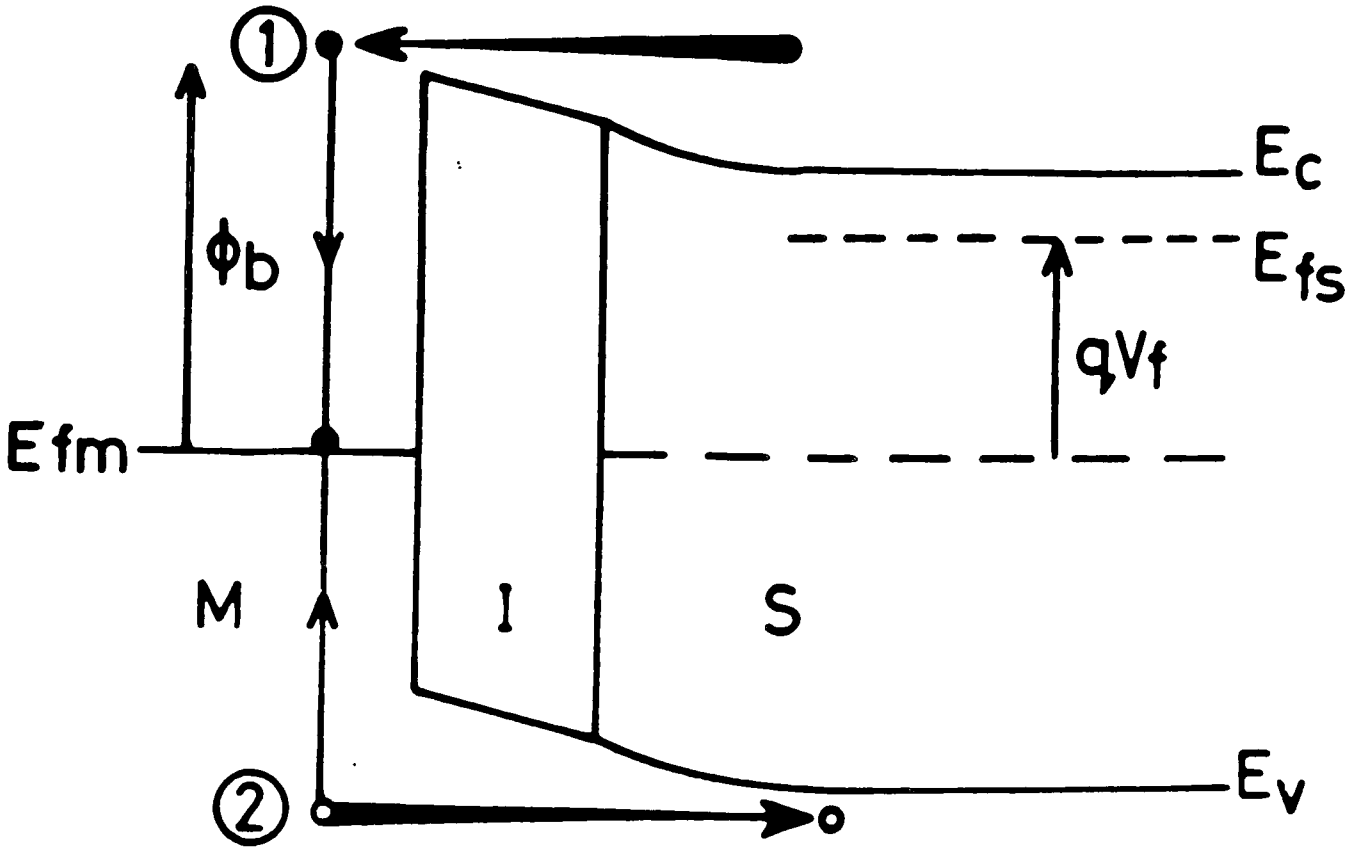

Figure 7.23 Schematic representation of hole injection by a two-stage Auger recombination process. ① Energetic electron enters metal, ② energetic hole injected into semiconductor.

near-ideal Schottky diodes with a barrier height to electrons ~0.8eV. The presence of a thin interfacial layer, constituting an additional barrier to the transport of carriers between the semiconductor and metal, was deduced. This layer did not cause sufficient band realignment to significantly raise the minority carrier injection ratio, and consequently no EL was detectable from these devices at drive current densities up to $\sim 10^{4} Am^{-2}$. Beyond this current the devices were prone to failure.

(ii) The incorporation of a phthalocyanine LB film insulator into the diodes limited the total current flow and El was detectable with a threshold voltage ~1V in forward bias and ~6V in reverse bias. For a forward bias $\gtrsim$3V the conductivity characteristics were dominated by a series resistance, believed to be a result from the interface between the ZnSeS epitaxial layer and the GaAs substrate on which it was grown.

(iii) Capacitance and conductivity measurements, made as a function of the number of LB film layers incorporated into the devices, suggested that the effective barrier height to electrons increased with film thickness, but that the diffusion potential in the semiconductor was unaltered.

(iv) The spectral distributions of EL emitted were consistent with radiative recombination from enhanced minority carrier injection in forward bias, and impact-ionisation in reverse bias. The EL output increased rapidly with forward bias up to ~10V, indicating that the degree of band realignment in the semiconductor was being reduced by the effect of series resistance.

(v) The power conversion efficiency of the devices was

strongly dependent upon insulator thickness, rising by over two orders of magnitude when was increased from ~9nm to ~18nm. The maximum external efficiency achieved was estimated as $2x10^{-4}$% for a device incorporating ten layers of phthalocyanine (~23nm). The efficiencies for greater insulator thicknesses are unknown due to difficulties in reliably depositing further layers of phthalocyanine.

(vi) The power conversion efficiencies achieved were disappointingly low in view of the estimated internal quantum efficiency of the ZnSeS films(17). This is thought to be partly a result of losses associated with series resistance effects. However, the mechanism by which holes in the valence band are replenished during forward bias EL is not properly understood, and could well be a limiting low efficiency process.

CHAPTER 8

CONCLUSIONS AND SUGGESTIONS FOR FURTHER WORK

The aims of this research were twofold, to demonstrate the dye sensitisation of a semiconductor with a dye in the form of an LB film, and to examine the properties of MIS light emitting diodes with a stable LB film as the dielectric.

It was shown that a merocyanine dye without any gross hydrophobic and hydrophilic substitutions behaved well as a Langmuir film at the air-water interface. The value of surface area per molecule calculated from the pressure-area characteristics of the dye film was consistent with that estimated by molecular modelling, suggesting that a monolayer had been formed. Incorporating the dye into a matrix of cadmium arachidate at a molecular ratio of 1:1 enabled it to be deposited as films onto various substrates using the LB film technique. The optical characteristics of LB films of the unsubstituted dye were compared and contrasted with those of a merocyanine dye with the amphiphilic substitutions normally associated with more conventional LB film materials. The absorption by both dyes as a function of film thickness obeyed the Beer-Lambert law, though the absorptivity of the unsubstituted dye chromophore was lower. Fluorescence spectra of the dyes indicated the presence of some dimeric structure in the films. When films of the dyes were

deposited onto polycrystalline zinc sulphide it was found that the presence of three monolayers of either dye reduced the d.c photoconductivity of the ZnS in the spectral range at which the dye absorbed most strongly. The filtering action of the dyes was shown to be insufficient for this effect, and it was proposed that the change in photoconductivity was indicative of a desensitisation process, explained in terms of hole injection by excited dye molecules. Although this was the complementary effect to that sought, it is believed that these results demonstrate the feasibility of spectrally sensitising a semiconductor with LB films of such dyes.

The incorporation of LB film layers of phthalocyanine as an insulator into gold/ zinc sulphur selenide structures was shown to enhance the properties of the system as an electroluminescent (EL) device. Au/ZnSeS structures were initially fabricated which behaved as near-ideal Schottky diodes with a barrier height to electrons ~0.8eV, but no EL was detectable from these devices up to their operating limits. The presence of a phthalocyanine insulating layer limited the current in the devices, and EL was detectable for forward biases $\gtrsim$1V. EL output increased rapidly with forward bias up to ~10V, indicating enhanced minority carrier injection with band realignment. The degree of band realignment was thought to be limited by a voltage drop associated with series resistance effects. Measurement of the electrical characteristics of these devices as a function of the number of deposited layers of phthalocyanine suggested that the effective barrier to electrons increased with insulator thickness, but that the diffusion potential in the semiconductor was unaltered. The device EL efficiency was

strongly dependent upon the insulator thickness, rising by over two orders of magnitude to a maximum of $2x10^{-4}$% achieved with ten layers of phthalocyanine (~23nm). The behaviour of the devices was explained by adapting the model used in conventional tunnelling injection theory. An alternative mechanism to tunnelling was required to explain the traversal of the insulator by carriers, and it was suggested that it may be the efficiency of this process which limits the overall device efficiency.

SUGGESTIONS FOR FURTHER WORK

There are a number of areas which could benefit from the extension of the work described in this thesis. The study of dyes as LB film materials was very successful in the development of the LB films themselves, but has yet to show the clear sensitisation process which should be possible with a dye in this form. The research undertaken was limited by the lack of availability of suitable substrate materials. However, recent developments in thin film sputtering techniques are allowing finer control of the properties of semiconductor materials deposited in this form. Work will shortly commence at Durham on the deposition of LB films onto sputtered zinc oxide, supplied by Plessey Ltd. It is hoped that it will prove possible to demonstrate the dye sensitisation of the photoelectrical properties of these films, in particular with the dye SC58497. If an effect is observed, the technique could then be extended to the fabrication of photodetector and solar cell devices for characterisation. As properties of phthalocyanine LB films become better understood, these too could be used in dye

sensitisation studies.

Future work on MIS based LEDs should first concentrate on the full characterisation of devices based upon MOCVD grown ZnSeS, with initially a reversion to classical LB films (i.e cadmium stearate and cadmium 22-tricosenoate) whose properties as LB films are at present better understood than those of phthalocyanine. This would help show whether the devices studied to date have reached a distinct optimum in insulator thickness, as has been reported for GaP MIS LEDs. Continuing work with phthalocyanine should be aimed at improving the stability of devices, which would probably benefit from encapsulation. It is already planned to extend the study of EL devices to MIS structures on gallium nitride substrates.

FIGURE CAPTIONS

Figure 2.1 Schematic representation of intramolecular energy transitions of organic materials.

Figure 2.2 Energy levels of dyes and a semiconductor depicting spectral sensitisation (a) by electron transfer, (b) by energy transfer (after West(4)).

Figure 2.3 Relations between energy levels of dyes and the energy bands of a semiconductor (after Dahne(6)).

Figure 2.4 Spectral distribution of the photoconductivity of ZnO powder. 1) Unsensitised; dyed with: 2) erythrosine; 3) pinacyanol; 4) cryptocyanine; 5) neocyanine; 6) xenocyanine (after Akimov(2)).

Figure 2.5 Demonstration of energy transfer by the fluorescence of LB film structures incorporating dyes (after Kuhn et al(8)).

Figure 3.1 Radiative recombination mechanisms in a semiconductor.

Figure 3.2 Luminous efficiency of the human eye vs incident light wavelength.

Figure 3.3 Schematic diagram of a p-n homojunction (a) in equilibrium and (b) under forward bias.

Figure 7.19 DC power conversion efficiency against number of layers of phthalocyanine for GaP MIS diodes. (After Batey et al(3)).

Figure 7.20 Quantum efficiency of ZnSe:Mn diodes measured at 20mA against estimated film thickness. (After Livingstone et al(19)).

Figure 7.21 Device degradation characteristics of electroluminescence from Au/LB film/ZnSeS MIS diodes. (a) From first switch on, (b) after 30 minutes recovery, (c) after 15 hours operation and 30 minutes recovery.

Figure 7.22 Proposed energy band diagrams for Au/phthalocyanine/ZnSeS devices: (a) $V \lesssim 1V$ (below threshold); (b) $1V \lesssim V \lesssim 10V$ (above threshold); and (c) $V \gtrsim 10V$.

Figure 7.23 Schematic representation of hole injection by a two-stage Auger recombination process. ① Energetic electron enters metal, ② energetic hole injected into semiconductor.

REFERENCES

CHAPTER 2

1. e.g H.Hada, Y.Yonezawa and H.Inaba, Chem.Lett., (1980) 467

2. I.A.Akimov, 'Spectral Sensitizations of Internal Photoeffect in Inorganic Semiconductors by Dyes' in "Elementary Photoprocesses in Molecules", Consultants' Bureau (1968)

3. H.W.Vogel, Ber.deut.Chem.Ges., 6 (1873) 1302

4. W.West, Photogr.Sci.Eng., 18 (1974) 35

5. W.West, Photogr.J., 88B (1948) 557

6. S.Dähne, Photogr.Sci.Eng., 23 (1979) 219

7. R.W.Gurney and N.F.Mott, Proc.Royal Soc., A164 (1938) 151

8. H.Kuhn, D.Moebius and H.Bucher, 'Spectroscopy of Monolayer Assemblies', in A.Weissberger and B.Rossiter (eds), Physical Methods of Chemistry, Vol.1, Part 3b, Wiley (1972)

9. e.g H.Meier, 'Organic Semiconductors', Verlag Chemie (1974)

10. H.Kuhn, 1980 Tokyo Symposium on Advances in Photography, Paper No.III-2 (1980) 199

11. T.Iwasaki, S.Oda, T.Sawada and K.Honda, Photogr.Sci.Eng., 25 (1981) 6

12. E.E.Jelley, Nature, 138 (1936) 1009

13. I.A.Akimov, Dokl.Akad.Nauk SSSR, 251 (1980) 135

14. W.Bauer and G.Heiland, J.Phys.Chem.Solids., 32 (1971) 2605

15. B.Broich and G.Heiland, Surface Science, 92 (1980) 247

16. J.Lagowski, H.C.Gatos and C.L.Balestra, J.Appl.Phys., 49 (1978) 2821

17. M.Vodenicharova and G.Hvedstrup Jensen, J.Phys.Chem.Solids, 36 (1975) 1241

18. H.Gerischer, Ber.Bunsenges.Phys.Chem., 77 (1973) 771

19. R.Memming, Faraday Disc., 58 (1974) 261

20. M.T.Spitler and M.Calvin, J.Chem.Phys., 66 (1977) 4294

21. P.Fromherz and W.Arden, J.Chem.Phys., 102 (1980) 6211

22. T.Moriizumi and K.Kudo, App.Phys.Lett., 38 (1981) 85

23. B.J.Mulder and J.De Jonge, Proc.Koninkl.Ned.Akad.Wetenschap., B66 (1963) 303

24. L.G.S.Brooker et al, J.Am.Chem.Soc., 73 (1951) 5332

25. F.M.Hamer in A.Weissberger (ed), 'Cyanine Dyes and Related Compounds', Wiley (1974)

26. M.M.Zwick and H.Kuhn, Z.Naturforsch, A17 (1962) 411

27. K.H.Drexhage in E.Wolf (ed), 'Progress in Optics XII', North Holland (1974)

28. K.Seefeld, D.Mobius and H.Kuhn, Helv.Chim.Act., 60 (1977) 2608

29. E.E.Polymeropoulos, D.Mobius and H.Kuhn, Thin Solid Films, 68 (1980) 173

30. D.Mobius, Acc.Chem.Res., 14 (1981) 63

31. T.L.Penner and D.Mobius, J.Am.Chem.Soc., 104 (1982) 7407

32. W.Arden and P.Fromherz, Ber.Bunsenges.Phys.Chem., 82 (1978) 874

33. H.Kuhn, Thin Solid Films, 99 (1983) 1

34. M.Sugi and S.Iizima, Thin Solid Films, 68 (1980) 199

35. M.Sugi, T.Fukui, S.Iizima and K.Iriyama, Bull.Electrotech.Lab, 43 (1979) 51

36. T.Fukui, M.Saito, M.Sugi and S.Iizima, Thin Solid Films, 109 (1983) 247

37. U.Itoh, K.Sakashita and Y.Igarashi, Thin Solid Films, 121 (1984) 7

38. I.Pockrand, A.Brillante and D.Mobius, J.Chem.Phys., 77 (1982) 6289

39. S.Baker, M.C.Petty, G.G.Roberts and M.V.Twigg, Thin Solid Films, 99 (1983) 53

CHAPTER 3

1. N.F.Mott, Proc.Cambridge Phil.Soc., 34 (1938) 568

2. W.Schottky and E.Spenke, Wiss.Veroff Siemens-Werken, 118(1939) 225

3. J.Bardeen, Phys.Rev., 71 (1947) 717

4. J.M.Andrews and J.C.Phillips, Phys.Rev.Lett., 35 (1975) 56

5. L.J.Brillson, Phys.Rev.B, 18 (1978) 2431

6. W.E.Spicer, I.Lindau, P.Skeath, C.Y.Su and P.Chye, Phys.Rev.Lett., 44 (1980) 420

7. J.L.Freeouf, Appl.Phys.Lett., 41 (1982) 285

8. A.M.Cowley and S.M.Sze, J.Appl.Phys., 36 (1965) 3212

9. e.g S.M.Sze, 'Physics of Semiconductor Devices', 2nd Ed, Wiley (1981) 250

10. D.L.Scharfetter, Solid State Electronics, 8 (1965) 299

11. H.A.Bethe, MIT Rad.Lab.Rep., 43-12 (1942)

12. C.R.Crowell and M.Beguwala, Solid State Electronics, 14 (1971) 1149

13. E.H.Rhoderick, J.Phys.D.,5 (1972) 1920

14. e.g E.H.Rhoderick, 'Metal-Semiconductor Contacts', Oxford Univ.Press, (1978)

15. C.R.Crowell and S.M.Sze, Solid State Electronics, 9 (1966) 1035

16. A.M.Goodman, J.Appl.Phys., 34 (1963) 329

17. R.H.Fowler, Phys.Rev., 38 (1931) 45

18. B.M.Arora, A.K.Srivastava and S.Guha, J.Appl.Phys., 53 (1982) 1820

19. H.C.Card and E.H.Rhoderick, J.Phys.D., 4 (1971) 1589

20. A.M.Cowley, J.Appl.Phys., 37 (1966) 3024

21. C.L.Chen and K.D.Wise, IEEE Trans.Electron Devices, 29 (1982) 1522

22. S.J.Fonash, J.Appl.Phys., 54 (1983) 1966

23. H.C.Card and E.H.Rhoderick, Solid State Electronics, 16 (1973) 36

24. J.Batey, M.C.Petty and G.G.Roberts, Proc.INFOS Conf.Eindhoven, North-Holland (1983) 141

25. J.Batey, M.C.Petty, G.G.Roberts and D.R.Wight, Electron.Lett., 20 (1984) 489

26. P.Christie, private communication

27. A.W.Livingstone, K.Turvey and J.W.Allen, Solid State Electronics, 16 (1973) 351

28. A.G.Fischer, Phys.Lett., 12 (1964) 313

29. A.G.Fischer, J.Electrochem.Soc., 118 (1971) 139C

30. e.g R.Mach and G.O.Muller, Phys.Stat.Sol.(a), 69 (1982) 11

CHAPTER 4

1. A.Pockels, Nature, 43 (1891) 437

2. Lord Rayleigh, Phil.Mag., 48 (1899) 321

3. I.Langmuir, J.Am.Chem.Soc., 39 (1917) 1848

4. K.B.Blodgett and I.Langmuir, Phys.Rev., 51 (1937) 964

5. G.L.Gaines Jnr, 'Insoluble Monolayers at Liquid-Gas Interfaces', Wiley (1966)

6. H.Kuhn, D.Moebius and H.Bucher, 'Spectroscopy of Monolayer Assemblies', in A.Weissberger and B.Rossiter (eds), Physical Methods of Chemistry, Vol.1, Part 3b, Wiley (1972)

7. G.G.Roberts,P.S.Vincett and W.A.Barlow, Phys.Technol., 12 (1981) 69

8. A.Barraud and M.Vandevyver, Thin Solid Films, 99 (1983) 221

9. I.R.Girling and D.R.J.Milverton, Thin Solid Films, 115 (1984) 85

10. C.W.Pitt and L.M.Walpita, Thin Solid Films, 68 (1980) 101

11. W.L.Procarione and J.W.Kaufman, Chem.Phys.Lipids, 12 (1974) 251

12. W.H.Simpson and P.J.Revcroft, Thin Solid Films, 6 (1970) 167

13. L.Y.Wei and B.Y.Woo, Biophys.J., 13 (1973) 215

14. A.Barraud, C.Rosilio and A.Ruaudel-Texier, J.Coll.Interface Sci., 62 (1977) 509

15. I.R.Peterson, G.J.Russell and G.G.Roberts, Thin Solid Films, 109 (1983) 371

16. P.S.Vincett, W.A.Barlow, F.T.Boyle, J.A.Finney and G.G.Roberts, Thin Solid Films, 60 (1979) 265

17. L.G.S.Brooker et al, J.Am.Chem.Soc., 73 (1951) 5332

18. H.Gruning and G.Heiland, Surf.Sci., 122 (1982) 569

19. K.Iriyama, F.Mizutani and M.Yoshiura, Chem.Lett., (1980) 1399

20. A.K.Ghosh and T.Feng, J.Appl.Phys., 49 (1978) 5982

21. J.Zyss, J.Non-Crystalline Sol., 47 (1982) 211

22. M.Sugi, M.Saito, T.Fukui and S.Iizima, Thin Solid Films, 88 (1982) L15

23. S.Baker, M.C.Petty, G.G.Roberts and M.V.Twigg, Thin Solid Films, 99 (1983) 53

24. S.Baker, G.G.Roberts and M.C.Petty, IEE Proc., 130-I (1983) 260

25. K.B.Blodgett, J.Am.Chem.Soc., 57 (1935) 1007

26. P.S.Vincett and G.G.Roberts, Thin Solid Films, 68 (1980) 135

27. Thin Solid Films, 68 (1980)

28. Thin Solid Films, 99 (1983)

29. G.G.Roberts, K.P.Pande and W.A.Barlow, Solid State Electron.Dev., 2 (1978) 169

30. J.P.Lloyd, M.C.Petty, G.G.Roberts, P.G.LeComber and W.E.Spear, Thin Solid Films, 99 (1983) 297

31. K.K.Kan, G.G.Roberts and M.C.Petty, Thin Solid Films, 99 (1983) 291

32. G.G.Roberts, M.C.Petty and I.M.Dharmadasa, IEE Proc., 128 (1981) 197

33. J.Batey, M.C.Petty, G.G.Roberts and D.R.Wight, Electron.Lett., 20 (1984) 489

34. I.R.Peterson, IEE Proc., 130-I (1983) 252

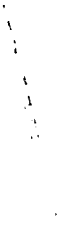

35. G.G.Roberts, M.C.Petty, P.J.Caplan and E.H.Poindexter, Proc.INFOS Conf.Eindhoven, North-Holland (1983) 20

36. G.G.Roberts, T.M.McGinnity, W.A.Barlow and P.S.Vincett, Solid State Commun., 32 (1979) 683

CHAPTER 5

1. H.Kuhn, D.Moebius and H.Bucher, 'Spectroscopy of Monolayer Assemblies', in A.Weissberger and B.Rossiter (eds), Physical Methods of Chemistry, Vol.1, Part 3b, Wiley (1972)

2. M.Sugi, M.Saito, T.Fukui and S.Iizima, Thin Solid Films, 88 (1982) L15

3. S.Baker, G.G.Roberts and M.C.Petty, IEE Proc.,130-I (1983) 260

4. A.E.Thomas,G.J.Russell and J.S.Woods, J.Crys.Growth, 63 (1983) 265

5. P.J.Wright and B.Cockayne, J.Crys.Growth, 59 (1982) 148

6. J.Batey, PhD Thesis, University of Durham (1983)

7. S.Baker, Private Communication

CHAPTER 6

1. H.Kuhn, D.Moebius and H.Bucher, 'Spectroscopy of Monolayer Assemblies', in A.Weissberger and B.Rossiter (eds), Physical Methods of Chemistry, Vol.1, Part 3b, Wiley (1972)

2. M.Sugi, M.Saito, T.Fukui and S.Iizima, Thin Solid Films, 88 (1982) L15

3. CRC Handbook of Chemistry and Physics, 58th edition (1978) F-215

4. P.S.Vincett, W.A.Barlow, F.T.Boyle, J.A.Finney and G.G.Roberts, Thin Solid Films, 60 (1979) 265

5. B.H.Carroll, Photogr.Sci.Eng., 21 (1977) 151

6. K.H.Drexhage in E.Wolf (ed), 'Progress in Optics XII', North Holland (1974)

7. S.Dähne, Photogr.Sci.Eng., 23 (1979) 219

8. J.Lagowski, H.C.Gatos and C.L.Balestra, J.Appl.Phys., 49 (1978) 2821

9. M.Vodenicharova and G.Hvedstrup Jensen, J.Phys.Chem.Solids, 36 (1975) 1241

10. H.Gerischer, Ber.Bunsenges.Phys.Chem., 77 (1973) 771

11. G.G.Roberts, T.M.McGinnity, W.A.Barlow and P.S.Vincett, Solid State Commun., 32 (1979) 683

12. A.E.Thomas,G.J.Russell and J.S.Woods, J.Crys.Growth, 63 (1983) 265

13. I.A.Akimov, Dokl.Akad.Nauk SSSR, 251 (1980) 135

14. M.Saito, M.Sugi, T.Fukui and S.Iizima, Thin Solid Films, 100 (1983)

CHAPTER 7

1. J.Batey, G.G.Roberts and M.C.Petty, Thin Solid Films, 99 (1983) 283

2. J.Batey, M.C.Petty and G.G.Roberts, Proc.INFOS Conf.Eindhoven, North-Holland (1983) 141

3. J.Batey, M.C.Petty, G.G.Roberts and D.R.Wight, Electron.Lett., 20 (1984) 489

4. J.Batey, PhD Thesis, University of Durham (1983)

5. J.Woods, Displays, April (1981) 251

6. Y.S.Park and B.R.Shin, in J.Pankove (ed), 'Electroluminescence', (1977) 133

7. P.S.Vincett and G.G.Roberts, Thin Solid Films, 68 (1980) 135

8. H.C.Card and E.H.Rhoderick, J.Phys.D., 4 (1971) 1589

9. A.M.Cowley, J.Appl.Phys., 37 (1966) 3024

10. S.J.Fonash, J.Appl.Phys., 54 (1983) 1966

11. A.M.Cowley and S.M.Sze, J.Appl.Phys., 36 (1965) 3212

12. e.g P.J.Martin, PhD Thesis, University of Durham (1980)

13. S.Baker, G.G.Roberts and M.C.Petty, IEE Proc., 130-I (1983) 260

14. Y.A.Vidadi, E.A.Chistyakov and L.D.Rozenshtein, Sov.Phys.- Solid State, 11 (1970) 1946

15. P.Christie, private communication

16. S.Baker, PhD Thesis, University of Durham (1985)

17. D.R.Wight, P.J.Wright and B.Cockayne, Electron.Lett., 18 (1982) 593

18. M.E.Oznan and J.Woods, Appl.Phys.Lett., 25 (1974) 489

19. A.W.Livingstone, K.Turvey and J.W.Allen, Solid State Electronics, 16 (1973) 351

20. H.Watanabe, T.Chikamura and M.Wada, Japan.J.Appl.Phys., 13 (1974) 357

21. A.G.Fischer, Phys.Lett., 12 (1964) 313

22. H.Card and B.L.Smith, J.Appl.Phys., 42 (1971) 5863